CENTER FOR RESEARCH AND ADVANCED STUDIES OF THE NATIONAL POLYTECHNIC INSTITUTE

PHYSICS DEPARTMENT

"Searching for new physics signatures in low-energy neutrino experiments"

by

Oscar Sanders Muñoz

In order to obtain the

Doctor of Science

degree, speciality in

Physics

Advisor: Ph. D. Omar Gustavo Miranda Romagnoli

Mexico City August, 2022

CENTRO DE INVESTIGACIÓN Y DE ESTUDIOS AVANZADOS
DEL INSTITUTO POLITÉCNICO NACIONAL

UNIDAD ZACATENCO
DEPARTAMENTO DE FÍSICA

"Búsqueda de señales de nueva física en experimentos de neutrinos de baja energía"

Tesis que presenta

Oscar Sanders Muñoz

para obtener el Grado de

Doctor en Ciencias

en la Especialidad de

Física

Director de tesis: Dr. Omar Gustavo Miranda Romagnoli

Ciudad de México Agosto, 2022

Agradecimientos

A mis **padres**, por haberme brindado todas las herramientas para desarrollarme profesionalmente durante todos estos años, concluyendo con la obtención de este título.

A mis **hermanos**, por estár siempre presentes en los buenos y malos momentos, mostrándome de lo que soy capaz.

A mi **esposa**, que siempre ha demostrado ser un apoyo incondicional, en las buenas y en las malas, y que si no fuera por ella tal vez hoy no estaría en este lugar.

A mi **hija**, por ser el pequeño motor que me impusla a esforzarme cada día más para que pueda lograr todas sus metas.

A mis **familiares**, por comprender mi profesión y apoyarme en lo posible.

A mis **amigo**s, por haber sido mis compañeros en este camino, siempre al pendiente de mi progreso y listos para dar un buen consejo.

A mis **profesores**, porque si no fuera por su esfuerzo, no habría adquirido los conocimientos necesarios para avanzar a lo largo de los años.

A mi asesor de tesis, el **Dr. Omar G. Miranda Romagnoli** por guiarme durante todo este proceso, siempre apoyándome desde el punto de vista profesional y también como un colega y amigo, sin su esfuerzo este trabajo no hubiera sido posible.

A mis sinodales, **Dr. Abdel Pérez Lorenzana**, **Dr. Eduard de la Cruz Burelo**, **Dr. Luis Jorge Flores Sandoval** y **Dr. Tonatiuh Matos Chassin** por su amabilidad y consejos que hicieron de este trabajo el mejor posible.

A todo el personal de **CINVESTAV**, pues su labor diaria permite que en conjunto podamos generar nuevo conocimiento para progreso de la humanidad.

Y finalmente al **CONACYT** por la beca para llevar a cabo mis estudios de Doctorado que llegan a su fin con este trabajo.

Este trabajo ha sido apoyado en parte por el proyecto **CONACYT** A1-S-23238.

Contents

Abstract

Coherent elastic neutrino-nucleus scattering (CEvNS) is a well-described process in the Standard Model. We needed more than 40 years to be detected for the first time by the collaboration COHERENT using a Cesium-Iodine detector and later one of liquid Argon. In this thesis, we study the possible application of this process to find bounds on different parameters that describe new physics, such as sterile neutrino oscillations, non-unitarity of the neutrino mixing matrix, and magnetic properties of the neutrino. We analyze futures detectors from the same COHERENT collaboration and new experiments still under construction using coherent elastic neutrino-nucleus scattering (CEvNS) or neutrino scattering with electrons (EvES).

Resumen

La dispersión elástica coherente entre neutrino y núcleo (CEvNS) es un proceso bien descrito en el modelo estándar. Necesitamos más de 40 años para que se detectara por primera vez por la colaboración COHERENT utilizando un detector de Cesio-Iodo y posteriormente uno de Argon líquido. En esta tesis estudiamos la posible aplicación de este proceso para encontrar cotas en distintos parámetros que describen nueva física como es el caso de oscilaciones de neutrinos estériles, no unitariedad de la matriz de mezcla de neutrinos y propiedades magnéticas del neutrino. Analizamos los futuros detectores de la misma colaboración COHERENT, y nuevos experimentos que aún están en construcción usando CEvNS o bien dispersión del neutrino con electrones(EvES).

Introduction

Within the Standard Model, neutrinos are particles that have no charge and zero mass. However, the discovery of neutrino oscillations has shown that neutrinos do actually have mass. This leads us to search for new physics beyond the Standard Model to explain how they obtain their mass. These considerations have guided us to new properties like a neutrino magnetic moment, NSI interactions, and non-unitarity of the neutrino mixing matrix, among others. Also, some anomalies that still cannot be explained in the context of neutrino oscillations between active states suggest the possible existence of sterile neutrinos, which are defined as having no SM gauge interactions.

Coherent Elastic Neutrino-Nucleus Scattering is a very useful process in the study of new physics. Since its cross section is well-determined within the Standard Model, any deviation from its prediction may be a sign of new physics. We take advantage of this and study the future perspective on different beyond the standard model physics with different experimental setups that have already measured and are planning to measure this process. The thesis is organized as follows:

First, we give a general introduction to neutrino physics and particle physics. In Chapter 3, we give a theoretical framework of all the physics scenarios considered, starting with the process of neutrino oscillations in the presence of light sterile neutrino states. Then, we study the non-unitarity of the neutrino mixing matrix that arises if the extra lepton states are heavy enough to forbid its participation in neutrino oscillations. And finally, we talk about neutrino magnetic properties in the context of a sterile neutrino dipole portal, in which a sterile neutrino state is produced at an electromagnetic interaction between a neutrino and a nucleus or an electron.

In chapters 4, 5, and 6, we present the formalism of the processes under study and the experimental setups considered for each case. Then in Chapter 7, we present the results obtained for each scenario, showing the different sensitivities that can be reached. Finally, in chapter 8, we give our conclusions to this thesis.

Chapter 1

Particle physics introduction

Particle physics studies the fundamental building blocks of matter, from the protons and neutrons that form the nucleus of the atoms to the quarks that form each of these particles. The study of the particles dates back to ancient Greece, where the Greek philosophers asked themselves what the matter was made of. Due to the technology available by then, their first answers emerged from thought experiments. They imagined that if one bread is cut by half continuously, there must be a piece that is impossible to cut further. This minimum piece of bread is what they called the atom, which means indivisible. It was not until the end of the 19th century when the discovery of the electron by J.J. Thomson started a more in-depth and formal study of the particles.

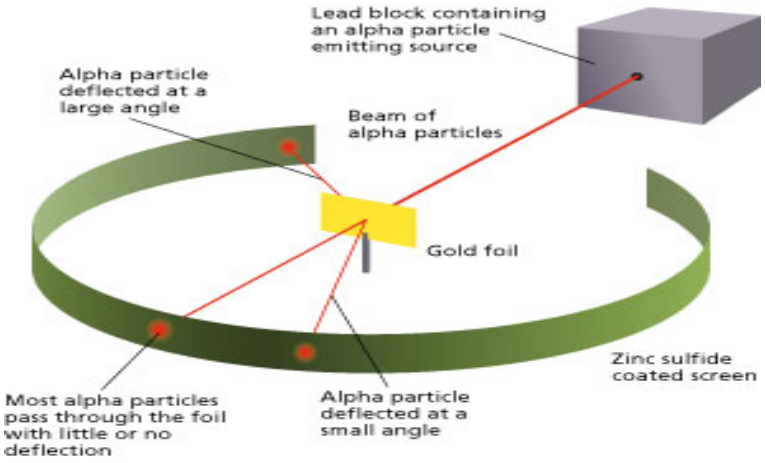

Figure 1.1: Rutherford scattering experiment was the first proof that the nucleus of a atoms was a very small concentration of mass and positive charge. The effect observed was like if a bullet got reflected by a paper sheet [1].

John Dalton gave the first scientific approach to solve the problem of the atom. By

studying the properties of gases, Dalton wrote some postulates that described the interaction of atoms in chemical reactions [2] . A century later, Thomson discovered that electrons were constituents of atoms, and imagined that they were suspended in a kind of positively charged paste like a pudding [3]. Rutherford's scattering experiment contradicted this idea. Rutherford's experiment consisted of a thin sheet of gold foil bombarded by a beam of α-rays [4], see Fig. 1.1. In accordance with Thomson's model, the α-rays should have been deflected in small angles since the atoms of gold were considered as diffusive spheres. With big surprise, Rutherford observed that most of the α-rays passed undisturbed, and some of them scattered at big angles, even a few of them scattered completely back to the beam source. With this result, Rutherford concluded that all the mass and positive charge of the atom were concentrated in a tiny volume at the center of the atom. He called hydrogen to the nucleus of the lightest atom.

Finally, in 1914 [5]Niels Bohr proposed a planetary-like model for hydrogen in which the electron is circling the proton like a planet going around the Sun. With this model, Bohr calculated the hydrogen spectrum and supposed that heavier atoms were composed of more protons supporting the same number of orbiting electrons. The problem with this idea was that larger atoms resulted in heavier than predicted by Bohr's Model. The solution to this problem came in 1932 with the discovery of the neutron by Chadwick. The neutron is an electrically neutral twin of the proton that solves the missing mass of the atoms by adding a certain number of neutrons to the nucleus of each element. Since the neutron is electrically neutral, the number of neutrons is somewhat flexible. This means that atoms of the same element could have a different number of neutrons, these atoms with a different number of neutrons but the same number of protons are called isotopes. In this way, by 1932, the protons, neutrons, and electrons were thought to be the only blocks of matter.

Despite the great progress achieved on the understanding of the composition of matter, there was still a question remaining. If the protons have positive charge, then there must be a repulsive force acting between them so what is holding them together in the nucleus. This force must be stronger than electromagnetism and also must have a very short range since we don't notice it in our daily lives. This force is called the strong force, and the first theory was proposed by Yukawa in 1934 [2]. As an analogy to electric and gravitational force, Yukawa assumed that the protons and neutrons where attached together due to some kind of field, and this field needed to be quantized. since the force has very short range, the mediator would be heavy with a mass between the

electron and the proton, that's why it was called the meson. Around 1937, different experiments observed a particle that matched Yukawa's meson, but there were some problems like the lifetime and the mass seemed to be different from the prediction. The problem was solved in 1947 [2] when Powell discovered that there were actually two particles from the cosmic rays, they called them the pion (π) and the muon (μ). The pion is the actual meson from Yukawa's theory, and it is produced on the atmosphere but decays to muons before reaching ground.

Later on, different particle decays were studied and in order to explain the possibility of certain interactions, different conservation rules were developed like Baryon number, Lepton number, and Strangeness conservation. With these new properties, Murray Gell-Mann introduced the so called Eightfold Way in 1961 [2] which is an arrange of Baryons and Mesons according to their charge and strangeness, this was useful for the prediction of new particles with properties that matches the missing spots in this configurations.

With all this particles, properties and interactions it was necessary to establish a framework to work with. The Standard Model(SM) is a periodic table like organization for elementary particles. In this theory, the building blocks of matter are classified into two groups called leptons and quarks. Each group consists of six particles, which are subdivided into three generations. The mass of these particles increases in each generation while their stability decreases. The first generation is formed of the lightest and most stable particles. Therefore all stable matter is made from these particles; the heavier particles decay to a more stable group.

The first generation of quarks consists of the "up quark" and the "down quark", the second by the "charm quark" and the "strange quark" and the third by "top quark" and "bottom quark". Each quark can come in three different "colors" and always mix in a "colorless" way, so they do not exist individually. This idea of the nonexistence of isolated quarks is called confinement. The particles formed by the quarks are called hadrons, and they are subdivided into two groups called baryons and mesons. Baryons are built with three quarks, while mesons with a quark and an anti-quark.

In the case of the Leptons, the first generation consists of the "electron" and the "electron neutrino", the second of the "muon" and the "muon neutrino" and the third one of the "tau" and the "tau neutrino". The electron, muon, and tau have electric charge and mass, while the neutrinos are electrically neutral and have negligible mass.

We can also classify the particles in fermions and bosons, the first ones with half-integer

spin and the second ones with integer spin. The name of each group corresponds to the statistics that describe them, that is, Fermi-Dirac or Bose-Einstein statistics. Each force has its own strength, range of action and boson, the gluon for the strong force, the photon carries the electromagnetic force, the W and Z bosons the weak force and the graviton for the gravity although it has not yet been found. Finally, the Higgs gives mass via the Higgs mechanism.

The four fundamental forces ordered from the weakest to the strongest are:

- The gravitational force: responsible for the attraction between objects with mass.
- The weak force: responsible for the radioactive processes like nucleus decays.
- The electromagnetic force: responsible for the interaction between charged particles.
- The color force: responsible for maintaining the quarks forming hadrons together.

Although gravity is not yet part of the Standard Model, it will still work well because the effect of gravity on the minuscule scale of particles is so weak that it can be negligible. However, the search for the graviton and the unification of gravity is an open problem nowadays.

1.1 Standard Model

The Standard Model is described by the gauge group

$$G_{SM} = SU(3)_C \times SU(2)_L \times U(1)_Y \tag{1.1}$$

with three fermion generations. Neutrinos have neither strong nor electromagnetic interactions, and we call active neutrinos to those having weak interactions. Since leptons do not have color charge, they do not participate in strong interactions. On the other hand, since neutrinos have no electric charge, they do not experience electromagnetic processes.

Despite Fermi theory of weak interaction described beta decay with great accuracy, there were some interactions at a different energy scale that the theory proved to be "wrong". The turning point in understanding this phenomenon was the hypothesis that weak interaction violates parity [6]. It was confirmed by the experiment of Wu (1957)

and was the key to understand the structure of weak interaction, allowing to conclude that for neutrinos, the spin and momentum have opposite directions, while, for anti-neutrinos the directions are the same. This is called positive and negative helicity for anti(neutrinos). The theoretical picture was completed by the universal V-A nature of the charged-current weak interaction.

The weak interaction can be due to a weak charge current (CC) between neutrinos and their corresponding charged leptons given by the Lagrangian [7]

$$-\mathcal{L}_{cc} = \frac{g}{\sqrt{2}} \sum_{l} \bar{\nu}_{Ll} \gamma^{\mu} l_{\bar{L}} W_{\mu}^{+} + h.c. \tag{1.2}$$

This interaction can be represented by the fundamental vertex shown in Figure 1.2, in which a negative lepton (e^-, μ^-, τ^-) converts into its corresponding neutrino, emitting a W^-, or if considered as an absorption, a W^+

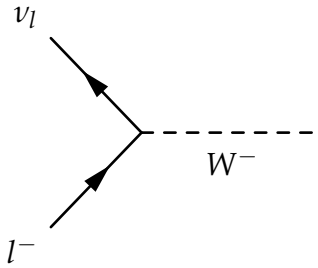

Figure 1.2: Fundamental weak charged current vertex.

On the other hand, the weak interaction can also be due to a neutral current (NC) given by [7]

$$-\mathcal{L}_{NC} = \frac{g}{2cos\theta_W} \sum_{l} \bar{f} \gamma^{\mu} f Z_{\mu}^{0}, \tag{1.3}$$

where f stands for any lepton or quark, with a fundamental vertex of the form shown in Figure 1.3.

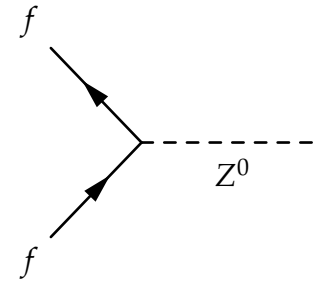

Figure 1.3: Fundamental weak neutral vertex.

With Eq. (1.3) it is possible to determine the decay width of the Z^0 boson into neutrinos. This value is proportional to the number of left-handed neutrinos and has the value $N_\nu = 2.9963 \pm 0.0074$, as reported by [8]. In this way, the SM must contain only three active neutrinos.

According to the SM, fermions masses come after a spontaneous symmetry breaking from the Yukawa interaction by coupling right-handed fermions with its left-handed doublet and the Higgs field. Since neutrinos do not have a right-handed counterpart in this model, Yukawa's mechanism leaves them massless. In the Fermi theory, the transition from a neutral lepton to a charged one is described by the leptonic charged current. This current is given by the V-A structure of weak interaction, so the current has the form:

$$V_\mu^{lept} - A_\mu^{lept} = e\gamma_\mu\nu - \bar{e}\gamma_\mu\gamma_5\nu = 2\bar{e}\gamma_\mu P_L\nu, \tag{1.4}$$

where $P_L = (1-\gamma_5)/2$. This indicates that the wave-functions of the neutrinos(anti-neutrinos) need to be of the form

$$\Psi_\nu(x) = e^{-ipx}P_L u, \tag{1.5}$$

$$\Psi_{\bar{\nu}(x)} = e^{-ipx}P_R u, \tag{1.6}$$

where u is a 4-spinor that obeys the Dirac equation. Considering the case of plane waves and in the ultra-relativistic limit where $p >> m$ we have $E \approx p$ so the Dirac Hamiltonian can be written as

$$H_D = \vec{\alpha}\cdot\vec{p} + \beta m \approx \vec{\alpha}\cdot\vec{p} = \vec{\Sigma}\cdot\vec{p}\gamma_5 \approx \vec{\Sigma}\cdot\vec{n}\gamma_5 E, \tag{1.7}$$

with

$$\vec{\alpha} = \begin{bmatrix} 0 & \vec{\sigma} \\ \vec{\sigma} & 0 \end{bmatrix}, \tag{1.8}$$

and where $\vec{n} = \vec{p}/p$ is the momentum direction.The projection of the spin in the direction of the momentum is called helicity and is given by $\vec{\Sigma}\cdot\vec{n}$ in the previous formula. For the case when the kinetic energy is much larger than the mass, we find that the

energy eigenstates satisfy

$$\vec{\Sigma} \cdot \vec{n} \Psi_{\nu}(x) \approx -\Psi_{\nu}(x), \tag{1.9}$$

$$\vec{\Sigma} \cdot \vec{n} \Psi_{\bar{\nu}(x)} \approx +\Psi_{\bar{\nu}}(x). \tag{1.10}$$

This means that in the ultra-relativistic limit, neutrinos have negative helicity whereas anti-neutrinos have positive helicity. But a problem arises if the mass of the neutrinos is non-zero, and there are two possible scenarios for this.

In the first case, the mass of neutrinos has the same character as the mass of other spin 1/2 charged particles. This type of mass shows a strict separation between particle and antiparticle states. This means that there are four distinct states in the rest frame, as for the neutron or the electron. Namely, two spin states for the neutrino and the two spin states for the anti-neutrino. The second hypothesis is the one proposed by Majorana. In this case, there are just 2 spin states, in other words, the particle and antiparticle coincide, the question of which of these hypothesis is correct is one of the most important open question in neutrino physics up to date. In theory, it may be possible to observe the difference between this two types of masses in some experiments.

The flavor neutrino fields $\nu_{lL}(x)$ are included into the SM charged and neutral current interactions

$$L_I^{CC} = -\frac{g}{\sqrt{2}} j_{\alpha}^{CC} W^{\alpha} + h.c. \tag{1.11}$$

$$L_I^{NC} = -\frac{g}{2cos\theta_w} j_{\alpha}^{NC} Z^{\alpha}, \tag{1.12}$$

where

$$j_{\alpha}^{CC} = \sum_{l=e,\mu,\tau} \nu_{\bar{l}L} \gamma_{\alpha} l_L, \tag{1.13}$$

$$j_{\alpha}^{NC} = \sum_{l=e,\mu,\tau} \nu_{\bar{l}L} \gamma_{\alpha} \nu_L, \tag{1.14}$$

are the charged leptonic and neutral leptonic currents.

In the Standard Model, fermions acquire their masses via a Yukawa coupling of the scalar Higgs doublet ϕ with a fermion right-handed and left-handed component. So for leptons we can create the coupling with their left-handed doublets L_L and their right-handed charged lepton fields E_R [9]

$$-L_{Yukawa} = Y^l_{ij}\bar{L}_{Li}\phi E_{Rj} + h.c. \tag{1.15}$$

Then, after the spontaneous symmetry breaking we get the masses

$$m^l_{ij} = Y^l_{ij}\frac{v}{\sqrt{2}}, \tag{1.16}$$

with v the vacuum expectation value of the Higgs field. Since there is no right-handed neutrinos, we can't build this Yukawa mass term for them, so neutrinos are massless at Lagrangian level. On the other hand, a neutrino mass term may be generated at loop level, but the only possible term that could be constructed is the bilinear $\bar{L}_L L^c_L$, where L^c_L is the charged conjugate field, $L^c_L = C\bar{L}^T_L$ and C is the charge conjugation matrix. But this term violates the total lepton symmetry by two units so it cannot be induced by loop corrections and is forbidden in the SM.

1.2 Neutrino physics

The understanding of neutrinos started in 1930, in this year the problem of the Beta decay, which is described by $A \rightarrow B + e^-$, emerged. From the theory of two-body decays, the energy of the electron is expected to have a constant energy that is function of the mass of the particles A and B given by

$$E = \left(\frac{m^2_A - m^2_B + m^2_e}{2m_A}\right)c^2. \tag{1.17}$$

However, when the energy of the electron is measured, we find that the electrons vary considerably in energy. Equation (1.17) only describes the maximum possible electron energy for a particular beta decay (see Fig. 1.4).

Wolfgang Pauli who was born in Vienna in 1900, at twenty-five, he recognized a fourth degree of freedom in the atomic spectra, which resulted to be the spin, whose impli-

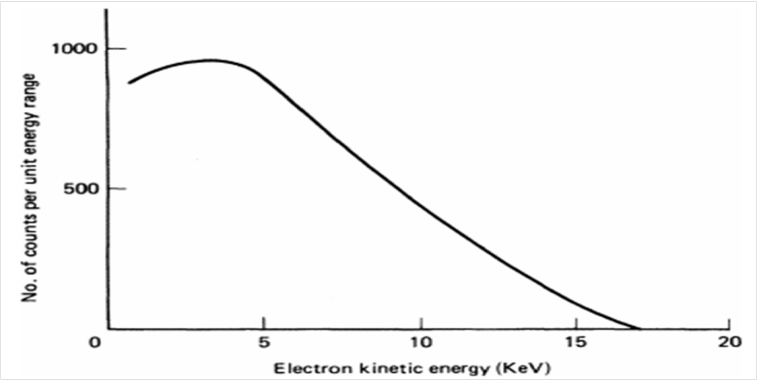

Figure 1.4: Electron energy spectrum for the Beta decay. The maximum energy is the one given by Eq. (1.17). This observation suggested that this process was violating energy conservation, but Fermi proposed the neutrino to solve this problem [2].

cations are now called Pauli Exclusion Principle, winning a Nobel Prize in 1945. On December 1930, he sent a letter talking about a possible solution to the beta decay spectrum, where he suggested that the process was a three-body decay and that the new particle was taking some of the electron energy as kinetic energy. Pauli suggested that this new particle had to be neutral, to conserve charge and called it neutron. It was on October 1931 in an International congress of Nuclear Physics, where Enrico Fermi got interest on Pauli's hypothesis.

In 1933 Fermi presented a theory of beta decay that incorporated Pauli's particle (which he called neutrino), in this theory (anti)neutrinos are created in association with β rays in certain nuclear decays. Since it was not detected, it should not have charge, and since the energy spectrum had a maximum energy equal to Eq. (1.17), it should be very light(presumably with zero mass).

On 1948, the existence of a new neutrino different from the one produced by electrons were suggested, this was demonstrated by Lederman,Schwartz, Steinberger in 1962(Nobel prize in 1988). Finally, evidence of the τ lepton, were collected since 1974. This τ neutrino was first observed by DONUT experiment on 2000. Nevertheless, the number of neutrinos was previously known from measurements of the invisible decay width of the Z boson on LEP experiment

$$N_\nu = \frac{\Sigma_Z^{invisible}}{\Sigma(Z_{\rightarrow}\nu\bar{\nu})_{SM}} = 2.9963 \pm 0.0074. \tag{1.18}$$

In order to differentiate between the neutrino and the anti-neutrino they were assigned a Lepton number, been +1 for the e^-, μ^-, τ^- and the ν's: and -1 for e^+, μ^+, τ^+ and

the $\bar{\nu}$'s. The Lepton number for the rest of the particles is 0. In this way, every decay should conserve the Lepton number, and so it could be determined which decays where possible and in which of them the neutrinos and anti-neutrinos were present.

Since there are three different neutrino flavors, each one has its own conservation law. The Lepton number is divided into the conservation of three new quantities called the electron, muon and tau number. With this information, we know which interactions are possible.

Dirac's theory played an important role for Fermi in his first development of the β decay theory. Therefore, we will show some of the most important results of the early studies of Quantum Mechanics.

We start with the stationary, one-dimensional Schrodinger equation [2]

$$\hat{H}\Psi = \left(-\frac{\hbar^2}{2m}\frac{\partial^2}{\partial x^2} + V\right)\Psi = E\Psi. \tag{1.19}$$

In this formulation, the physical quantities are expressed as differential operators

$$x \to \hat{x} = x, p \to \hat{p} = \frac{\hbar}{i}\frac{\partial}{\partial x}, E \to \hat{E} - \frac{\hbar}{i}\frac{\partial}{\partial t}, \tag{1.20}$$

where x is the position, p is the momentum and E is the energy. If we use the non-relativistic expression for energy $E = \frac{p^2}{2m} + V$ on a wave function Ψ using this relation, we get

$$E\Psi = \left(\frac{p^2}{2m} + V\right)\Psi = \left(-\frac{\hbar^2}{2m}\frac{\partial^2}{\partial x^2} + V\right)\Psi. \tag{1.21}$$

Therefore, the Schrodinger equation is a statement of energy conservation.

If we make the same process but consider the relativistic formulation of energy

$$E^2 = (pc)^2 + (mc^2)^2, \tag{1.22}$$

we get the so called Klein-Gordon equation, sometimes called the relativistic Schrodinger

equation,

$$\left(-\frac{\hbar^2}{c^2}\frac{\partial^2}{\partial t^2}+\hbar^2\frac{\partial^2}{\partial x^2}\right)\Psi=(mc)^2\Psi, \tag{1.23}$$

which can be written in more simplified form by using the special relativity notation and the Einstein's summation convention

$$(\partial_\mu\partial^\mu+m^2)\Psi=0. \tag{1.24}$$

The problem with this equation is that it neglects spin and is unable to model the Hydrogen spectrum, which has good experimental data in that times. The first attempt to include spin in quantum mechanics was developed by Jordan and Heisenberg in 1926, but later, Pauli developed his own theory which fit into the current understanding much better.

If we consider now the time-independent Schrodinger equation in the Heisenberg's formalism

$$\hat{H}\Psi=E\Psi, \tag{1.25}$$

this is an eigenvalue equation with H an operator, Ψ an eigenvector, and E the energy eigenvalue. We can also have, in the same manner, an operator associated to orbital angular momentum L. In this case, a particle with angular momentum l, and z projection m, can be described by an angular wave function Y_{lm},

$$L^2Y_{lm}=(l(l+1)\hbar^2Y_{lm}, \tag{1.26}$$

$$L_zY_{lm}=m\hbar Y_{lm}. \tag{1.27}$$

As an analogy, Pauli defined a new operator S associated to spin which had three components, each of which was a 2x2 Pauli matrix

$$S_x=\frac{\hbar}{2}\sigma_x, S_y=\frac{\hbar}{2}\sigma_y, S_z=\frac{\hbar}{2}\sigma_z, \tag{1.28}$$

where

$$\sigma_x = \begin{bmatrix} 0 & 1 \\ 1 & 0 \end{bmatrix}, \sigma_y = \begin{bmatrix} 0 & -i \\ i & 0 \end{bmatrix}, \sigma_z = \begin{bmatrix} 1 & 0 \\ 0 & -1 \end{bmatrix}. \tag{1.29}$$

He discovered that with this operator, the eigenvalue equation is exactly analogous to the original angular momentum one. Therefore, defining s as the spin quantum number and s_z as its projection into the $z - axis$ he found

$$S^2\chi_\pm = s(s+1)\hbar^2\chi_\pm, \tag{1.30}$$

$$S_z\chi_\pm = s_z\hbar\chi_\pm, \tag{1.31}$$

with eigenvectors given by

$$\chi_+ = \begin{bmatrix} 1 \\ 0 \end{bmatrix}, \chi_- = \begin{bmatrix} 0 \\ 1 \end{bmatrix}. \tag{1.32}$$

The problems with Pauli's theory were its non-relativistic character and that it failed to predict the gyro magnetic ratio by a factor of two.

The solution to all this problems was developed by Dirac in his equation. He forced this equation to be first order in all variables, as opposed to Schrodinger and Klein-Gordon equations, and he got to the final equation form

$$(i\gamma^\mu\partial_\mu - m)\Psi = 0, \tag{1.33}$$

which holds for the following 4x4 Dirac or γ-matrices

$$\gamma^0 = \begin{bmatrix} I & 0 \\ 0 & -I \end{bmatrix}, \gamma^1 = \begin{bmatrix} 0 & \sigma_x \\ -\sigma_x & 0 \end{bmatrix}, \tag{1.34}$$

$$\gamma^2 = \begin{bmatrix} 0 & \sigma_y \\ -\sigma_y & 0 \end{bmatrix}, \gamma^3 = \begin{bmatrix} 0 & \sigma_z \\ -\sigma_z & 0 \end{bmatrix}. \tag{1.35}$$

Dirac equation looks explicitly as

$$\sum_{k=1}^{4}\left(\sum_{\mu=0}^{3} i(\gamma^{\mu})j_k\partial_{\mu} - m\delta_{jk}\right)\Psi_k = 0;\ j \in \{1,2,3,4\}. \tag{1.36}$$

The object Ψ is called Dirac spinor and is analogous to the χ from Pauli except that in this case the Dirac spinor has 4 components, two of these components provide information about the possible spin value states, while the other two correspond to their negative energy states, that was a mystery for some years. Later, Dirac proposed that they represent new type of particles with negative energy, and the anti-electron was discovered on 1932, making Dirac's equation a great success. Dirac equation explained correctly the Hydrogen spectrum and predicted the correct value of the gyro magnetic ratio.

Beta decay was described by Fermi using Dirac's theory, which was the available theory for describing Quantum electrodynamics. In QED, the process $p \rightarrow p + \gamma$ described by the Lagrangian

$$L = ej_{\mu}^{(em)}A^{\mu} = e(\bar{u_p}\gamma_{\mu}u_p)A^{\mu}, \tag{1.37}$$

where e is the charge of the proton, u_p is the proton Dirac spinor, γ_{μ} is a Dirac matrix, and A^{μ} is the photon Dirac spinor. The current in this case is the electromagnetic current of the proton given by $j_{\mu}^{(em)} = \bar{u_p}\gamma_{\mu}u_p$. Fermi used this current to describe the β decay. He replaced the electromagnetic current with a term that corresponds to the transition between the neutron and the proton $j_{\mu}^{n\rightarrow p} = (\bar{u_p}\gamma_{\mu}u_n)$. He also replaced the photon spinor, A^{μ}, with the transition between the electron and the neutrino $j_{\nu\rightarrow e} = (\bar{u_e}\gamma^{\mu}u_{\nu})$. The electric charge constant was replaced with a new coupling constant, G, that we know as the Fermi coupling constant, G_F. All this analysis results in

$$L_{\beta} = G_F j_{\mu}^{n\rightarrow p} j_{\nu\rightarrow e}^{\mu} = G_F(\bar{u}_p\gamma_{\mu}u_n)(\bar{u}_e\gamma^{\mu}u_{\nu}). \tag{1.38}$$

This interaction is a contact interaction, which means that it is evaluated at the same point in space and time. This theory of β decay also explains other processes such as electron-capture ($e^- + p \rightarrow n + \nu$) or inverse β Decay ($\bar{\nu} + p \rightarrow n + e^+$). Despite different problems that the theory had, it was a great step in the understanding of the

Symmetry	Conserved quantity
Translation in space	Momentum
Translation in Time	Energy
Rotation in Space	Angular momentum
Reflection in Space	Parity

Table 1.1: Symmetries with their associated conserved quantities

weak interaction and is useful for low energy processes.

Parity Violation and the $\theta - \tau$ puzzle

Symmetries and conservation laws are related in physics. Noether's theorem states that if a system is symmetric under some transformations, there must be a conserved quantity within the system associated with that symmetry. The simplest example is when a system is identical when using a translation in a certain direction. The momentum along that direction conserves. Some of the most fundamental symmetries are shown in table 1.1.

One important conserved quantity for particle physics is parity. This is the result of a transformation of the form $\vec{r} \rightarrow -\vec{r}$. A system is symmetric under parity if $\Psi(r) = \Psi(-r)$ and anti-symmetric if $\Psi(r) = -\Psi(-r)$. The parity of the system is the result of the eigenvalue equation $\hat{P}\Psi(r) = p\Psi(r)$. Parity is a multiplicative quantum number. That is, the product of the constituents is the one that should be preserved, rather than the sum.

In 1924 [2], German-American physicist Otto Laporte, noted that when an atomic state transition from one state to another emitting a photon, the wavefunction always changes its parity. This is called "Laporte's rule" and it is just a statement of the law of conservation of parity. Later, in 1927, Eugene Wigner proved that Laporte's rule is a direct consequence of reflection symmetry of the electromagnetic force. Parity conservation was used to derive different particle quantum numbers and properties. But there raised a problem with two positively charged strange particles, the τ^+ and the θ^+, in which the following decays had been observed:

$$\tau^+ \rightarrow \pi^+\pi^+ + \pi^-, \tag{1.39}$$

$$\theta^+ \rightarrow \pi^+\pi^0. \tag{1.40}$$

Let's analyze the parities of these decays. The pions have an intrinsic parity of -1. This parity is obtained from applying parity conservation to pion capture by deuteron ($\pi + d \rightarrow n + n$). Now we need to take into account the spatial contribution to parity. The τ, θ, and the pions have intrinsic spins of 0. The total angular momentum is given by $J = L + S$, where L is the external angular momentum which is 0 for this case. For both decays the total initial angular momentum is 0.

- θ decay: The orbital angular momentum of the π's is zero [10] to conserve the total angular momentum. With this, the spatial contribution to parity is $(-1)^L = (-1)^0 = +1$ (This extra term comes from the angular part of the spatial wave function, $Y_l^m(\theta, \phi)$). So the total parity is $P = P_{\pi^+} P_{\pi^0} P_{spatial} = (-1)(-1)(+1) = +1$. So at the end by parity conservation $P(\theta) = +1$

- τ decay: In this case, the orbital angular momentum has 2 components, one given the angular momentum between the two π^+ and the other by the remaining π^- and the center of mass of the two π^+. Again, this sum must be equal to 0 to conserve to conserve total angular momentum. So the two components must have equal magnitude. So for this case, the spatial component of the parity is the product of both parities $P_{spatial} = (-1)^L(-1)^L) + 1$. So at the end $P(\tau) = P_{\pi^+} P_{\pi^+} P_{\pi^-} P_{spatial} = (-1)^3(+1) = -1$

As can be seen, there were two particles with almost identical properties such as mass and lifetime, but with apparently two different parities. This was a question that Lee and Yang attempted to solve on April 1956 at the sixth Rochester conference on High Energy Nuclear Physics in Rochester , New York.

As a first attempt, Lee and Yang proposed a solution called parity doubling, in which particles with odd strangeness were hypothesized to come in pairs, one with even parity and the other with odd. With this solution they were trying to maintain the principle of parity conservation in Weak interaction safe. At the 1956 Rochester Conference, Martin Block and Richard Feynman discussed if parity conservation was really inviolable, this conversation resulted on Feynman proposing that parity violation may be a possibility. With this, Lee and Yang began an analysis of the experimental data available to evaluate if the law of parity conservation held.

They noticed that there was no evidence of parity conservation in weak interactions, contrary to the strong interaction in which there was solid evidence. Lee and Yang mentioned that if parity violation were true, then certain quantities called pseudoscalars would have a non-zero average value and suggested different experiments to measure

these quantities.

The experiment proposed by Lee and Yang was the analysis of the process ${}^{60}Co(J^p = 5^+) \rightarrow^{60} Ni(4^+) + e^- + \bar{\nu}_e$ decay. In this case, the pseudoscalar to be measured was the projection of the electron's momentum on the spin (J) of the Cobalt nucleus. This experiment was performed by Madame Wu (Chien-Shiung Wu) [11]. On December 27, Wu's group came up with the amazing results. The average value of the pseudoscalar given by the projection of the electron's momentum onto the spin of the Cobalt nucleus was not zero and reflection symmetry was violated. This was not the only experimental evidence of parity violation, as different experiments confirmed this observation.

After this result, Lee and Yang suggested [10] that all neutrinos are left handed and all anti-neutrinos, right handed. This was proven to be correct a year later by Goldhaber measuring the neutrino helicity directly. Let us mention some consequences of the parity violation in weak interaction.

For neutrinos, the Dirac equation reads

$$i\gamma_\mu \partial^\mu \Psi - m_\nu \Psi = 0. \tag{1.41}$$

We will work in the chiral representation since it is easier to account the helicity of the neutrino, so the Dirac matrices takes the form

$$\gamma^0 = \begin{bmatrix} 0 & I \\ I & 0 \end{bmatrix}, \ \vec{\gamma} = \begin{bmatrix} 0 & -\vec{\sigma} \\ \vec{\sigma} & 0 \end{bmatrix}, \tag{1.42}$$

where $\vec{\sigma}$ is Pauli's spin operator. For the 4-component Dirac spinor in the chiral representation we will use

$$\Psi = \begin{pmatrix} \Psi_R \\ \Psi_L \end{pmatrix}, \tag{1.43}$$

where Ψ_R and χ are two component Weyl spinors. From Eq. (1.41) we get

$$i \begin{bmatrix} 0 & I \\ I & 0 \end{bmatrix} \begin{bmatrix} \frac{\partial \Psi_R}{\partial t} \\ \frac{\partial \Psi_L}{\partial t} \end{bmatrix} + i \begin{bmatrix} 0 & -\vec{\sigma} \\ \vec{\sigma} & 0 \end{bmatrix} \begin{bmatrix} \vec{\nabla} \Psi_R \\ \vec{\nabla} \Psi_L \end{bmatrix} - m_\nu \begin{bmatrix} \Psi_R \\ \Psi_L \end{bmatrix} = 0. \tag{1.44}$$

This gives two coupled equations

$$i\frac{\partial \Psi_L}{\partial t} - i\vec{\sigma}\cdot\vec{\nabla}\Psi_L = m_\nu \Psi_R, \tag{1.45}$$

$$i\frac{\partial \Psi_R}{\partial t} + i\vec{\sigma}\cdot\vec{\nabla}\Psi_R = m_\nu \Psi_L, \tag{1.46}$$

Since the neutrino mass was either zero or negligibly small, these equations decoupled leading to

$$p\Psi_L + \vec{\sigma}\cdot\vec{p}\Psi_L = 0, \tag{1.47}$$

$$p\Psi_R + -\vec{\sigma}\cdot\vec{p}\Psi_R = 0, \tag{1.48}$$

or

$$h\Psi_L = \frac{\vec{\sigma}\cdot\vec{p}}{p}\Psi_L = (-1)\Psi_L, \tag{1.49}$$

$$h\Psi_R = \frac{\vec{\sigma}\cdot\vec{p}}{p}\Psi_R = (1)\Psi_R. \tag{1.50}$$

These are the eigenvalue equations for helicity, so we get that the two component spinor Ψ_R is right-handed and that χ is left-handed. The observation that neutrinos were only left-handed leads to vanishing components of Ψ_R, resulting in a two component theory for the neutrino.

Finally, in Eq. (1.38) we talked about Fermi theory for the β decay as an analogy to QED. If we wanted to treat this process in a general form, we would need to start from the generalized Hamiltonian for the process

$$H_w = \sum_i \frac{G_i}{2}(\bar{u}_p O_i u_n)(\bar{u}_e O_i u_\nu) + h.c., \tag{1.51}$$

where O_i can be any of the bilinear forms. Note that the product for any case is a scalar, i.e. remain unchanged under a spatial inversion $\vec{r} \to -\vec{r}$. And considering that as we mentioned, weak interaction do not conserve Parity, this Hamiltonian is not a satisfactory description since it is not symmetric under spatial inversion. If we add a

pseudoscalar which have odd parity we can make this product with odd parity, so

$$(\bar{u}_p O_i u_n)(\bar{u}_e O_i u_\nu) + (\bar{u}_p O_i u_n)(\bar{u}_e O_i C_i \gamma_5 u_\nu) = [\bar{u}_p O_i u_n][\bar{u}_e O_i (1 + C_i \gamma 5) u_\nu], \quad (1.52)$$

where the first term is a scalar and the second one a pseudoscalar with C_i a constant. With this, the new parity violation Hamiltonian reads

$$H_w = \sum_i \frac{G_i}{2} [\bar{u}_p O_i u_n][\bar{u}_e O_i (1 + C_i \gamma 5) u_\nu] + h.c. \quad (1.53)$$

After some work and remembering that neutrinos are left-handed, it was specified that Fermi theory was only a particular case of a more general V-A theory for the weak interaction, so the final Hamiltonian is

$$H_w = \frac{G_f}{\sqrt{2}} [\bar{u}_p \gamma_\mu (1 - g_A \gamma_5) u_n][\bar{u}_e \gamma^\mu (1 - \gamma_5) u_\nu] + h.c. \quad (1.54)$$

Chapter 2

Theoretical framework

Now we will set the formalism of the different physics scenarios beyond the Standard Model considered in this thesis. All of them consider the existence of extra sterile neutrino states with different characteristics. If the neutrinos are light enough, they will take place into oscillations, if they are heavy then they won't participate but the unitary of the neutrino mixing matrix is violated. Finally, we talk about the neutrino magnetic properties from which a "dipole portal" may allow a transition from the active to the sterile states, induced by a magnetic coupling.

2.1 Neutrino oscillations

The first idea of neutrino oscillations was introduced by Bruno Pontecorvo on 1957 [12]. He proposed that leptons might have a phenomenon analogous to $K^0 \leftrightarrows \bar{K}^0$ oscillation, and mentioned in his paper the possibility of neutrino oscillations. Later, a special paper dedicated to neutrino oscillations was published by him on 1958 [13]. He suggested that neutrino-antineutrino oscillations could take place if the lepton number were violated. This phenomenon requires neutrinos to be massive, in contradiction with the then common belief that they were massless. At that time, only the electron neutrino was known, so he assumed that there must exist a weaker interaction which does not conserve the lepton number. By assuming maximum mixing, he concluded that neutrinos and anti-neutrinos are particle mixtures, this is, combinations of two neutral Majorana particles

$$|\bar{\nu}_R\rangle = \frac{1}{\sqrt{2}}(\nu_1 + \nu_2), \tag{2.1}$$

$$|\nu_R\rangle = \frac{1}{\sqrt{2}}(\nu_1 - \nu_2), \tag{2.2}$$

where $\bar{\nu}_R$ is the state of the right-handed anti-neutrino, ν_R is the state of the right-handed neutrino, which does not take part in weak interaction. As a result of the mixing, oscillations between $\nu_R \leftrightarrow \bar{\nu}_R$ become possible. Pontecorvo suggested that this oscillations may only be observable on astronomical scale due to the big oscillation length.

Later, around the time when the muon neutrino was discovered oi 1962, the idea of neutrino masses and mixing was discussed by Maki, Nakagawa, and Sakata [14]. They assumed that the fields of the neutrinos ν_e, ν_μ are connected with the fields of neutrinos with definite mass ν_1, ν_2 by an orthogonal transformation

$$\begin{aligned} \nu_e &= \cos\theta\nu_1 + \sin\theta\nu_2, \\ \nu_\mu &= -\sin\theta\nu_1 + \cos\theta\nu_2. \end{aligned} \tag{2.3}$$

In their paper, they didn't consider the phenomenon of neutrino oscillations, however, they mentioned the possibility of a transmutation of ν_μ into ν_e and the possible influence in the interpretation of the Brookhaven experiment, which was working at the time. On 1967, B. Pontecorvo published a second paper on neutrino oscillations [15], in which he considered the transition $\nu_e \leftrightarrow \nu_\mu$ and also oscillations between flavor and sterile neutrinos. He also considered the solar neutrino oscillations, so he predicted that the flux of the solar electron neutrino could be half the expected one, anticipating the solar neutrino problem. The existence of neutrino oscillations were confirmed between 1998 and 2002 with the discoveries of atmospheric and solar neutrino oscillations by the Super-Kamiokande [16] and the Sudbury Neutrino Observatory (SNO) [17], [18], and later confirmed by the KamLAND experiment [19].

Neutrino oscillations have been used to explain phenomena like the solar neutrino deficit, the anomaly in atmospheric neutrinos, and the excess of events in the LSND (Liquid Scintillation Neutrino Detector) experiment that reports evidence of the transition $\bar{\nu}_\mu \to \bar{\nu}_e$ among others [20]. However, some of these new phenomena are difficult

to explain considering only three neutrino flavors. For this reason, it has been proposed the existence of a fourth sterile neutrino that does not interact due to charged or neutral current. Moreover, the effect of two or three sterile neutrinos has also been analyzed [21].

2.1.1 Neutrino oscillation formalism

As mentioned earlier, for each lepton (e^-, μ^- and τ^-) there exists a neutral state called neutrino, which is associated to each of them separately. These states are called flavor eigenstates or weak interaction eigenstates.

Lets assume that neutrinos have masses. Thus, there is a spectrum of neutrino mass eigenstates $v_i = \nu_1, \nu_2, ...$ each with mass m_i. However, experimentally we can only distinguish between neutrinos by its flavor, depending if the neutrino interacts with a e,μ, or τ. The mixing may be described with the observation of each flavour of neutrinos as a superposition of mass eigenstates. Thus, we can consider a linear combination of three mass states, which are the physical neutrinos traveling freely. The relation between these states is

$$|\nu_\alpha\rangle = \sum_i U^*_{\alpha i} |\nu_i\rangle . \tag{2.4}$$

Where $U_{\alpha i}$ may be written in a matrix form that would look like

$$U = \begin{pmatrix} U_{e1} & U_{e2} & U_{e3} \\ U_{\mu 1} & U_{\mu 2} & U_{\mu 3} \\ U_{\tau 1} & U_{\tau 2} & U_{\tau 3} \end{pmatrix}, \tag{2.5}$$

where U is unitary, so

$$UU^+ = U^+U = I. \tag{2.6}$$

So we can express each mass eigenstate as a superposition of flavours

$$|\nu_i\rangle = \sum_\alpha U_{\alpha i} |\nu_\alpha\rangle . \tag{2.7}$$

If we assume that there are only 3 mass eigenstates, the Lagrangian can be expressed in mass eigenstates terms as

$$L = \bar{\nu} m \nu = \begin{pmatrix} \bar{\nu}_1 & \bar{\nu}_2 & \bar{\nu}_3 \end{pmatrix} \begin{pmatrix} m_1 & 0 & 0 \\ 0 & m_2 & 0 \\ 0 & 0 & m_3 \end{pmatrix} \begin{pmatrix} \nu_1 \\ \nu_2 \\ \nu_3 \end{pmatrix}, \tag{2.8}$$

but it can also be expressed in a flavour basis, as

$$L = \begin{pmatrix} \bar{\nu}_\alpha & \bar{\nu}_\mu & \bar{\nu}_\tau \end{pmatrix} \begin{pmatrix} M_{11} & M_{12} & M_{13} \\ M_{21} & M_{22} & M_{23} \\ M_{31} & M_{32} & M_{33} \end{pmatrix} \begin{pmatrix} \nu_\alpha \\ \nu_\mu \\ \nu_\tau \end{pmatrix}. \tag{2.9}$$

If there was no mixing, M would be diagonal.

Since neutrinos only participate in weak interactions and very weakly in gravity, it is difficult to detect them. But recalling Fig. 1.2 the fundamental weak charged current vertex shows that neutrinos can interact on the flavor base with its corresponding lepton, and this charged lepton can be easily detected. At the end of the travel of the neutrino through a distance L, the neutrino reacts with the detector making it possible to identify its flavor in some experiments. If the flavour of the neutrino has changed through its journey, we can identify this as due to neutrino flavor oscillation.

Since each ν_α is a superposition of ν_i's we have to individually add the contribution from each mass state in order to find the oscillation probability $P(\nu_\alpha \to \nu_\beta)$.

The total amplitude will depend on three factors:

- The amplitude for ν_i when $\bar{\nu}_\alpha$ is produced at the source.
- The amplitude for ν_i to propagate from source to detector.
- The amplitude for ν_i when $\bar{\nu}_\beta$ is detected at the detector

The total amplitude of flavor changing is given by:

$$Amp(\nu_\alpha \to \nu_\beta) = \sum_i U_{\alpha i} Prop(\nu_i) U^*_{\beta i}. \tag{2.10}$$

Now we will find the value of $Prop(\nu_i)$. If we consider the rest frame of the neutrino,

its state vector as a function of time τ, follows the Schrodinger equation:

$$i\frac{\partial}{\partial\tau}\left|\nu_i(\tau)\right\rangle = m_i\left|\nu_i(\tau)\right\rangle, \tag{2.11}$$

whose solution is given by

$$\left|\nu_i(\tau)\right\rangle = e^{-m_i\tau}\left|\nu_i(0)\right\rangle, \tag{2.12}$$

so the amplitude of ν_i travelling for time τ_0 is given by

$$\langle\nu_i(0)|\nu_i(\tau_0)\rangle = e^{-m_i\tau_0}. \tag{2.13}$$

So, if τ_i is the proper time of the neutrino to travel from the source to the detector,

$$Prop_{rest}(\nu_i) = \langle\nu_i(0)|\nu_i(\tau_i)\rangle = e^{-m_i\tau_i}, \tag{2.14}$$

we need it in the Lab frame, so we need a Lorentz transformation to find the corresponding expression in the lab frame. By Lorentz invariance $x_\mu p^\mu$,

$$m_i\tau_i = E_i t - p_i L. \tag{2.15}$$

Using the relation and considering that neutrinos are extremely light $m_i^2 << E^2$,

$$p_i = \sqrt{E^2 - m_i^2} \approx E - \frac{m_i^2}{2E}, \tag{2.16}$$

so we have

$$m_i\tau_i \approx Et - EL + \frac{m_i^2}{2E}L. = E(t-L) + \frac{m_i^2}{2E}L \tag{2.17}$$

Where we have used the same energy for different mass eigenstates.This is possible because only phases with same energy are detected. The term $E(t-L)$ is common to every interfering mass eigenstates. Thus, considering only the i-dependent part we

have

$$Prop(\nu_i) = e^{-\frac{m_i^2}{2E}L}. \tag{2.18}$$

So we have

$$Amp(\nu_\alpha \to \nu_\beta) = \sum_i U_{\alpha i} e^{-\frac{m_i^2}{2E}L} U^*_{\beta i}. \tag{2.19}$$

Finally,the oscillation probability $P(\nu_\alpha \to \nu_\beta)$ is given by

$$P(\nu_\alpha \to \nu_\beta) = |Amp(\nu_\alpha \to \nu_\beta)|^2, \tag{2.20}$$

$$\left(\sum_i U_{\alpha i} e^{-\frac{m_i^2}{2E}L} U^*_{\beta i}\right)^* \left(U_{betai} \sum_j U_{\alpha j} e^{-\frac{m_j^2}{2E}L} U^*_{\beta j}\right), \tag{2.21}$$

$$\sum_i \sum_j U^*_{\alpha i} U_{\beta i} U_{\alpha j} U^*_{\beta j} e^{i\frac{L}{2E}(m_j^2 - m_i^2)}, \tag{2.22}$$

$$= \sum_i U^*_{\alpha i} U_{\beta i} U_{\alpha i} U^*_{\beta i} + \sum_{i \neq j} U^*_{\alpha i} U_{\beta i} U_{\alpha j} U_{\beta j} e^{i\frac{L}{2E}\Delta m^2_{ji}}, \tag{2.23}$$

where

$$\Delta m^2_{ji} = (m_j^2 - m_i^2). \tag{2.24}$$

In order to proceed,we need to consider the following relation for the exponential function

$$e^{iA} = \cos A + i \sin A \to 1 - 2\sin^2 \frac{A}{2} + i \sin A. \tag{2.25}$$

Now, by expanding the exponential function in Eq. (2.23) we get

$$P(\nu_\alpha \to \nu_\beta) = \sum_i U^*_{\alpha i} U_{\beta i} U_{\alpha i} U^*_{\beta i} + \sum_{i \neq j} U^*_{\alpha i} U_{\beta i} U_{\alpha j} U^*_{\beta j} - 2 \sum_{i \neq j} U^*_{\alpha i} U_{\beta i} U_{\alpha j} U^*_{\beta j} sin^2(\Delta m^2_{ji} \frac{L}{4E}) + i \sum_{i \neq j} U^*_{\alpha i} U_{\beta i} U_{\alpha j} U^*_{\beta j} sin(\Delta m^2_{ji} \frac{L}{2E}).$$

Now we will work with every single term, first we have

$$P_3 = \sum_{i \neq j} U^*_{\alpha i} U_{\beta i} U_{\alpha j} U^*_{\beta j} sin^2(\Delta m^2_{ji} \frac{L}{4E}) \tag{2.26}$$

$$= \sum_{i > j} U^*_{\alpha i} U_{\beta i} U_{\alpha j} U^*_{\beta j} sin^2(\Delta m^2_{ij} \frac{L}{4E}) + \sum_{i < j} U^*_{\alpha i} U_{\beta i} U_{\alpha j} U^*_{\beta j} sin^2(\Delta m^2_{ji} \frac{L}{4E}) \tag{2.27}$$

$$= \sum_{i > j} U^*_{\alpha i} U_{\beta i} U_{\alpha j} U^*_{\beta j} sin^2(\Delta m^2_{ij} \frac{L}{4E}) + \sum_{i > j} U^*_{\alpha j} U_{\beta j} U_{\alpha i} U^*_{\beta i} sin^2(\Delta m^2_{ij} \frac{L}{4E}) \tag{2.28}$$

$$= \sum_{i > j} sin^2(\Delta m^2_{ij} \frac{L}{4E}) (U^*_{\alpha i} U_{\beta i} U_{\alpha j} U^*_{\beta j} + U^*_{\alpha j} U_{\beta j} U_{\alpha i} U^*_{\beta i}) \tag{2.29}$$

$$= \sum_{i > j} sin^2(\Delta m^2_{ij} \frac{L}{4E}) (U^*_{\alpha i} U_{\beta i} U_{\alpha j} U^*_{\beta j} + U_{\alpha i} U^*_{\beta i} U^*_{\alpha j} U_{\beta j}) \tag{2.30}$$

$$= \sum_{i > j} sin^2(\Delta m^2_{ij} \frac{L}{4E}) (U^*_{\alpha i} U_{\beta i} U_{\alpha j} U^*_{\beta j} + (U^*_{\alpha i} U_{\beta i} U_{\alpha j} U^*_{\beta j})^*) \tag{2.31}$$

$$= 2 \sum_{i > j} Re(U^*_{\alpha i} U_{\beta i} U_{\alpha j} U^*_{\beta j}) sin^2(\Delta m^2_{ij} \frac{L}{4E}). \tag{2.32}$$

Now for the last term we have

$$P_4 = \sum_{i\neq j} U^*_{\alpha i} U_{\beta i} U_{\alpha j} U^*_{\beta j} sin(\Delta m^2_{ji} \frac{L}{2E}) \tag{2.33}$$

$$= -\sum_{i>j} U^*_{\alpha i} U_{\beta i} U_{\alpha j} U^*_{\beta j} sin(\Delta m^2_{ji} \frac{L}{2E}) + \sum_{i<j} U^*_{\alpha i} U_{\beta i} U_{\alpha j} U^*_{\beta j} sin(\Delta m^2_{ji} \frac{L}{2E}) \tag{2.34}$$

$$= -\sum_{i>j} U^*_{\alpha i} U_{\beta i} U_{\alpha j} U^*_{\beta j} sin(\Delta m^2_{ji} \frac{L}{2E}) + \sum_{i>j} U^*_{\alpha j} U_{\beta j} U_{\alpha i} U^*_{\beta i} sin(\Delta m^2_{ij} \frac{L}{2E}) \tag{2.35}$$

$$= \sum_{i>j} sin(\Delta m^2_{ij} \frac{L}{2E})(U^*_{\alpha j} U_{\beta j} U_{\alpha i} U^*_{\beta i} - U^*_{\alpha i} U_{\beta i} U_{\alpha j} U^*_{\beta j}) \tag{2.36}$$

$$= \sum_{i>j} sin(\Delta m^2_{ij} \frac{L}{2E})((U_{\alpha j} U^*_{\beta j} U^*_{\alpha i} U_{\beta i})^* - U^*_{\alpha i} U_{\beta i} U_{\alpha j} U^*_{\beta j}) \tag{2.37}$$

$$= \sum_{i>j} sin(\Delta m^2_{ij} \frac{L}{2E})(-2iIm(U^*_{\alpha i} U_{\beta i} U_{\alpha j} U^*_{\beta j})) \tag{2.38}$$

$$= -2i \sum_{i>j} Im(U^*_{\alpha i} U_{\beta i} U_{\alpha j} U^*_{\beta j}) sin(\Delta m^2_{ij} \frac{L}{2E}). \tag{2.39}$$

Now for the first two terms we have

$$P_1 + P_2 = \sum_i U^*_{\alpha i} U_{\beta i} U_{\alpha i} U^*_{\beta i} + \sum_{i\neq j} U^*_{\alpha i} U_{\beta i} U_{\alpha j} U^*_{\beta j} \tag{2.40}$$

$$= \sum_i \sum_j U^*_{\alpha i} U_{\beta i} U_{\alpha j} U^*_{\beta j} \tag{2.41}$$

$$= \sum_i (U^*_{\alpha i} U_{\beta i}) \sum_j (U_{\alpha j} U^*_{\beta j}) \tag{2.42}$$

$$= |\sum_i U_{\alpha i} U^*_{\beta i}|^2. \tag{2.43}$$

In order to evaluate this term, we will use the unitary property of U. We have

$$U = \begin{pmatrix} U_{e1} & U_{e2} & U_{e3} \\ U_{\mu 1} & U_{\mu 2} & U_{\mu 3} \\ U_{\tau 1} & U_{\tau 2} & U_{\tau 3} \end{pmatrix}, \; U^+ = \begin{pmatrix} U^*_{e1} & U^*_{\mu 1} & U^*_{\tau 1} \\ U^*_{e2} & U^*_{\mu 2} & U^*_{\tau 2} \\ U^*_{e3} & U^*_{\mu 3} & U^*_{\tau 3} \end{pmatrix}, \tag{2.44}$$

$$UU^{+} = \begin{pmatrix} \sum_i U_{ei}U_{ei}^* & \sum_i U_{ei}U_{\mu i}^* & \sum_i U_{ei}U_{\tau i}^* \\ \sum_i U_{\mu i}U_{ei}^* & \sum_i U_{\mu i}U_{\mu i}^* & \sum_i U_{\mu i}U_{\tau i}^* \\ \sum_i U_{\tau i}U_{ei}^* & \sum_i U_{\tau i}U_{\mu i}^* & \sum_i U_{\tau i}U_{\tau i}^* \end{pmatrix} = \begin{pmatrix} 1 & 0 & 0 \\ 0 & 1 & 0 \\ 0 & 0 & 1 \end{pmatrix}. \tag{2.45}$$

In other words, we can write this as

$$\begin{aligned} \sum_i U_{\alpha i}U_{\beta i}^* = 1 \rightarrow \alpha = \beta, \\ 0 = \delta_{\alpha\beta} \rightarrow \alpha \neq \beta. \end{aligned} \tag{2.46}$$

Where δ is the Kronecker delta function.

So finally we get

$$P_1 + P_2 = \delta_{\alpha\beta}. \tag{2.47}$$

Finally we have the expression for the oscillation probability

$$\begin{aligned} P(\nu_\alpha \rightarrow \nu_\beta) &= \delta_{\alpha\beta} - 2 \cdot 2 \sum_{i>j} Re(U_{\alpha i}^* U_{\beta i} U_{\alpha j} U_{\beta j}^*) sin^2(\Delta m_{ij}^2 \frac{L}{4E}) \\ &\quad + i \left(-2i \sum_{i>j} Im(U_{\alpha i}^* U_{\beta i} U_{\alpha j} U_{\beta j}^*) sin(\Delta m_{ij}^2 \frac{L}{2E}) \right) \\ &= \delta_{\alpha\beta} - 4 \sum_{i>j} Re(U_{\alpha i}^* U_{\beta i} U_{\alpha j} U_{\beta j}^*) sin^2(\Delta m_{ij}^2 \frac{L}{4E}) \\ &\quad + 2 \sum_{i>j} Im(U_{\alpha i}^* U_{\beta i} U_{\alpha j} U_{\beta j}^*) sin(\Delta m_{ij}^2 \frac{L}{2E}). \end{aligned}$$

For anti-neutrinos we assume CPT invariance so under this assumption the process $\bar{\nu}_\alpha \rightarrow \bar{\nu}_\beta$ is the CPT-mirror image of $\nu_\beta \rightarrow \nu\alpha$,

$$P(\bar{\nu_\alpha} \rightarrow \bar{\nu_\beta}) = P(\nu_\beta \rightarrow \nu_\alpha). \tag{2.48}$$

The results of this is just a change in the last term of the oscillation probability, so:

$$
\begin{aligned}
P(\bar{\nu_\alpha} \to \bar{\nu_\beta}) &= \delta_{\alpha\beta} - 2 \cdot 2 \sum_{i>j} Re(U^*_{\alpha i} U_{\beta i} U_{\alpha j} U^*_{\beta j}) sin^2(\Delta m^2_{ij} \frac{L}{4E}) \\
&+ i \left(-2i \sum_{i>j} Im(U^*_{\alpha i} U_{\beta i} U_{\alpha j} U^*_{\beta j}) sin(\Delta m^2_{ij} \frac{L}{2E}) \right) \\
&= \delta_{\alpha\beta} - 4 \sum_{i>j} Re(U^*_{\alpha i} U_{\beta i} U_{\alpha j} U^*_{\beta j}) sin^2(\Delta m^2_{ij} \frac{L}{4E}) - \\
&2 \sum_{i>j} Im(U^*_{\alpha i} U_{\beta i} U_{\alpha j} U^*_{\beta j}) sin(\Delta m^2_{ij} \frac{L}{2E}).
\end{aligned}
$$

If neutrinos were massless, then all the mass squared differences would be zero, so at the end the oscillation probability would become zero too. It is useful to note that neutrino oscillations do not arise from interaction with matter because we considered vacuum since the beginning. Also, if there was no leptonic mixing, all off-diagonal terms in $U_{\alpha i}$ would be zeros, so again the oscillation probability would become zero.

It is useful to change from natural units to SI, this allow us to use more easily the different experimental setups considered in this thesis. By dimensional analysis, it is possible to find that the correct expression on S.I. is

$$
\begin{aligned}
\Delta m^2_{ij} \frac{L}{4E}|_{Natural} &= \Delta m^2_{kg} \frac{L_{meter}}{4R_{Joule}} \frac{c^3}{\hbar} && (2.49) \\
&= 1.27 \Delta m^2_{ij}(eV^2) \frac{L(km)}{E(GeV)}. && (2.50)
\end{aligned}
$$

Note that in the final equation we only have square mass differences and it doesn't contain the mass of each mass eigenstate explicitly, we cannot find out the mass of each eigenstates, so we have two possible orderings for the mass of the eigenstates, as shown in Fig. 2.1. The left one is called normal ordering (NO) and the right one inverted ordering (IO). The absolute mass scale is not known, but future neutrino experiments aim to solve this problem.

Lets consider the case in which only two mass eigenstates ν_1 and ν_2 were significant, and correspondingly the two flavour states are ν_e and ν_μ. The matrix representing this

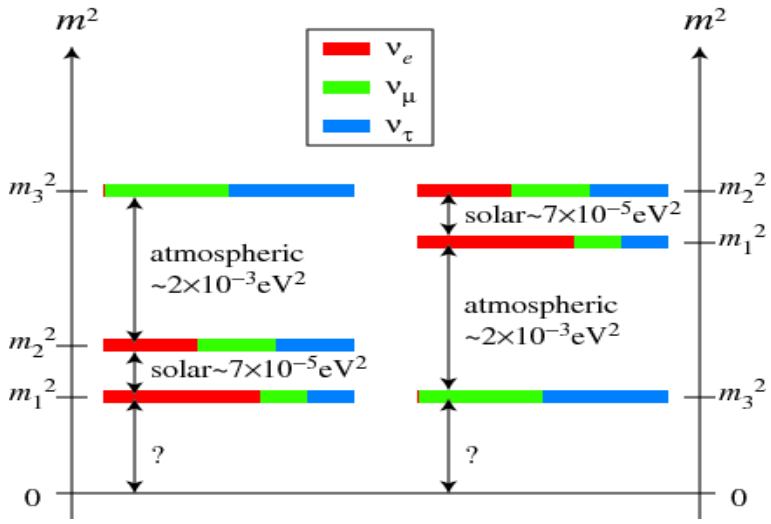

Figure 2.1: Possible orderings for the mass eigenstates of neutrinos. Left case(NO) considers ν_3 in the top of the scale and right case(IO) takes ν_3 to the bottom [**?**].

mixing is of the form

$$U = \begin{pmatrix} U_{e1} & U_{e2} \\ U_{\mu 1} & U_{\mu 2} \end{pmatrix} = \begin{pmatrix} cos\theta & sin\theta \\ -sin\theta & cos\theta \end{pmatrix} \tag{2.51}$$

and

$$U^+ = \begin{pmatrix} U_{e1}^* & U_{\mu 1}^* \\ U_{e2}^* & U_{\mu 2}^* \end{pmatrix} = \begin{pmatrix} cos\theta & -sin\theta \\ sin\theta & cos\theta \end{pmatrix}. \tag{2.52}$$

Using this we can find the relation that simplifies

$$4U_{\alpha 2}^* U_{\beta 2} U_{\alpha 1} U_{\beta 1}^* = -4 \sin\theta \cos\theta \cos\theta \sin\theta. = -\sin^2 2\theta \tag{2.53}$$

Thus for $\alpha \neq \beta$ we find

$$P(\nu_\alpha \to \nu_\beta) = \delta_{\alpha\beta} - (-\sin^2 2\theta) \sin^2(\Delta m_{ij}^2 \frac{L}{4E} + 2(0) \sin\left(\Delta m_{ij}^2 \frac{L}{2E}\right) \tag{2.54}$$

$$= sin^2 2\theta \sin^2\left(\Delta m_{ij}^2 \frac{L}{4E}\right). \tag{2.55}$$

It is useful to note that the same relation applies for anti-neutrinos since the last term vanishes for a real U matrix.

We don't know the total number of mass eigenstates for sure. However, the fact that there are at least three, can be easily understood from studying solar and atmospheric neutrinos. We attribute solar neutrinos to the splitting to ν_1 and ν_2

Assuming mixing among the three known neutrinos (ν_e, ν_μ, ν_τ), as a superposition of three massive states, the mixing matrix can be parametrized as [22]

$$U = \begin{bmatrix} c_{12}c_{13} & s_{12}c_{13} & s_{13}e^{-i\delta_{CP}} \\ -s_{12}c_{23} - s_{12}s_{13}s_{23}e^{i\delta_{CP}} & c_{12}c_{23} - c_{12}s_{13}s_{23}e^{i\delta_{CP}} & c_{13}s_{23} \\ s_{12}s_{23} - c_{12}s_{13}s_{23}e^{i\delta_{CP}} & -c_{12}s_{23} - s_{12}s_{13}c_{23}e^{i\delta_{CP}} & c_{13}c_{23} \end{bmatrix}, \tag{2.56}$$

where $c_{ij} = cos\theta_{ij}$ and $s_{ij} = \sin\theta_{ij}$.

In order to understand these phenomena, let us suppose that a neutrino is produced in the time $t = 0$ with a well-defined momentum p, from Eq. (2.4), we have that, for a time t, the wave function is given by

$$\psi(x,t) = \sum_m U_{lm}\nu_m e^{ip_\nu x}e^{-iE_m t}. \tag{2.57}$$

If we assume that $M_m << p_v$ we have that $E_m \approx p_\nu + \frac{M_m^2}{2p_\nu}$, and the neutrino will be traveling at a speed close to the speed of light, and so for a time t we will have that $x = t$ (taking $c = 1$). If we write the mass eigenstates as a linear combination of the flavor states inverting the matrix U we get

$$\psi(x,x) = \sum_{l'}\left(\sum_m U_{lm}e^{-i(\frac{M_m^2}{2p_\nu})x}U^*_{l'm}\right)\nu_{l'}. \tag{2.58}$$

So we see that the wave function is a superposition of all the neutrino flavors. The probability amplitude that the neutrino changes from a flavor l to l' traveling a distance x is given by the coefficient of $\nu_{l'}$. If we assume that CP is conserved, we can take U as a real matrix and the probability that a neutrino changes its flavor to l' given a distance

x will be given by

$$P(l \to l', x) = \sum_m U_{lm}^2 U_{l'm}^2 + \sum_{m' \neq m} U_{lm} U_{lm'} U_{l'm'} U_{l'm} cos\left(2\pi \frac{x}{L_{mm'}}\right) \tag{2.59}$$

where we can see that the function has an oscillatory pattern through the distance of the form

$$\cos\left(\frac{2\pi x}{L_{mm'}}\right), \tag{2.60}$$

where the term $L_{mm'}$ is called the oscillation length between ν_m and $\nu_{m'}$, and is given by

$$L_{mm'} = \frac{4\pi p_\nu}{\Delta m_{mm'}^2}. \tag{2.61}$$

Note that if $x << L_{mm'}$ the neutrino maintains in its original flavor, and if $x >> L_{mm'}$ the oscillatory pattern vanish. The distance X in which the oscillatory pattern vanishes is given by

$$X \approx \frac{p_\nu}{\delta p_\nu} L_{mm'}, \tag{2.62}$$

where δp_ν is the momentum spread of the beam. Therefore, if the distance x is greater than X, the pattern vanishes. However, it is still possible to find a neutrino that changed flavor, but the probability is no longer a function of the distance traveled. It is important to say that the oscillatory pattern can be seen if the distance is of the order of the oscillation length. Neutrino oscillations can be detected in two ways: With appearance experiments in which $\nu_l \to \nu_{l'}$ is sought, or disappearance, in which a reduction in the neutrino flux of a certain flavor is observed.

For the particular case in which there are only two neutrino flavors and two mass eigenstates participating appreciably in the mixing, we have the relation

$$\nu_\alpha = \nu_1 \cos\theta + \nu_2 \sin\theta, \tag{2.63}$$

$$\nu_\beta = -\nu_1 \sin\theta + \nu_2 \cos\theta. \tag{2.64}$$

In this way, the oscillation length will be given by

$$L = \frac{4\pi p_\nu}{\Delta m^2}; \tag{2.65}$$

therefore, the probability for a transition from one flavor to another is

$$P(\nu_\alpha \to v_\beta, x) = \sin^2(2\theta)\sin^2(\pi\frac{x}{L}), \tag{2.66}$$

and the probability that a neutrino remains in the same flavor eigenstate at a distance x is given by

$$P(\nu_\alpha \to \nu_\beta, x) = 1 - \sin^2 2\theta \sin^2 \delta_{12}. \tag{2.67}$$

With $\delta_{12} = 1.27\frac{\frac{\Delta m^2}{1eV2}\cdot\frac{x}{1km}}{\frac{p_\nu}{1GeV}}$.

Neutrino oscillations were confirmed for the first time in 1998, in the Super-Kamiokande experiment [23], where the neutrinos produced by the collisions of cosmic rays in the atmosphere were analyzed. More evidence of the existence of the neutrino oscillations have been found in appearance and disappearance experiments ([20], [24]). Since the Standard Model assumes that neutrinos do not have mass, neutrino oscillations are physics beyond Standard Model.

2.2 Sterile neutrinos

As mentioned in the previous chapters, there are three generations of leptons in the Standard Model that are grouped in $SU(2)_L$ doublets. Where L indicates that these quantum fields are eigenstates of the left-handed helicity operator $P_L = \frac{1}{2}(1-\gamma_5)$. They have a definite mass and obey the Dirac equation, and the flavor eigenstates ν_α are linear combinations of ν_i fields

$$\begin{pmatrix}\nu_e\\ \nu_\mu\\ \nu_\tau\end{pmatrix} = V\begin{pmatrix}\nu_1\\ \nu_2\\ \nu_3\end{pmatrix}, \tag{2.68}$$

where V is the 3x3 unitary matrix.

The interactions of leptons with the W boson mix all mass eigenstates as can be seen from the Lagrangian

$$L = -\frac{g}{\sqrt{2}} \sum_{\alpha=e,\mu,\tau} \sum_{i=1,2,3} V_{\alpha i} \bar{\nu}_i \gamma^\mu P_L l_\alpha W_\mu + h.c., \tag{2.69}$$

where $V_{\alpha i}$ is the matrix element of V. $\bar{\nu}_i$, l_α and W_μ are quantum fields of the neutrino with mass m_i, lepton of flavor α and W-boson, respectively and γ^μ is a Dirac 4x4 matrix.

The smallness of the masses an their mixture in the interactions with the W-boson and charged leptons give rise to the previously discussed effect of neutrino oscillations. This effect was useful to explain the Solar and atmospheric neutrino problems. But, there are some anomalies that cannot be described by a three neutrino model with the given values of Δm^2 as can be seen in Fig. 2.2, in which the region for atmospheric and solar neutrinos is well explained in a 3-neutrino active oscillation scenario, but for reactor antineutrinos the existence of a fourth sterile neutrino may explain the anomaly.

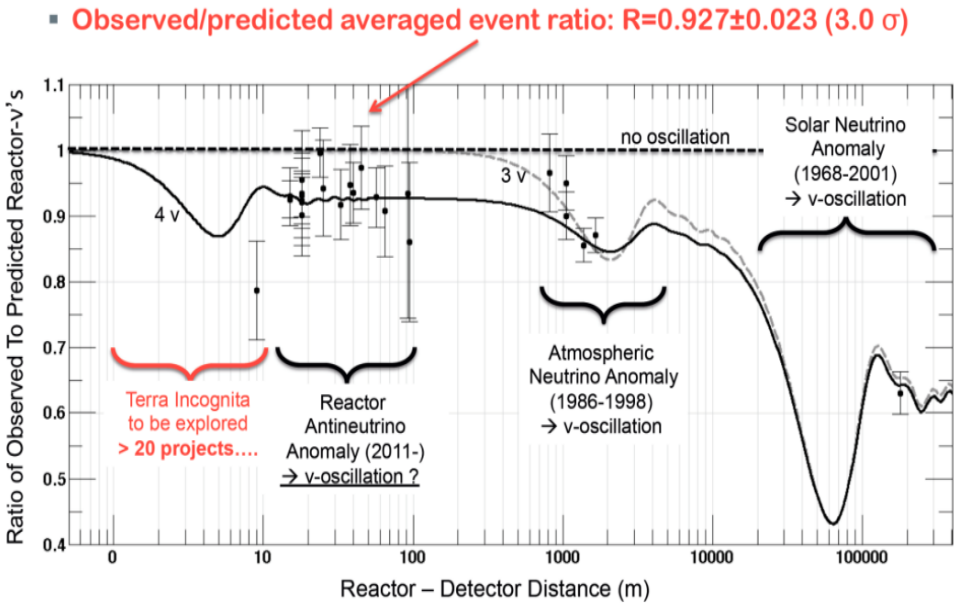

Figure 2.2: Observed/predicted ratio for different baselines [25].

2.2.1 Experimental hints for eV-mass sterile neutrinos

There are different experiments that find some anomalies when measuring neutrino fluxes. These anomalies may be explained by considering neutrino oscillations from

active to sterile states, if so, the Δm^2 needed is of the order of $1eV^2$. In this thesis, we will work with this scenario and find the possible constraints on these parameters.

Reactor antineutrino anomaly (RAA)

These anomalies refer to a deficit observed in reactor experiments. Reactor neutrino experiments were important for the understanding and determination of neutrino oscillation parameters in the 3-neutrino model. KamLAND experiment provides the most precise determination of the "solar" parameters Δm^2_{21} and improved our knowledge of θ_{12}. Double Chooz [26], Daya Bay [27] and Reno [28] experiments determined the smallest of the three known neutrino mixing angles, θ_{13} and confirmed to be non-zero. These experiments are also sensitive to the effective mass-squared difference $|\Delta m^2_{31}|$ with a precision comparable to that of accelerator based experiments.

The RAA problem arose in experiments that measured the θ_{13} parameter after the neutrino flux at nuclear reactors were re-evaluated. With this calculations, an increase of the fluxes prediction of few percent as compared to the Schreckenbach et al. prediction was revealed. Earlier predictions were in good agreement with the experimental data, but in updated predictions, an electron antineutrino rate deficit of more than 6% is observed for neutrino experiments between 6-100 meters from reactor.Fig. 2.3 shows the ratios between experimental and expected rates. This deficit is known as the RAA and the significance is about 2.8σ.

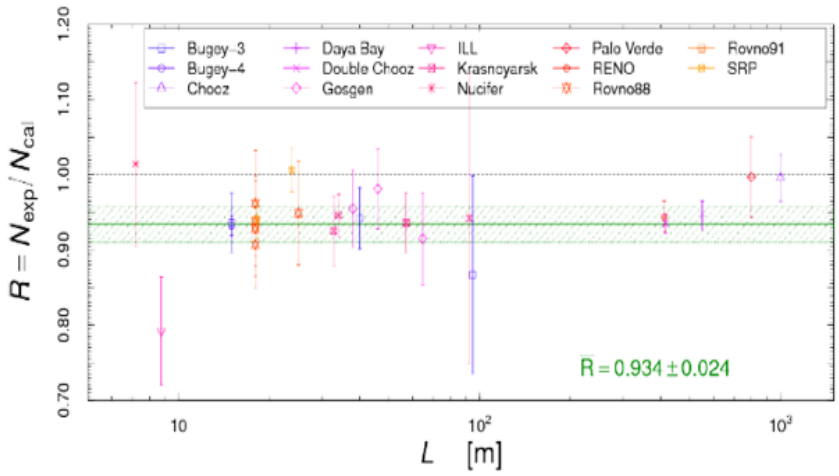

Figure 2.3: Ratio of reactor data and predicted flux as a function of reactor detector distance L [29].

Despite the RRA triggered the search for sterile neutrino oscillations as a possible scenario, other alternative explanations based on nuclear physics were also considered. In

the case that the disappearance of $\bar{\nu}_e$ due to short-baseline oscillation provide the explanation of the RAA, this suppression should depend only on the neutrino energy and not on the emitting fission isotope. Daya Bay tested this assumption as well as RENO experiment. These experiments observed a fuel-dependent variation of the inverse beta decay with respect to the predictions. This disfavors the oscillation hypothesis as sole source of the RAA as well as different modelling of fission isotopes [30]. However, a combined analysis with global rate data shows a preference for oscillations with respect to individual isotope-dependent suppression [31]. It is also possible to have hybrid models.

Double Chooz, Daya Bay, and RENO observed a distortion in the neutrino spectrum known as the reactor "shape anomaly" that consists of an excess in the measured reactor neutrino spectrum compared to the predicted around 5 MeV. A similar pattern was observed by NEOS data. But the spectra shape reported by Bugey 3 seems inconsistent with the previous experiments. This anomaly is more likely attributed to nuclear and reactor physics, so sterile neutrinos may not explain it.

Gallium Anomaly

Another problem is observed in the calibration of radio chemical experiments using radioactive sources in this case, a deficit in the detection of neutrinos is observed with respect to the prediction. The neutrino experiments GALLEX [32] and SAGE [33], which study solar neutrinos, tested their performance using neutrinos from ^{51}Cr and ^{37}Ar sources. Both GALLEX and SAGE used a ^{51}Cr source for calibration, if the calibrations are averaged and compared to the predicted neutrino signal, a deficit of 15% is observed with a 3σ significance, this comparison is shown in Fig. 2.4. This is known as the Gallium anomaly.

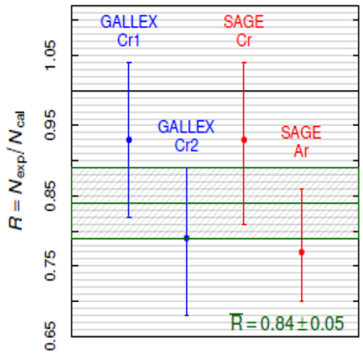

Figure 2.4: Measured to predicted ratio of neutrino-induced signal rate in the gallium experiments GALLEX and SAGE [29].

LSND anomaly

The first anomalies that arose the idea of sterile neutrinos is the one of the Liquid Scintillator Neutrino Detector (LSND) experiment, in which the result can be interpreted as an appearance of $\bar{\nu}_e$ in a pure $\bar{\nu}_\mu$ beam [34]. In this experiment, protons of 800 MeV were aimed at a target to generate low-energy pions which then are stopped by a material before decaying. This produces ν_e, ν_μ and $\bar{\nu}_\mu$ but no $\bar{\nu}_e$. The decay of π^- is suppressed by capture on the target atoms.

LSND observed an unexpected excess of $\bar{\nu}_e$-like events that can be interpreted as $\bar{\nu}_\mu \rightarrow \bar{\nu}_e$ appearance oscillations. The problem is that it needs a high Δm^2 incompatible with the present three active flavor oscillation picture. It is useful to mention that KARMEN experiment did not observed such excess, KARMEN excludes great part of the allowed parameter space when interpreted as an active flavor oscillation, but still if both experimental results are considered, the range of allowed values is still considerable.

MiniBooNE anomaly

The Mini Booster Neutrino Experiment (MiniBooNE) was considered initially as a test for the results obtained by the LSND experiment. The neutrino sources as well as the experimental conditions were changed so that it was not affected by the same uncertainties, but the L/E ratio was the same since it determines the sensitivity to the oscillation frequency and to Δm^2

For this experiment, protons of energy 8 GeV from the Fermilab Booster collision on a fixed beryllium target, producing π's and K's. Then, these mesons are focused by long magnetic collimators and decay-in-flight. The polarity can be selected by the magnetic field of the collimator, so that neutrinos and antineutrinos can be studied. This results on a spectrum with maximum energy of 1250 MeV. In both modes neutrinos and antineutrino, it was discovered an excess of electron-like events in the low-energy region. This is compatible with the l/E ratio of the LSND result. Later in 2018, the significance of the anomaly was corroborated to 4.7σ.

Interpretation of the anomalies

If the previous anomalies are interpreted as due to neutrino oscillations from active to sterile neutrino states, the measured deviations allow us to determine the preferred regions of the oscillation parameters. Fig. 2.5 shows the best regions obtained for the different experiments previously mentioned.

The first two panels shows the allowed parameter space of the reactor and gallium

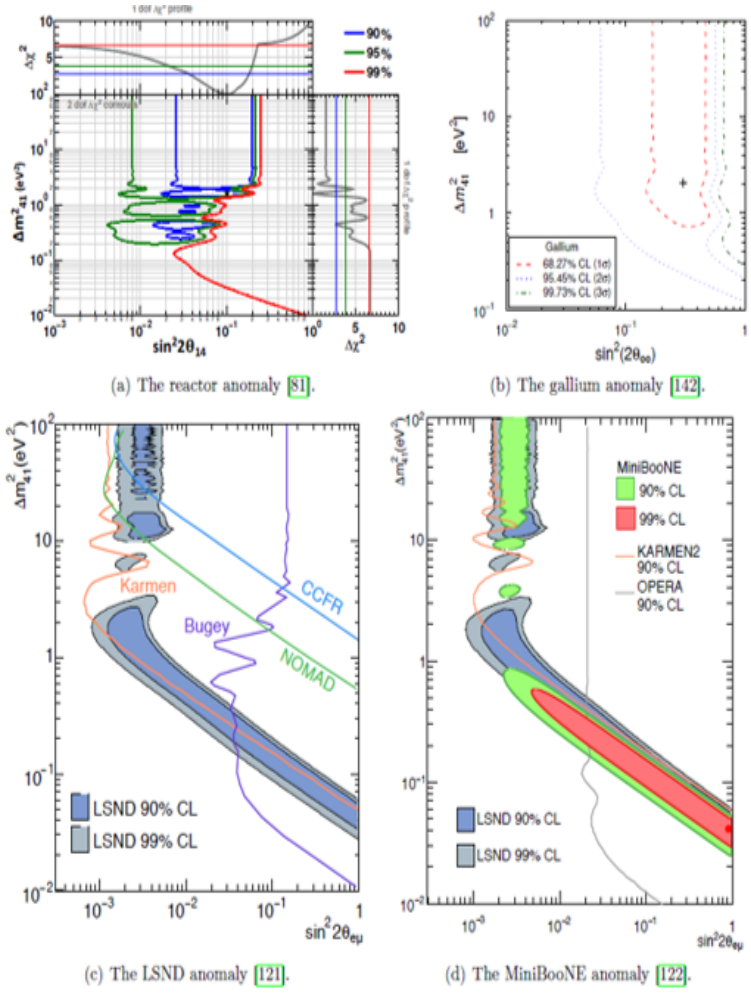

(a) The reactor anomaly [81]. (b) The gallium anomaly [142].

(c) The LSND anomaly [121]. (d) The MiniBooNE anomaly [122].

Figure 2.5: Regions allowed for the different anomalies [29].

anomalies, respectively. The interpretation as sterile neutrino oscillations relies on electron (anti) neutrino disappearance. They are sensitive to the mixing amplitude $\sin^2(2\theta_{14})$, corresponding to the mixing matrix element U_{e4}, as well as the corresponding mass square splitting Δm^2_{41}.

The lower panels shows the preferred region for the LSND and MiniBooNE experiments where they looked for $\bar{\nu_\mu} \rightarrow \bar{\nu_e}$ appearance searches. It can be seen that there is a good agreement between the results in the panel (d). For this case, the effective mixing angle corresponds to the product of mixing matrix elements $|U_{e4}|^2|U^2_{\mu 4}|$, also, the observed Δm^2can be almost directly related to the ν_e disappearance anomalies. All four are very well described under the (3+1) oscillation framework including the additional sterile state. Comparing this with the mass eigenstates associated to the active flavors, the preferred region for Δm^2_{41} is large as of order of $1eV^2$.

2.2.2 Vacuum oscillations in the presence of sterile neutrinos

Suppose that in addition to the three flavor eigenstates, there exist one extra single neutrino state. Then as an extension we will have

$$\begin{pmatrix} \nu_e(x) \\ \nu_\mu(x) \\ \nu_\tau(x) \\ \nu_s(x) \end{pmatrix}_L = U \begin{pmatrix} \nu_1(x) \\ \nu_2(x) \\ \nu_3(x) \\ \nu_4(x) \end{pmatrix}_L = \begin{pmatrix} U_{e1} & U_{e2} & U_{e3} & U_{e4} \\ U_{\mu 1} & U_{\mu 2} & U_{\mu 3} & U_{\mu 4} \\ U_{\tau 1} & U_{\tau 2} & U_{\tau 3} & U_{\tau 4} \\ U_{s1} & U_{s2} & U_{s3} & U_{s4} \end{pmatrix} \begin{pmatrix} \nu_1(x) \\ \nu_2(x) \\ \nu_3(x) \\ \nu_4(x) \end{pmatrix}_L . \tag{2.70}$$

The oscillation formula is the same as the one for oscillation between active states, given in Eq.(2.49). For this case, the matrix can be parametrized by 6 mixing angles, 3 "Dirac phases" and in the case of Majorana neutrinos, 3 additional "Majorana phases". The additional mixing angles are denoted by θ_{14}, θ_{24} and θ_{34}. Also, it is possible to parametrize the active-sterile mixing by the matrix entries $U_{e4}, U_{\mu 4}$ and $U_{\tau 4}$. We can write the 4x4 matrix as $U = U_{34}U_{24}U_{14}U_{23}U_{13}U_{12}P$, where U_{ij} is a unitary rotation in the (i,j) plane and P a diagonal matrix containing the Majorana phases, for the Dirac case P=1, from which we have

$$U_{e4} = s_{14}, \tag{2.71}$$

$$U_{\mu 4} = c_{14}s_{24}, \tag{2.72}$$

$$U_{\tau 4} = c_{14}c_{24}s_{34}. \tag{2.73}$$

If we focus on the case in which the forth neutrino mass $m_4 >> m_{1,2,3}$ is well separated from the other mass eigenstates, we get

$$\Delta m^2_{SBL} \equiv \Delta m^2_{41} \simeq \Delta m^2_{42} \simeq \Delta m^2_{43} >> |\Delta m^2_{31}|, |\Delta m^2_{32}|, \Delta m^2_{21}. \tag{2.74}$$

where Δm^2_{SBL} represents the value reported by short-baseline experiments which is around $1eV^2$. The spectrum of the case (3+1) in which $m_4 \simeq \sqrt{\Delta m^2_{SBL}} >> m_{1,2,3}$ is favored with respect to the (1+3) case $m_{1,2,3} \simeq \sqrt{\Delta m^2_{SBL}} >> m_4$ by cosmological considerations, in the later case the sum of the masses would be much larger. For short baseline experiment, we have the condition $\Delta m^2_{atm} L/E << \Delta m^2_{SBL} L/E \lesssim 1$ we can do the approximation $\Delta m^2_{31} = \Delta m^2_{21} = 0$ which implies that $\Delta m^2_{43} = \Delta m^2_{42} = \Delta m^2_{41} = \Delta m^2_{SBL}$.

From this, we get that the survival probability is given by

$$P(\nu_\alpha \to \nu_\alpha) = \sin^2 2\theta^{SBL}_{\alpha\alpha} \sin^2\left(\frac{\Delta m^2_{41} L}{4E}\right), \sin^2 2\theta^{SBL}_{\alpha\alpha} \equiv 4|U_{\alpha 4}|^2(1-|U_{\alpha 4}|^2), \quad (2.75)$$

and for appearance probabilities

$$P(\nu_\alpha \to \nu_\beta) = \sin^2 2\theta^{SBL}_{\alpha\beta} \sin^2\left(\frac{\Delta m^2_{41} L}{4E}\right), \sin^2 2\theta^{SBL}_{\alpha\beta} \equiv 4|U_{\alpha 4}U_{\beta 4}|^2. \quad (2.76)$$

2.3 Non-unitarity

The understanding of neutrinos has changed over the years. Nowadays, we know that these particles have mass, but the process from which they obtain it is one of the current challenges of neutrino physics. One possibility is that its mass comes from mixing with heavy-fermion states. These leptons can come in an arbitrary number. The mixture of heavy leptons with the usual three neutrinos makes the mixing matrix a non-unitary one since these states are not kinematically accessible.

For this thesis, we will relax the unitarity approximation and study its consequences. We consider isosinglets neutrinos above 100 GeV, too heavy to participate in oscillations or low-energy decay processes. We will see that current experiments involving electron and muon neutrinos can be effectively described in terms of three real parameters and one CP violation phase.

We will work with a representation of the mixing matrix, which factorizes the parameters associated with the heavy leptons from those describing oscillations of light neutrinos.

Now, we will show the effects of the heavy leptons couplings to the light states in the light-neutrino sector. We can write the rotation matrix U^{nxn} using Okubo's notation as [35]

$$U^{nxn} = w_{n-1n} w_{n-2n} ... w_{1n} w_{n-2n-1} w_{n-3n-1} ... w_{1n-1} ... w_{23} w_{13} w_{12}, \quad (2.77)$$

where $w_{ij}(i<j)$ stands for the usual complex rotation matrix

$$w_{13} = \begin{bmatrix} c_{13} & 0 & e^{-i\phi_{13}}s_{13} \\ 0 & 1 & 0 \\ -e^{i\phi_{13}}s_{13} & 0 & c_{13} \end{bmatrix}, \tag{2.78}$$

with $s_{ij} = sin\theta_{ij}$ and $c_{ij} = cos\theta_{ij}$. This matrix can be expressed in general as

$$(w_{ij})_{\alpha\beta} = \delta_{\alpha\beta}\sqrt{1-\delta_{\alpha i}\delta_{\beta j}s_{ij}^2 - \delta_{\alpha j}\delta_{\beta i}s_{ij}^2} + \eta_{ij}\delta_{\alpha i}\delta_{\beta j} + \eta_{ij}\bar{\delta_{\alpha j}}\delta_{\beta i}, \tag{2.79}$$

where $i<j$ and $s_{ij}^2 = sin^2\theta_{ij}$, $\eta_{ij} = e^{-\phi_{ij}}sin\theta_{ij}$ and $\bar{\eta_{ij}} = -e^{i\phi_{ij}}sin\theta_{ij}$.

This expression can be decomposed as

$$U^{nxn} = U^{n-N}U^N, \tag{2.80}$$

with

$$U^N = w_{N-1N}w_{N-2N}...w_{1N} \tag{2.81}$$

$$U^{n-N} = w_{n-1n}w_{n-2n}...w_{1n}w_{n-2n-1}w_{n-3n-1}...w_{1N+1}. \tag{2.82}$$

When working with more than three neutrinos, we can write U^{nxn} as

$$U^{nxn} = U^{NP}U^{SM} \tag{2.83}$$

with

$$U^{NP} = w_{n-1n}w_{n-2n}...w_{1n}w_{n-2n-1}w_{n-3n-1}...w_{3n-1}w_{2n-1}w_{1n-1}...w_{34}w_{24}w_{14} \tag{2.84}$$

and

$$U^{SM} = w_{23}w_{13}w_{12}. \tag{2.85}$$

The complete $n \times n$ matrix, U^{nxn} may be written as

$$U^{nxn} = \begin{bmatrix} N & S \\ V & T \end{bmatrix}, \tag{2.86}$$

where N is the 3×3 matrix with the standard neutrino terms.

N can be parametrized as

$$N = N^{NP} U^{3x3} = \begin{bmatrix} \alpha_{11} & 0 & 0 \\ \alpha_{21} & \alpha_{22} & 0 \\ \alpha_{31} & \alpha_{32} & \alpha_{33} \end{bmatrix} U^{3x3}, \tag{2.87}$$

where U^{3x3} is the usual unitary form of the 3x3 leptonic mixing matrix.

From the previous considerations, the coupling of the n charged current interaction states can be described by a rectangular matrix

$$K = (NS) \tag{2.88}$$

The extra heavy fermions mixed with the light neutrinos would imply the effective nonunitary of the 3x3 light neutrino mixing matrix. The unitary condition takes the form

$$KK^{+} = NN^{+} + SS^{+} = I, \tag{2.89}$$

$$NN^{+} = \begin{bmatrix} \alpha_{11} & \alpha_{11}\alpha_{21}^{*} & \alpha_{11}\alpha_{31}^{*} \\ \alpha_{11}\alpha_{21} & \alpha_{22}^{2} + |\alpha_{21}^{2}| & \alpha_{22}\alpha_{32}^{*} + \alpha_{21}\alpha_{31}^{*} \\ \alpha_{11}\alpha_{31} & \alpha_{22}\alpha_{32} + \alpha_{31}\alpha_{21}^{*} & \alpha_{33}^{2} + |\alpha_{31}|^{2} + |\alpha_{32}|^{2} \end{bmatrix}. \tag{2.90}$$

By considering this new matrix, we will see that for this case, if we consider the oscillation of neutrinos between two active states, there will appear an oscillation effect at zero distances which is a result of the non-unitarity of the neutrino mixing matrix. In an analogous way, it is possible to obtain that the oscillation probability for this case is the same as for the unitary case except for the first term

$$P(\bar{\nu_\alpha} \to \bar{\nu_\beta}) = \tag{2.91}$$

$$= |\sum_i N_{\alpha i} N^*_{\beta i}|^2 - 4\sum_{i>j} Re(N^*_{\alpha i} N_{\beta i} N_{\alpha j} N^*_{\beta j}) sin^2(\Delta m^2_{ij} \frac{L}{4E}) \tag{2.92}$$

$$- 2\sum_{i>j} Im(N^*_{\alpha i} N_{\beta i} N_{\alpha j} N^*_{\beta j}) sin(\Delta m^2_{ij} \frac{L}{2E}). \tag{2.93}$$

To find the first term, we can see that the tern NN^+ explicitly is

$$NN^+ = \begin{bmatrix} \sum_i N_{ei} N^*_{ei} & \sum_i N_{ei} N^*_{\mu i} & \sum_i N_{ei} N^*_{\tau i} \\ \sum_i N_{\mu i} N^*_{ei} & \sum_i N_{\mu i} N^*_{\mu i} & \sum_i N_{\mu i} N^*_{\tau i} \\ \sum_i N_{\tau i} N^*_{ei} & \sum_i N_{\tau i} N^*_{\mu i} & \sum_i N_{\tau i} N^*_{\tau i} \end{bmatrix}. \tag{2.94}$$

Now if we consider the case where the distances between the detector and the source are very small, the terms with the sines will become zero. As a result, the value of the oscillation probability for these zero distances won't be zero, so the final oscillation probability for each case is

$$P_{\mu e} = \alpha^2_{11} |\alpha_{21}|^2, \tag{2.95}$$

$$P_{\mu\mu} = (|\alpha_{21}|^2 + \alpha^2_{22})^2, \tag{2.96}$$

$$P_{\mu\tau} = |\alpha_{22}\alpha^*_{21} + \alpha_{21}\alpha^*_{31}|^2. \tag{2.97}$$

and for the case of the transition from electron neutrino, we find

$$P_{ee} = \alpha^4_{11}, \tag{2.98}$$

$$P_{e\mu} = (\alpha_{11}\alpha^*_{21})^2, \tag{2.99}$$

$$P_{e\tau} = |\alpha_{11}\alpha^*_{31}|^2. \tag{2.100}$$

These parameters need to obey the following triangular inequalities

$$|\alpha_{21}| \leq \sqrt{(1-\alpha_{11}^2)(|-\alpha_{22}^2)}, \tag{2.101}$$

$$|\alpha_{31}| \leq \sqrt{(1-\alpha_{11}^2)(|-\alpha_{33}^2)}, \tag{2.102}$$

$$|\alpha_{32}| \leq \sqrt{(1-\alpha_{22}^2)(|-\alpha_{33}^2)}. \tag{2.103}$$

2.4 Neutrino electromagnetic properties

Neutrino electromagnetic properties were first mentioned in 1930 by Pauli when he postulated its existence. In extended versions of the Standard Model with right-handed neutrinos, the magnetic moment of massive neutrinos is not zero in general, and the value depends on the neutrino mass. These properties are important because of their connection to the fundamentals of neutrino physics. They can help distinguish between Dirac and Majorana neutrinos. It is also helpful to prove physics beyond the Standard Model since the only electromagnetic property expected in the SM for the neutrinos is the charge radius. Also, discovering new electromagnetic properties would lead us to new physics beyond the Standard Model [36–39].

We can describe the interaction between a fermionic field f(x) and the electromagnetic field $A^\mu(x)$ with the Hamiltonian [40]

$$H_{em}^{(f)} = j_\mu^{(f)}(x)A^\mu(x) = q_f \bar{f}(x)\gamma_\mu f(x)A^\mu(x) \tag{2.104}$$

with q_f the charge of the fermion. We do not have electromagnetic interactions with neutrinos at tree-level since their charge is zero. However, we can have such interactions from loop diagrams at higher order of perturbative expansion of the interaction. The electromagnetic interaction of a neutrino field $\nu(x)$ in the one-photon approximation is described by the effective Hamiltonian

$$H_{em}^{(\nu)} = j_\mu^{(\nu)}(x)A^\mu(x) = \bar{\nu}(x)\Lambda_\mu \nu(x)A^\mu(x) \tag{2.105}$$

where $j_\mu^{(\nu)}(x)$ is the neutrino effective electromagnetic current four-vector and Λ_μ is a 4x4 matrix in spinor space, such that $j_\mu^{(\nu)}(x)$ transforms as a four-vector. The Feynman diagrams in Fig. 2.6 show the one-photon coupling of a neutrino.

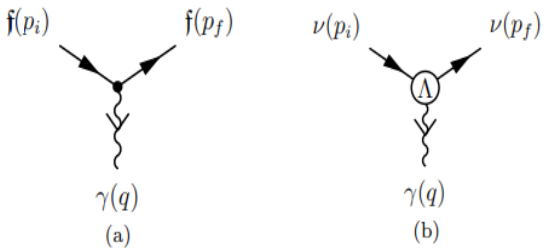

Figure 2.6: Tree-level coupling of a charged fermion with a photon and a neutrino with a photon [40].

The Diagram in Fig. 2.6 includes charge and magnetic form factors. The neutrino part of the diagram is considered by the matrix element

$$\left\langle \nu(p_f,h_f)\right| j_\mu^{(\nu)}(x)\left|\nu(p_i,h_i)\right\rangle, \tag{2.106}$$

where $p_i(p_f)$ and $h_i(h_f)$ are the four-momentum and helicity of the initial (final) neutrino. This can be written as

$$\left\langle \nu(p_f)\right| j_\mu^{(\nu)}(x)\left|\nu(p_i)\right\rangle = e^{i(p_f-p_i)\cdot x}\left\langle \nu(p_f)\right| j_\mu^{(\nu)}(0)\left|\nu(p_i)\right\rangle. \tag{2.107}$$

If we consider that the neutrinos are free particles described by free Dirac fields, we have

$$\left\langle \nu(p_f)\right| j_\mu^{(\nu)}(0)\left|\nu(p_i)\right\rangle = \bar{u}(p_f)\Lambda_\mu(p_f,p_i)u(p_i). \tag{2.108}$$

The electromagnetic properties of the neutrinos are included in the function $\Lambda_\mu(p_f,p_i)$, which we can write in their most general form as

$$\Lambda_\mu(p_f,p_i) = f_1(q^2)q_\mu + f_2(q^2)q_\mu\gamma_5 + f_3(q^2)\gamma_\mu \tag{2.109}$$
$$+f_4(q^2)\gamma_\mu\gamma_5 + f_5(q^2)\sigma_{\mu\nu}q^\nu + f_6(q^2)\epsilon_{\mu\nu\rho\gamma}q^\nu\sigma^{\rho\gamma}, \tag{2.110}$$

where $f_kj(q^2)$ are six Lorentz-invariant form factors and q is the four-momentum of the photon. We know that the Hamiltonian and the electromagnetic field are Hermitian, so

the effective current needs to be Hermitian too. From this, we can find that

$$\Lambda_\mu(q) = \gamma^0 \Lambda_\mu^\dagger(-q)\gamma^0. \tag{2.111}$$

From this, using the properties of the Dirac matrices, we can find the following constraints on the form factors

$$f_2, f_3, f_4 \rightarrow real, \tag{2.112}$$

$$f_1, f_5, f_6 \rightarrow imaginary. \tag{2.113}$$

These number of independent parameters can be reduced by imposing current conservation. This is something required by gauge invariance, in which the Hamiltonian is invariant under a transformation $A^\mu(x) \rightarrow A^\mu(x) + \partial^\mu \phi(x)$. This requirement implies that

$$\left\langle \nu(p_f) \right| \left[P^\mu, j_\mu^{(\nu)}(0) \right] \left| \nu(p_i) \right\rangle = 0, \tag{2.114}$$

so in the momentum space, we have this constrain as

$$q^\mu \bar{u}(p_f) \Lambda_\mu(q) u(p_i) = 0. \tag{2.115}$$

This implies that

$$f_1(q^2)q^2 + f_2(q^2)q^2\gamma_5 + 2m f_4(q^2)\gamma_5 = 0. \tag{2.116}$$

If we use the fact that γ_5 and the unity matrix are linearly independent, we obtain

$$f_1(q^2) = 0, \; f_4(q^2) = -f_2(q^2)q^2/2m. \tag{2.117}$$

Therefore, in the most general case, we have the function $\Lambda_\mu(q)$ defined in terms of

four form factors

$$\Lambda_\mu(q) = f_Q(q^2)\gamma_\mu - f_M(q^2)i\sigma_{\mu\nu}q^\nu + f_E(q^2)\sigma_{\mu\nu}q^\nu\gamma_5 + f_A(q^2)(q^2\gamma_\mu - q_\mu \not{q})\gamma_5, \quad (2.118)$$

where $f_Q = f_3$, $f_M = if_5$, $f_E = -2if_6$ and $f_A = -2f_2/2m$ are the real charge, dipole magnetic and electric, and anapole neutrino form factors. If we only consider the coupling with a real photon ($q^2 = 0$), we get

$$f_Q(0) = q, f_M(0) = \mu, f_E(0) = c, f_A(0) = a, \quad (2.119)$$

where q, μ, c, and a are, respectively, the neutrino charge, magnetic moment, electric moment, and anapole moment. Finally, it is useful to note that for Majorana neutrinos, the diagonal charge and dipole magnetic and electric form factors are zero. Anapole form factor is the only possible diagonal non-zero term for Majorana neutrinos [40]. But they can have as many off-diagonal(transition) form factors as Dirac neutrinos.

Chapter 3

CEvNS

The first theoretical approach to Coherent elastic neutrino-nucleus scattering (CEvNS) was made by Daniel Z. Freedman in 1974 [41] after an observation of a possible weak neutral current neutrino-nucleus interaction. The interaction between a neutrino and a nucleus may be complex, but if the momentum transfer is small enough, the internal structure of the nucleus can be ignored. As a result, an enhancement of the scattering cross-section, can be observed. In this section we will discuss this process and the detectors capable of detecting it.

3.1 Theory

Despite its theoretical prediction in 1974, this process took more than four decades to be detected. Its neutral-current nature implies that the only experimental signature consists of nuclear recoils with very low energy of about eV to keV. Since measuring this process is different for each detector technology, from now on, when we refer directly to the energy of the nuclear recoil, we will use the term eVnr.

Neutral current neutrino-nucleus scattering occurs due to the exchange of a Z^0 boson, as seen in Fig.3.1. The CEvNS occurs when the neutrinos interact with two or more particles, and the particles amplitude in the target adds up. Consequently, the differential cross section is proportional to the square of the number of particles in the target.

As a basic condition, the wavelength of the incident particle, or the wavelength of the momentum transfer ($q = |\vec{q}|$), has to be very big compared to the nucleus or atom radius (R), that is, $qR << 1$. CEvNS can be observed by measuring the very low recoil

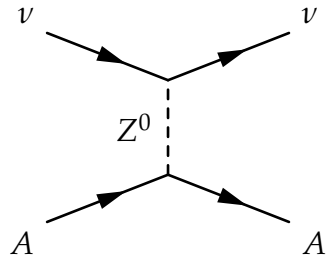

Figure 3.1: Feynman diagram of the neutrino-nucleus scattering. This process is neutral current mediated by the Z^0 boson.

energy of the nucleus (T). If E is the neutrino energy, we will have that $T << E$ and the momentum transfer can be approximated to $q^2 \approx 2MT$ with M the nuclear mass and $T_{max} \approx 2E^2/M$ [42]. The cross-section of this process is obtained in the Appendix and is given by

$$\frac{d\sigma}{dT} = \frac{G_F^2}{4\pi} Q_w^2 |F(q^2)|^2 M[1 - \frac{T}{E} - \frac{MT}{2E^2}] \tag{3.1}$$

Since the CEvNS is predicted in the Standard Model, it can be very useful to detect it and test its validity; this process can be sensitive to other types of physics beyond the Standard Model [43].

3.2 EvES

Electron-neutrino elastic scattering (EvES) is a process quite similar to CEvNS. In this case, a neutrino scatters from an electron. For this process, the cross-section is given by

$$\left(\frac{d\sigma_{\nu_\alpha - e^-}}{dE_r}\right)_{SM}^{free} = \frac{2G_F^2 m_e}{\pi}\left(g_L^2 + g_R^2\left(1 - \frac{E_r}{E_\nu}\right)^2 - g_L g_R \frac{m_e E_r}{E_\nu^2}\right), \tag{3.2}$$

where the left handed, $g_L = (g_V - g_A)/2$ and right-handed, $g_R = (g_V - g_A)/2$ are expressed as

$$g_V = -\frac{1}{2} + 2\sin^2\theta_w + \delta_{\alpha e}, \tag{3.3}$$

$$g_A = -\frac{1}{2} + \delta_{\alpha e}, \tag{3.4}$$

in which α represents a neutrino flavor e, μ, or τ, and the $\delta_{\alpha e}$ ensures that for any case different from the electron, the only contribution is from the neutral current. This equation applies to free electrons. To consider binding effects, we weight the free EvES cross-section using the step approximation

$$\left(\frac{d\sigma_{\nu_\alpha - e^-}}{dE_r}\right)_{SM} = \frac{1}{Z}\left[\sum_{i=1}^{Z}\Theta(E_r - B_i)\right]\left(\frac{d\sigma_{\nu_\alpha - e^-}}{dE_r}\right)_{SM}^{free} \tag{3.5}$$

where B_i is the i-th atomic sub(shell) binding energy, and Θ is a step function. In this manner, it is possible to quantify the impact of the atomic ionization.

Chapter 4

Experimental setups for CEvNS

Despite the utility of CEvNS to probe the Standard Model, its experimental measurement was not easy to realize due to the low recoil energies of the nucleus. The COHERENT collaboration, whose primary objective was to measure CEvNS, observed this process for the first time in 2017 using a CsI[Na] detector [44]. Up to date, there are more experimental measurements and different experiments under construction which aim to measure this process for different studies. The following chapter, introduces the different experiments considered for the analysis. We will present all the important details for each experiment, and in the next chapter, we will talk about the statistical analysis used and the results for each case.

4.1 COHERENT COLLABORATION

As we mentioned, COHERENT COLLABORATION reported the first measurement of CEvNS in 2017. They have already reported two new measurements, one using a LAr detector [45] and the second using CsI [44]. For this reason, different subsystems are considered in the present work. Here, we will explain the details of each experimental setup considered for the different physics analyses. We will mention each detector subsystem and specify its properties, such as mass, threshold, baseline, etc. The COHERENT experiments consist of a set of four detectors capable of observing low-energy nuclear recoils: a CsI[Na] scintillating crystal, p-type point-contact germanium detectors, a single-phase liquid argon, and an array of NaI[Ti] crystals, located at the Spallation Neutron Source(SNS) at Oak Ridge National Laboratory(ORNL). Before explaining each one of the detectors, let us introduce one of the most relevant aspects of

the collaboration, the neutrino source.

π-DAR neutrino source

The Coherent Collaboration uses a process called pion decay at rest to produce neutrinos. In this process, protons are accelerated to high energies (hundred of MeV to GeV) and collide with a target to produce hadrons. Some of these protons will produce a large number of pions. These pions are focused into a decaying pipe. Some will decay in flight (DIF) and transfer some of their momenta to the emitted neutrinos. On the other hand, if the pions lose energy in a dense material, they will stop and decay-at-rest (DAR). Here, negative pions are captured by nuclei.

The final neutrino production is from stopped pions with the decay $\pi^+ \rightarrow \mu^+ + \nu_\mu$ producing a prompt mono-energetic beam of 29.792 MeV of ν_μ [44]. On the other hand, the μ^+ produced in the pion decay decay-at-rest produces a $\bar{\nu_\mu}$ and ν_e in the form $\mu_+ \rightarrow e^+ + \bar{\nu_\mu} + \nu_e$ with a well-defined spectrum which is shown in Fig. 4.1. The respective fluxes from 0 to $52.8 MeV$ are given by [46]

$$\begin{aligned} \frac{dN_{\nu_\mu}}{dE} &= \eta\delta\left(E - \frac{m_\pi^2 - m_\mu^2}{2m_\pi}\right), \\ \frac{dN_{\bar{\nu_\mu}}}{dE} &= \eta\frac{64E^2}{m_\mu^3}\left(\frac{3}{4} - \frac{E}{m_\mu}\right), \\ \frac{dN_{\nu_e}}{dE} &= \eta\frac{192E^2}{m_\mu^3}\left(\frac{3}{4} - \frac{E}{m_\mu}\right). \end{aligned} \tag{4.1}$$

The pion decays at $\tau = 26.033$ ns, while the muon decays at 2.187 μs [47]. This difference in production time allows us to separate the neutrinos in prompt and delayed beams. This can be seen in Fig. 4.2. It reduces the background by considering the timing information for the expected neutrino flux for each time interval. For proton energies of about 1 GeV, the decay-in-flight component is suppressed, resulting in a clean neutrino flux. A dense material improves the likelihood of pions stopping before decaying. This kind of neutrino source has been used in different experiments, but now we will talk about what makes the SNS a specially good choice considering its properties.

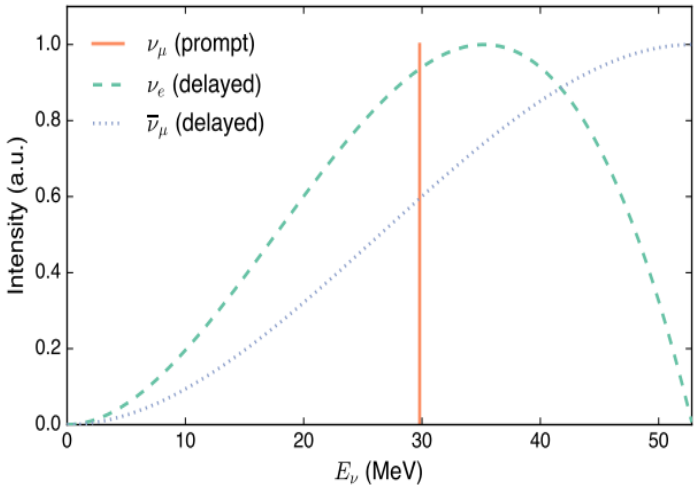

Figure 4.1: The energy spectrum of the neutrinos produced at the SNS is well defined in the interval $0 - 52.8 MeV$. The mono-energetic beam of ν_μ is represented as a vertical line [48].

Spallation Neutron Source

The Spallation Neutron Source (SNS) located at Oak Ridge National Laboratory started as a neutron source for different purposes in 2007. The SNS runs at 1 GeV proton energy and 1.4 MW beam power [47]. Hydrogen ions are accelerated through a linear accelerator, losing their two electrons and passing a thin foil before entering an accumulator ring. Around 1000 proton pulses are accumulated in the ring to create short bunches of $\approx 10^{14}$ protons. These protons are directed to a liquid mercury target. Protons move around the accumulator ring about 262 meters each loop, and the time it takes sets the maximum duration of the proton pulse on the target. The SNS generates 400 nanosecond bursts of protons on target at 60 Hz frequency, allowing good control of the backgrounds and simultaneously measuring neutrino signals and backgrounds.

The neutrinos produced per flavor per proton on target are between 0.15 to 0.5 for protons between 0.775 and 1.425 GeV. For 1 GeV protons at 1.4 MW, the predicted flux is $4.7 \times 10^7 cm^{-2} s^{-1}$ at 20m from the target, with a 99% of the total flux from π^+ DAR. There is a plan for a second target station using solid tungsten as a target [47]. For this, the power will increase to 2.8 MW, and the proton beam will be split into two targets, one with 45 Hz and the other with 15 Hz, improving the steady-state background.

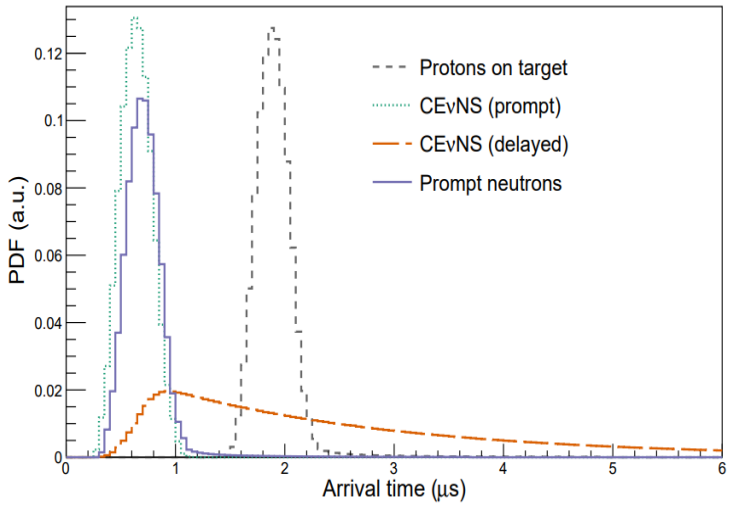

Figure 4.2: Timing distribution of the neutrino flux [48].

Experimental program

The COHERENT collaboration consists of multiple detector subsystems. These detectors have been implemented since their creation in 2014. The main objective of each detector is to measure Coherent Elastic neutrino-nucleus Scattering (CEvNS) at the SNS, but they also can be used for dark matter searches. Table 4.1 shows the different detectors as well as their main properties, such as mass, technology, and distance from the source.

Table 4.1: Current and future COHERENT detector subsystems [47,49].

Target	Technology	Mass(kg)	Distance(m)	Date
Csi[Na]	Scintillating crystal	14.6	19.6	2015
Pb,Fe	Liquid scintillator	1000	19	2015
NaI[Ti]	Scintillating crystal	185	21	2016
LAr	Noble scintillator	24	27.5	2017
LAr	Noble scintillator	612	27.5	proposed
D_2O	Cherenkov	600	600	2022
Ge	HPGe PPC	18	21	2022
NaI[Ti]	Scintillating crystal	3388	24	2022
CryoCsI	Scintillating crystal	TBD	TBD	proposed

There are different backgrounds that need to be considered in CEvNS detection. Anything that may be detected as a signal of nuclear recoil is considered in this background. We can separate this into two kinds of backgrounds, steady-state and beam-related. The

steady-state background is anything that is not related to the production of the neutrino flux. This depends on the type of detector and its location, and the beam-related background depends on the neutrino flux production. As we mention, the timing information of the SNS helps in the reduction of these backgrounds. The most important backgrounds are due to neutrons generated during the neutrino flux production, which can be divided into:

- Beam-related Neutrons(BRN). This background result from the neutrons produced at the SNS that arrives in time with the beam. So it is important to shield the detector from this and use a correct model to characterize it.
- Neutrino-induced Neutrons(NIN). Neutrinos from the beam may interact with the shielding materials producing neutrons, these neutrons may be detected by the CEvNS detector, and it is a non-negligible background

COHERENT measurements

The first ever measurement of CEvNS was performed by the COHERENT collaboration using a 14.6 kg CsI[Na] scintillator exposed to the SNS. This process was observed at a 6.7-sigma confidence level. The detector was deployed at a distance of 19.6 m from the SNS target. Table 4.2 shows some of the parameters that are represented by a single value.

Table 4.2: Parameters for the first measurement of CEvNS by COHERENT collaboration using a CsI detector [48].

Parameter	Unit	Value
DEcay-at-rest neutrino production	$\nu/flavor/SNSproton$	0.08 $\pm$0.008
SNS beam exposure	GW-hr	7.47594
CsI[Na] quenching factor	%	8.78 $\pm$1.66
CsI[Na] light yield at 59.94 keVee	PE/KeVee	13.348 $\pm$0.019

The quenching factor is a particularly important parameter. It tells us the ratio between the energy measured from the electron-recoil process and the real energy from the nuclear-recoil of the nucleus caused by the neutrino. This is especially useful since the number of events is calculated using the nuclear-recoil energy, but the experimental data is usually given in electron-equivalent energy or Photo-electrons. We can obtain this magnitude by multiplying T_{ee} by the light yield.

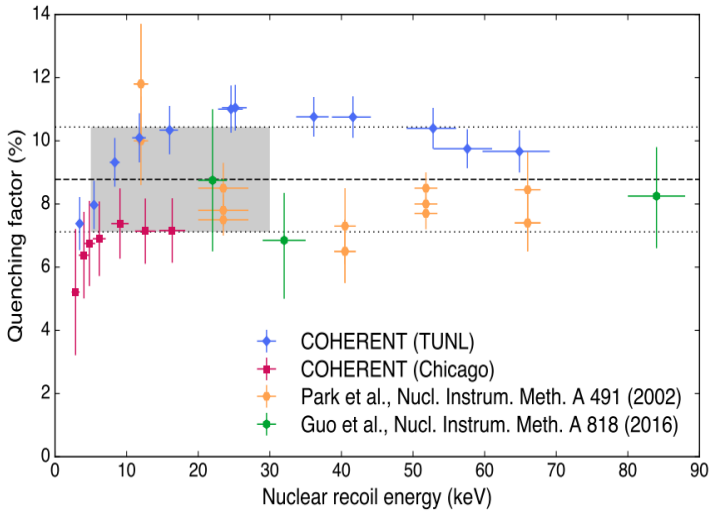

Figure 4.3: Measurements for the determination of the quenching factor [48].

The efficiency represents the fraction of the total number of events that actually need to be considered. This value depends on the energy of the photoelectron measured. For this case, the acceptance efficiency is given by the equation [48]

$$f(x) = \frac{a}{1 + exp(-k(x - k_0))}\Theta(x - 5) \tag{4.2}$$

where $\Theta(x)$ is a modified Heaviside step function with the parameters:

$$a = 0.6655^{+0.0212}_{-0.0384}, \tag{4.3}$$
$$k = 0.4942^{+0.0335}_{-0.0131}, \tag{4.4}$$
$$x_0 = 10.8507^{+0.1838}_{-0.3995}, \tag{4.5}$$

with the function defined as

$$0, x < 5, \tag{4.6}$$
$$0.5, 5 \leq x < 6, \tag{4.7}$$
$$1x \geq 6. \tag{4.8}$$

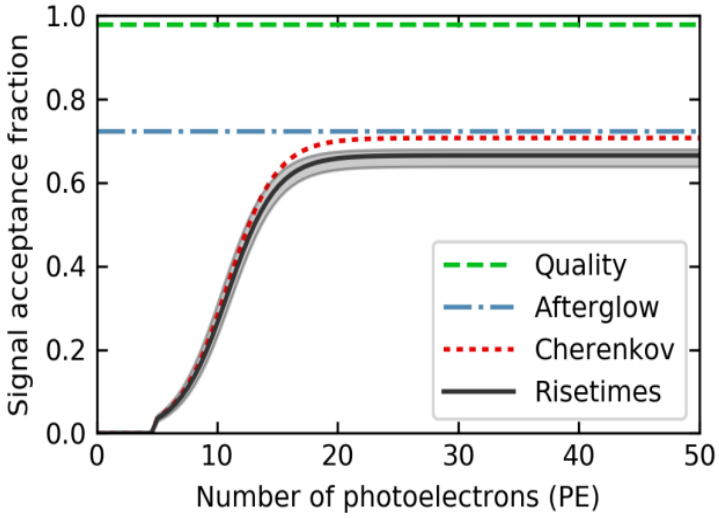

Figure 4.4: Acceptance efficiency curve for the CsI[Na] detector [48].

Fig 4.5 shows the experimental data obtained for these measurements. With all the considerations mentioned and after a likelihood analysis, the observed number of events was 134 ± 22, and the SM prediction was 173 ± 48. The systematic uncertainties considered were [50] 5% for signal acceptance, 5% form factor, 10% neutrino flux, and 25% quenching factor for a total of 28%.

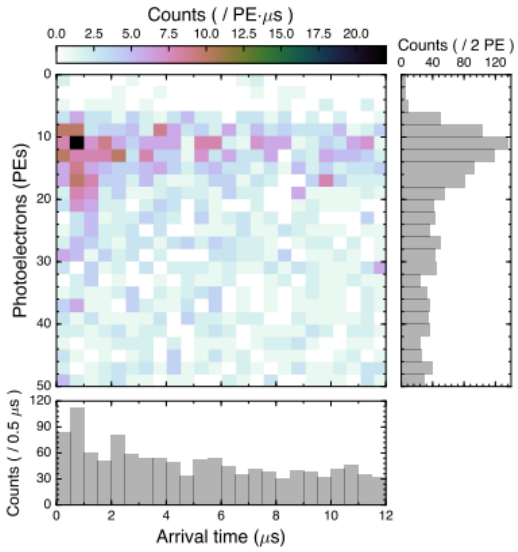

Figure 4.5: 2-D data from for coincidence region. The data is reported in both photoelectrons and Arrival time [48].

Later on 2020, a new measurement was reported by COHERENT using a LAr detector called CENNS-10, which consists of an active mass of 24 kg single-phase argon

detector, deployed at a distance of 27.5 m from the SNS target. This detector can suppress background by pulse-shape discrimination, distinguishing between nuclear recoils from electronic recoils. The Quenching factor for this detector reduces its uncertainty with respect to the CsI one, as the relation is given by [45]

$$QF = (0.246 \pm 0.0006) + ((7.8 \pm 0.9) \times 10^{-4} keVnr^{-1})T, \tag{4.9}$$

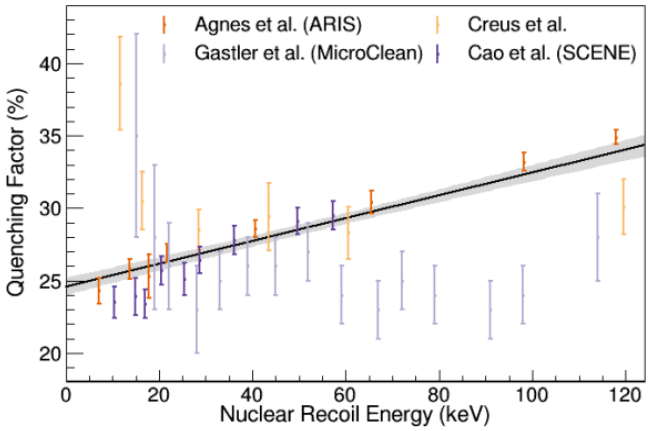

Figure 4.6: Quenching factor for the CENNS-10 experiment [45].

the fit and error bands are shown in Fig. 4.6. The analysis was performed with 13.7×10^{22} protons-on-target by two independent groups, and both of them observed an excess of more than 3σ over the background. The results are shown in Fig. 4.7, and the detectors keeps collecting data for more precise results.

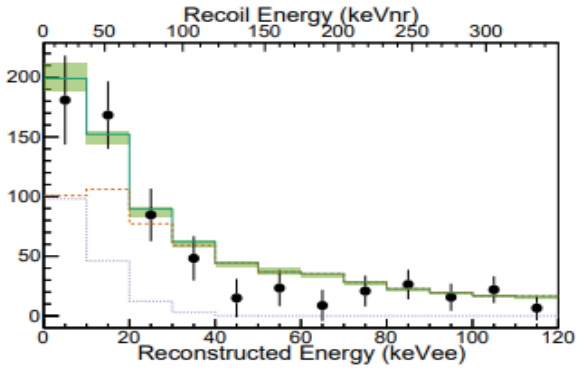

Figure 4.7: Best fit for one of the analysis on reconstructed energy [45].

Finally, on 2021, new results with more data collected were reported by the COHERENT collaboration using the previous CsI detector. This was more than double the data

previously reported with reduced systematic uncertainties and an updated quenching factor model. The new analysis resulted in an observation of 306 ± 20 CEvNS events, which is consistent with the prediction of 341 ± 11 and is shown in Fig. 4.8.

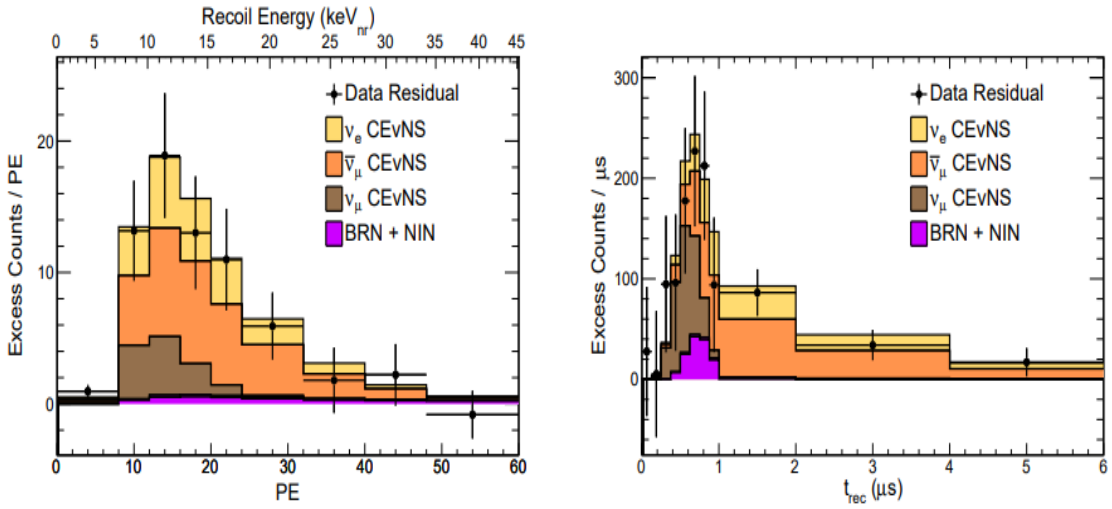

Figure 4.8: Results from the new data obtained for CsI detector. For each plot the excess counts are represented in bins that have a width of two PE each. The events for each flavor of the neutrinos are shown [45].

After we have discussed the most important experiment regarding CEvNS, we will mention more experiments under construction that aim to measure CEvNS with different technologies and configurations. When we talk about the sensitivity obtained for each type of physics we will talk in more detail about the analysis performed for each case.

4.2 Coherent Captain Mills and European Spallation Source

Coherent "CAPTAIN" Mills (CCM) is a short baseline neutrino experiment located at Los Alamos National Laboratory in the Lujan FAcility. This experiment plans to detect neutrinos via CEvNS using a liquid Argon detector. This is a Cryogenic Apparatus for Precision Test of Argon Interaction with neutrinos. For this experiment, the neutrino source is produced just as in the case of the SNS, the difference is that, in this case, the target is made of tungsten. This experiment plans to install a large 7 ton liquid argon detector with an expected threshold of 1keV. This will be placed 20m from the source with the goal of searching for sterile neutrinos.

The European Spallation Source(ESS) which is located in Lund, Sweden, is a European Research Infrastructure Consortium(ERIC) constructed with the most powerful neutron source in the world. There is no official information ab the exact configurations that the experiment will consider, but for this work, we follow two proposals: i) a 10kg liquid argon detector with ultra-low 0.1 KeV threshold, ii)a 1ton liquid argon detector with 20 KeV threshold, both of them located at 20m from the source.

The main difference between ESS, SNS, and CCM is the power reached in each experiment. The CCM is scheduled to reach 5MW with a goal energy of 2 GeV by 2023, SNS aims to reach 1.3MW, and the CCM 80kW. As a result, a magnitude increase of about one order in the ESS neutrino flux with respect to SNS is expected. Although the power of the proton beam at Lujan is 1-2 orders of magnitude smaller than in SNS and ESS, in contrast to the other two, the CCM experiment can deploy very large ton-scale detectors. Another big difference is that of the proton beam pulse timing. For the SNS, it provides 60 Hz of 1 μ wide proton on target spills, while for ESS, we have a 14 Hz fo 2.8ms spills, reducing the relative capability of separating the neutrino flavors with timing information.

Chapter 5

Experimental setups for EvES

The nature of electron-neutrino scattering allows us to study some of the physics considered in this thesis with experiments that can measure this process. There is not much difference between this process and CEvNS, so making an analysis using EvES experiments is a straightforward process. We will see that the region covered by this experiment is different from the one of CEvNS, so this is useful as a complement.

XENON1T

The XENON1T experiment reported results from searches with low-energy electron recoil [51]. We considered this experiment primarily to calibrate our computations with previous studies of these results. But we also observed the effect of including the step function correction commented on Eq. (3.5), which was not used in previous works.

TEXONO

TEXONO collaboration has already reported a measurement of EvES using reactor neutrinos at the Kuo-Sheng Nuclear Power Station with a CsI[Ti] scintillating crystal array [52]. The mass of the detector was 187 kg with an average $\bar{\nu}_e$ flux of $6.4 \times 10^{12} cm^{-2} s^{-1}$.

^{51}Cr Source

Besides using the different neutrino sources previously discussed. We explored different prospects using a low-energy monochromatic ν_e ^{51}Cr source for both EvES and CEvNS. For EvES we examined a LXe detector with three different configurations. The important parameters of each case are resumed in Fig. (5.1). The cylindrical LXe detector is at 1 m from the source. It has a height and diameter of 1.38m, corresponding to a 6 tonnes mass.

For CEvNS we focused on a proposal previously done [53] with various detectors with different sub-KeV capabilities. We considered a cylindrical 2000 cm^3 detector for different targets, with materials such as Si, Ge, sapphire (Al_2O_3) and calcium tungstate ($CaWO_4$). The detector will be placed at 25 cm from the source, with an average neutrino flux of $1.1 \times 10^{13} cm^{-2} s^{-1}$. For this case we consider a fixed threshold of $8eV_{nr}$, and for the neutrino flux we need to consider for different contributions with neutrino energies (427, 432, 747, 752) keV from the ^{51}Cr decay, with a relative strength of 9, 1, 81, and 9 % with an exposure time of 55.4 days.

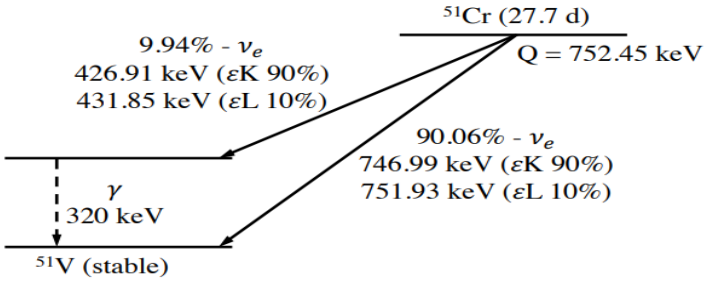

Figure 5.1: ^{51}Cr decay process [53].

Chapter 6

Experimental results

In this section, we will show all the different analyses we performed for each new physics scenario in their corresponding experimental setup. We will explain how we performed the statistical calculation for each case and show the plots obtained. For each subsection, we show the results for the corresponding beyond the standard model physics from all the experiments that we studied.

6.1 Sensitivity to weak mixing angle and nuclear physics

The weak mixing angle parameter is one of the most important parameters of the SM, and any deviation from its prediction will be an indicator of new physics. With this motivation, we performed a χ^2 analysis of this parameter for three future configurations of the COHERENT experiment and for the actual experimental results obtained with the Liquid Argon detector.

First, for the future configurations we used a χ^2 function given by

$$\chi^2 = \left(\frac{N^{exp} - (1+\alpha)N^{th}(X) - (1+\beta)N^{bg}}{\sigma} \right)^2 + \left(\frac{\alpha}{\sigma_\alpha} \right)^2 + \left(\frac{\beta}{\sigma_\beta} \right)^2 \tag{6.1}$$

where N^{exp} is the measured number of events, which we will consider as the one given by the SM since we are working with futuristic experiments; $N^{th}(X)$ is the predicted number of events as a function of the weak mixing angle; N^{bg} is the expected background which we will consider to be 10% of the predicted number of events; the statis-

tical uncertainty given by $\sigma = N^{exp}$; finally, the nuisance parameters α and β will have the uncertainties σ_α and σ_β, respectively.

The final results are shown in Fig. 6.1 and summarized in table 6.1. We present four different scenarios for each detector material. Each one considers different systematic uncertainties to illustrate what would be the sensitivity to this parameter. We can see that a first measurement with a big uncertainty will lead to large errors due to normalization and quenching factors, among other systematic uncertainties.

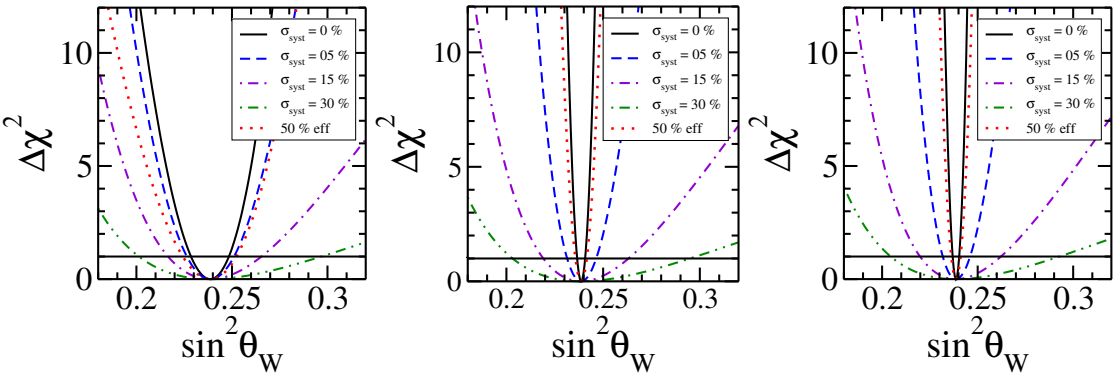

Figure 6.1: Expected sensitivity to $\sin^2\theta_W$ for the different detectors under consideration: Germanium, Argon, and NaI, respectively. The different curves are for a 100 % efficiency and no systematic errors (solid), for a systematic error of 5 % (dashed), 15 % (dashed-dotted), and 30 % (dashed double-dotted). Finally, the case of an efficiency of 50 % and no systematic error is also shown (dotted line) [54].

The first scenario of $\sigma = 30\%$ is similar to the first measurement reported by the COHERENT collaboration. A case with $\sigma = 15\%$ is more realistic after the detectors are better characterized, and the background is reduced. A case with $\sigma = 0$ is also displayed to see what may be the best possible results and to have a better idea of the potential of each detector. Finally, a scenario with an efficiency of 50% and $\sigma = 5\%$ is also shown. For all the previous cases, except for the case of no error, we considered a background error of $\sigma = 10\%$. Table 6.1 shows the expected sensitivity at 90 % C.L. As expected, the detector with the larger mass, such as the NaI case, will give the best constraints, considering that the systematic errors must be under control. But also, the Ge detector, with its modest mass of 10 kg, may give competitive measurements for this parameter if the errors are well controlled.

Now, we will work with actual measurements obtained from the COHERENT collaboration. These results were obtained after the publication of the previous results. The measurements are from the CENNS-10 experiment, which is a LAr detector with a mass

Experiment	50 % eff	100 % eff	$\sigma_{syst} = 5$ %	$\sigma_{syst} = 30$ %
Ge	5.9	4.2	5	20
Ar	1.2	0.9	3	19
NaI	1.0	0.7	3	19

Table 6.1: Expected sensitivity, in percent, to the weak mixing angle. For each experiment we show the 1σ expected sensitivity in the case of a 50 % (100 %) efficiency of the experiment. For a non-zero systematic error of 5 (30) %, the efficiency was considered to be of 100 %.

of 10 kg. For this, we used the following χ^2 function

$$\chi^2(X) = \min_{\alpha} \left(\frac{(N_{meas} - N_{theor}(X)[1+\alpha])^2}{\sigma^2_{stat}} + \left(\frac{\alpha}{\sigma_\alpha}\right)^2 \right) \tag{6.2}$$

where N_{meas} represents the 159 events measured and $N_{theor}(X)$ is the theoretical prediction. For this case we got, $\sigma_{stat} = \sqrt{N_{meas} + N_{BRN}}$, where $N_{BRN} = 563$ is the number of background due to beam related neutrons. Finally, the systemic error is $\sigma_\alpha = 8.5\%$. The result obtained is shown in Fig. 6.2 with a comparison to the previous result from the CsI detector, which can be seen that it is a notable improvement. With this, we can obtain that the result from the CENNS-10 data is

$$\sin^2\theta_W = 0.258^{+0.048}_{-0.050}. \tag{6.3}$$

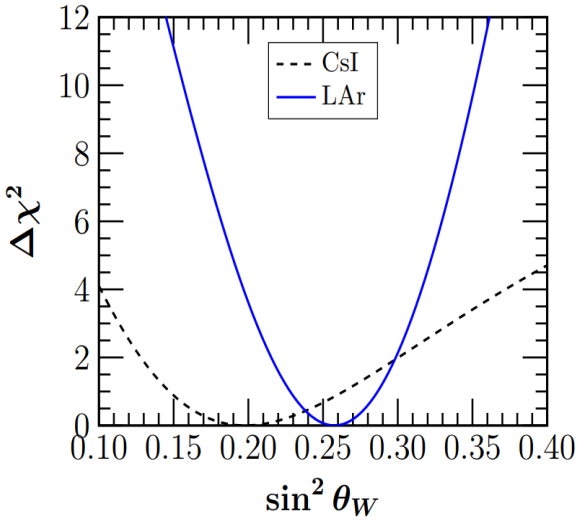

Figure 6.2: Sensitivity for the weak mixing angle. Results of CsI and LAr for comparison [55].

Finally, another parameter that can be obtained from this data is the neutron mean radius R_n for the Argon isotope. This parameter is predicted theoretically with a value of $R_n = 3.36fm$. Still, its determination helps to better understand the background for CEvNS for experiments that aim to detect Dark Matter. The analysis for this parameter is shown in Fig. 6.3. The average neutron rms radius for the CsI is also displayed just for convenience. Note that R_n for Argon is more constrained with respect to the CsI. In the end, the limit at 90 % C.L. for the rms radius of Argon is

$$R_n < 4.33fm. \tag{6.4}$$

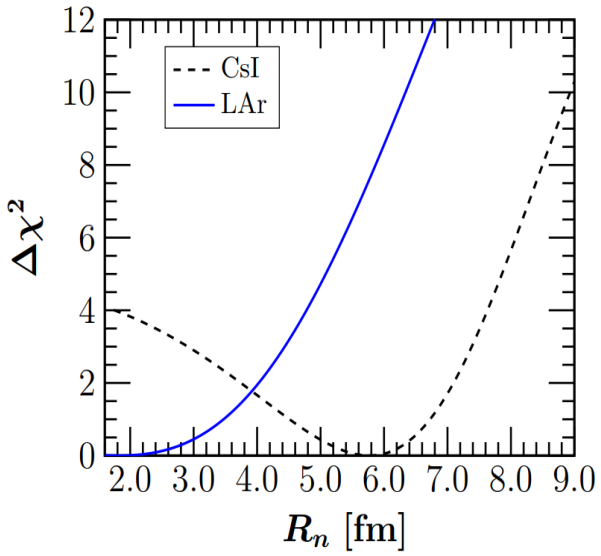

Figure 6.3: Sensitivity to the neutron rms radius [55].

6.2 Sensitivity to sterile neutrino oscillations

In this section, we study the possibility of measuring the neutrino oscillations parameters. First, we make this analysis for the NaI, LAr, and Ge detectors with the first considerations proposed by the COHERENT COLLABORATION. For this case, the expected number of events at each detector is given by

$$N^{th} = N_D \int_T A(T)dT \int_{E_{min}}^{52.8MeV} dE \sum_\alpha \frac{dN_\alpha}{dE}\frac{d\sigma}{dT} \tag{6.5}$$

Table 6.2: Experimental setups considered for the first analysis from the COHERENT collaboration detectors

	Threshold	Baseline	Det. Tec.	Fid. Mass
^{72}Ge	5keV	22m	HPGe PPC	10kg
$^{23}Na^{127}I$	13KeV	28m	Scintillator	2000kg
^{40}Ar	20keV	29m	Liquid Scintillator	1000kg [1ex]

In order to find the number of events, we need to consider the correct parameters for each experimental configuration. The number of N and Z, and the acceptance function must be in accordance with the detector used. In a previous chapter, we discussed the experimental setups we would consider. Some of the proposals have changed over time, so we will give the exact parameters used at the moment when needed. For this first approach, we used the setups resumed in Table. 6.2. From this, one of the parameters that will change for each case is the number of protons on target

$$N = \frac{N_A M_{det}}{M}, \tag{6.6}$$

where N_A is the Avogadro Number, M_{det} is the mass of the detector, and M is the molar mass of the material.

Once we have the theoretical number of events, we perform a likelihood analysis using a χ^2 function. The form of this function will vary over each experiment and the physics under consideration, so that we will specify it in each case. For the present analysis, we will use a least-squares function given by

$$\chi^2 = \left(\frac{N^{exp} - (1+\alpha)N^{th}(X) - (1+\beta)N^{bg}}{\sigma} \right)^2 + \left(\frac{\alpha}{\sigma_\alpha} \right)^2 + \left(\frac{\beta}{\sigma_\beta} \right)^2, \tag{6.7}$$

N^{exp} and N^{th} are, respectively, the experimental and theoretical number of events in each bin; α and β are nuisance parameters that quantify the systematic uncertainty of the signal rate, with a standard deviation that may vary for different cases. Since these experiments are still in installation, we don't have experimental data to compare and analyze the possible values for the oscillations parameters. The theoretical number of events will be given by taking the SM interactions of the neutrinos with the detector. On the other hand, the experimental number of events will be calculated considering the neutrino oscillations from the source to the detector. This effect will be considered in a 3+1 scheme in which one sterile neutrino is considered. This is possible due to

the short distance from the neutrino source to the detector. By neglecting oscillation between the three active states, the oscillation probability from active to sterile states can be studied in a two-flavor approximation

$$P_{\nu_\alpha \nu_s} = \sin^2 2\theta_{\alpha\beta} \sin^2 \left(\frac{1.27 \Delta m^2_{i4} L}{E_\nu} \right). \tag{6.8}$$

We will consider two different cases. First, the $\nu_e \rightarrow \nu_s$ oscillation and then the corresponding case for muon (anti)neutrinos. That is, we only consider either $\sin\theta_{ee}$ or $\sin\theta_{\mu\mu}$ different from zero at a time and compute its effect in the electron (muon) neutrino number of events. To take into account the possible sterile neutrino oscillation, we consider the survival probability as

$$P_\alpha = 1 - \sin^2 2\theta_{\alpha\alpha} \sin^2 \left(\frac{1.27 \Delta m^2_{i4} L}{E_\nu} \right). \tag{6.9}$$

After multiplying the oscillation probability by the neutrino flux and integrating it over the neutrino energy spectrum, the expected number of events in these two cases will be given by

$$N^{th} = N_D \int_T A(T) dT \int_{E_{min}}^{52.8 MeV} dE \sum_\alpha \frac{dN_\alpha}{dE} P_\alpha(\theta_{\alpha\alpha}, \Delta m^2_{i4}) \frac{\mathrm{d}\sigma}{\mathrm{d}T}, \tag{6.10}$$

With these considerations, the chi-squared function will be calculated using Eqs. (6.5) and (6.10) as the theoretical and experimental number of events, respectively. In this case, since neutrino oscillation probability is a function of two variables ($\sin^2 2\theta_{\alpha\alpha}, \Delta m^2_{i4}$), we will take the χ^2 function as the one described in Eq. (6.7) with $N^{th}(X) = N^{th}(\sin^2 2\theta_{\alpha\alpha}, \Delta m^2_{i4})$ as in Eq. (6.10).

Table 6.3: Significance for different number of parameters

Significance	Number of parameters		
α	1	2	3
0.68	1	2.30	3.50
0.90	2.71	4.61	6.25
0.99	6.63	9.21	11.30

The confidence limits are given as a function of the number of varying parameters and

summarized in Table 6.3.

In Figs. 6.4 and 6.5, we show the sensitivity to the allowed regions of the parameters $\sin^2 2\theta_{\alpha\alpha}$ and Δm^2_{i4} for the different systematic errors and efficiencies that we have already discussed. The results are shown at 90 % CL.

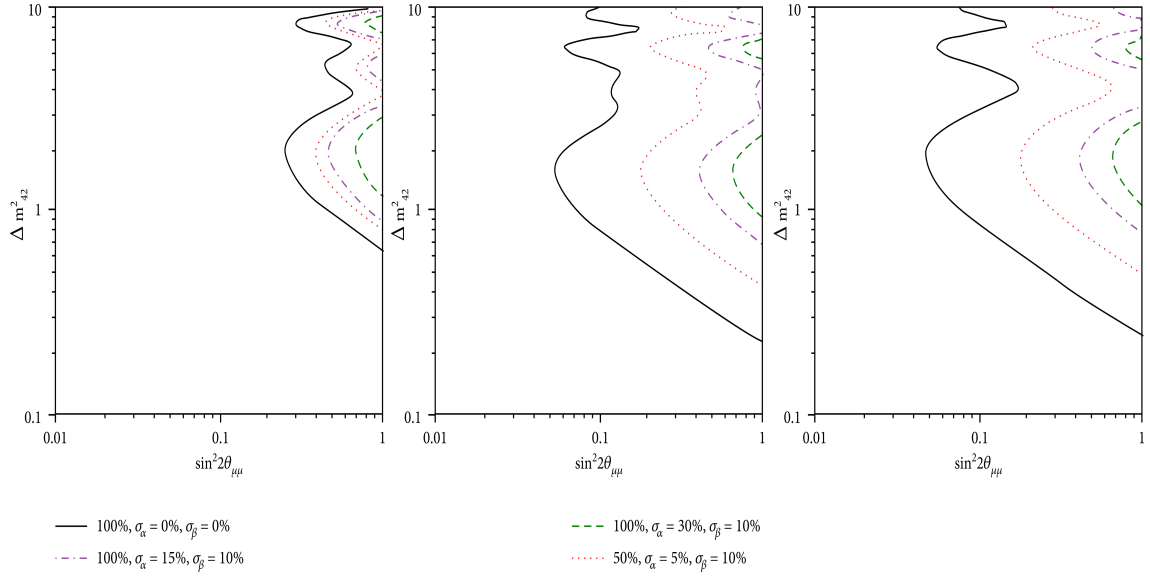

Figure 6.4: Expected sensitivity for muon neutrino oscillation into a sterile neutrino state for each experiment under consideration: Gr (left), Ar (middle), and NaI (right), respectively. The different curves are for different combinations of the considered uncertainties [54].

The material that presented the best sensitivity in the delimitation was the very massive NaI detector, thanks to the large number of events that are expected. The difference between the argon and germanium expectations was limited; however, the germanium showed a better result with respect to the Argon, despite being a less massive detector.

From the analysis carried out, we can conclude that of the three proposed materials, the one that could present the best results according to the given conditions is the NaI. We can also conclude that the increase in mass is not the only important factor in improving the sensitivity of the results. This way, NaI can be considered the best candidate for future experiments focused on oscillations to sterile states. Among the considerations that could be improved for the analysis presented here is the acceptance taken for each material. Although we consider it as a step function from the energy threshold in these cases, this is not the reality, as can be seen in the case of acceptance for the CsI. In addition, the distance to each detector could have been varied to study if it could improve the sensitivity. Finally, the study could be done by combining the detectors to improve

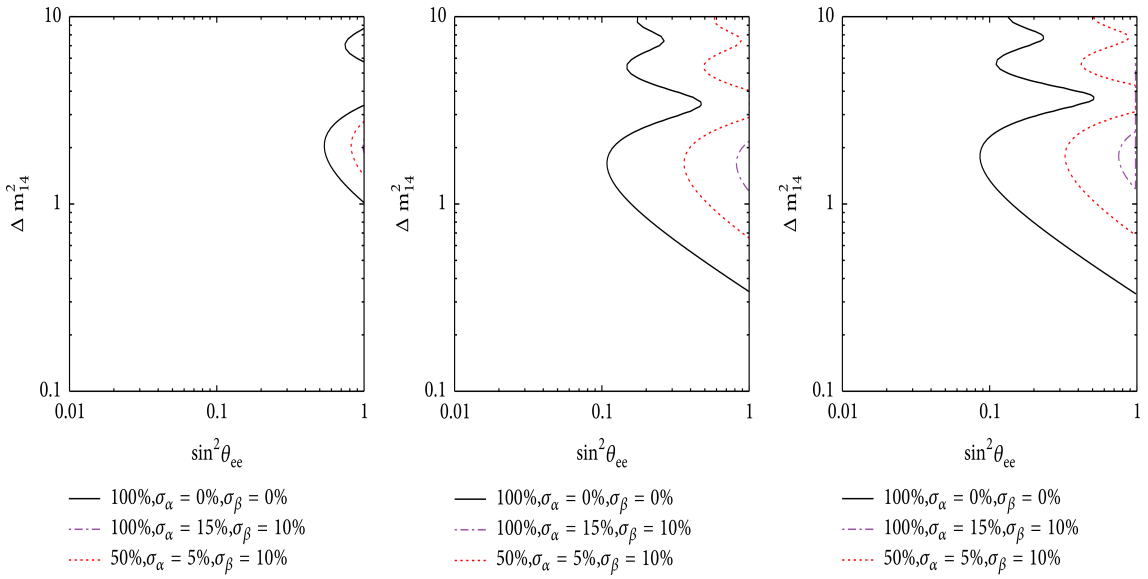

Figure 6.5: Expected sensitivity for electron neutrino oscillation into a sterile neutrino state for each experiment under consideration: Gr (left), Ar (middle), and NaI (right), respectively. The different curves are for different combinations of the considered uncertainties [54].

the sensitivity of the final results.

It should be mentioned that the results presented here do not plan to be competitive in the current delimitation of the parameters used but rather to give an idea of how the results of the COHERENT experiment could be used in the area of sterile neutrino oscillations.

For the previous results, we used a fixed distance of the detector to the source that was established by the experimental proposals. But we mentioned that the oscillation probability is a function of this distance, so there must be a value that gives the best results because the oscillation probability is at maximum. This analysis can be pushed further by studying the effect of varying the distance to each detector. For this study, we will consider the CCM, the ESS with two configurations, one with 10kg and one with 1 ton of mass, and the CENNS-610, which corresponds to the LAr detector from the COHERENT COLLABORATION but with a mass of 610 kg. For the ESS, the 1-ton configuration is to be considered more like an ideal case since it is not a real consideration for the experiment at the moment. But the high intense neutrino beam motivated us to consider also this case.

First, we explore the best baseline for light sterile neutrino searches. For this, we fix the important parameters for this process, that is $\Delta m^2_{41} = 1eV^2$ and $\sin^2\theta^2_{14} = 0.1$ for the

Table 6.4: Experimental setups considered

	CENSS	CCM	ESS
mass	610 kg	7 ton	10kg(1 ton)
threshold(keVnr)	20	1	0.1(20)
$N_{POT}(10^{23}/yr)$	1.5	0.177	2.8
r	0.08	0.0425	0.3
baseline (m)	28.4	20	20

electron neutrino and $\sin^2\theta_{24}^2 = 0.1$ for the muon neutrino. With this, we evaluate the following χ^2 as a function of the baseline L

$$\chi^2 = \left(\frac{N_{SM} - N_{new}}{\sqrt{N_{SM}}}\right)^2, \tag{6.11}$$

where N_{SM} is the number of events expected in the SM case, and N_{new} is the number of events with the extra contributions, which for this case is the neutrino oscillation process.

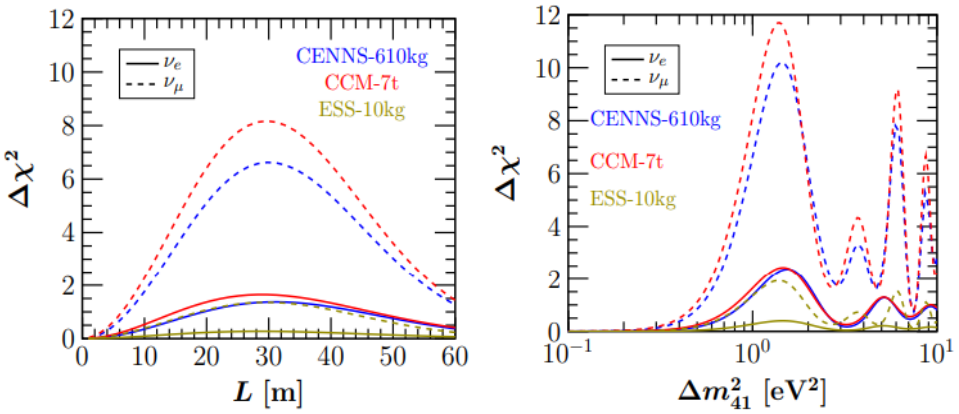

Figure 6.6: (left) sensitivity with respect to the baseline L for a fixed mass splitting $\Delta m^2_{41} = 1eV^2$ for $\sin^2 2\theta_{14} = 0.1$ for both ν_e and ν_μ. (right) sensitivity with respect to the mass splitting Δm^2_{41} for a fixed value of $L = 30m$ and $\sin^2 2\theta_{14} = 0.1$ [56].

The results obtained with this study are shown in Fig. 6.6. Here. we can see a comparison of the experiments. Note that the ESS with a mass of 1 ton is on a different plot due to the big difference with respect to the other three in Fig. 6.7. We also show the sensitivity to the distances for electron and muon neutrinos separately to see each contribution. In all cases, the maximum sensitivity is around $L = 30m$, which is close to the baseline considered in each experiment. From these plots, we also see that we can

expect the best results from CENNS and CCM and also that we get better results for muon-like events. We get very similar sensitivities for CENNS and CCM despite the large difference in their masses. This is explained by the high neutrino flux available from the SNS, which can compensate for the low mass with respect to the CCM. Also, considering a 1-ton mass on the ESS combined with its very intense neutrino beam can, of course, give a better result that all the previous considerations.

We also found it useful to study the sensitivity of these experiments to mass splittings. For this, we fixed $\sin^2 2\theta_{14} = 0.1$ or $\sin^2 2\theta_{24} = 0.1$ and the baseline at $L = 30m$. With this, we confirm that CENNS and CCM have better performance, and also, we get a better sensitivity with muon-like events. For our chosen values of the mixing angle, the best mass splitting values are at 1.5 and 6 eV^2

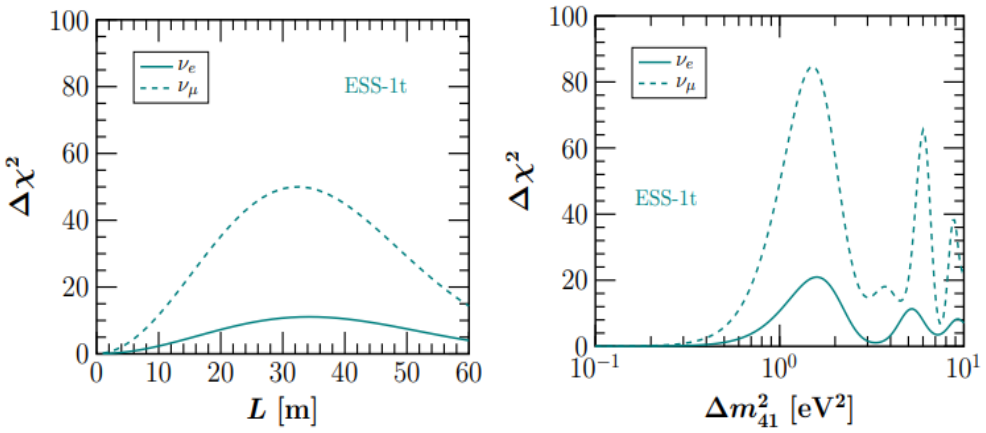

Figure 6.7: same as Fig. 6.6 for the future ESS of 1 ton detector [56].

Now we can find the sensitivities to the sterile neutrino oscillation parameters. For this, we simultaneously vary the mixing angle $\sin^2 2\theta_{i4}$ and the mass splitting Δm^2_{42} for different baselines. For each case in Fig. 6.8, we find the curves at 90% C.L. The results are quite promising. We can observe overall the same behavior that we observed when varying only the distance and the mass splitting. The future configuration of the ESS may become competitive with current oscillation studies.

Finally, the CENNS-610 is the experiment that gives us more information about its planned configuration, so for this case, we can go a little further and perform a more realistic analysis considering the expected baseline of 28.4 m and adding a systematic

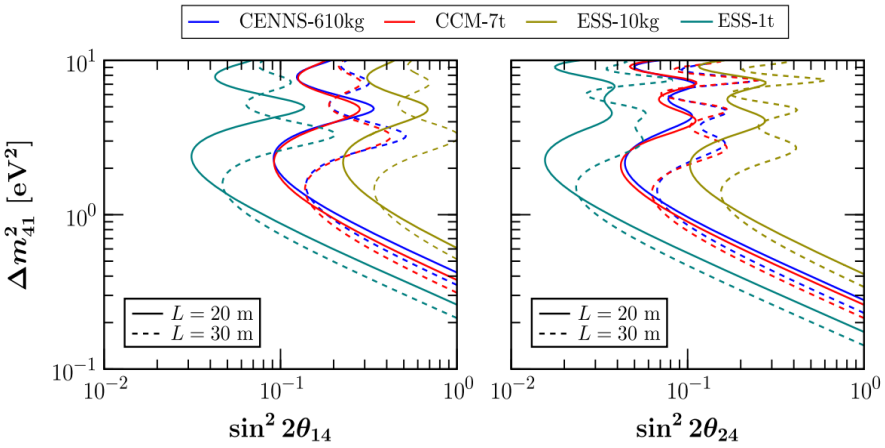

Figure 6.8: 90 % C.L. sensitivity curves for different baselines and experiments [56].

uncertainty. So for this case the χ^2 is calculated as:

$$\chi^2 = min_a \left(\frac{(N_{SM} - N_{osc}(1+a))^2}{(\sigma_{stat})^2} + \left(\frac{a}{\sigma_{sys}} \right)^2 \right). \tag{6.12}$$

The regions obtained for this are shown in Fig. 6.9 with $\sigma_{sys} = 2\%$ and $\sigma_{sys} = 5\%$.

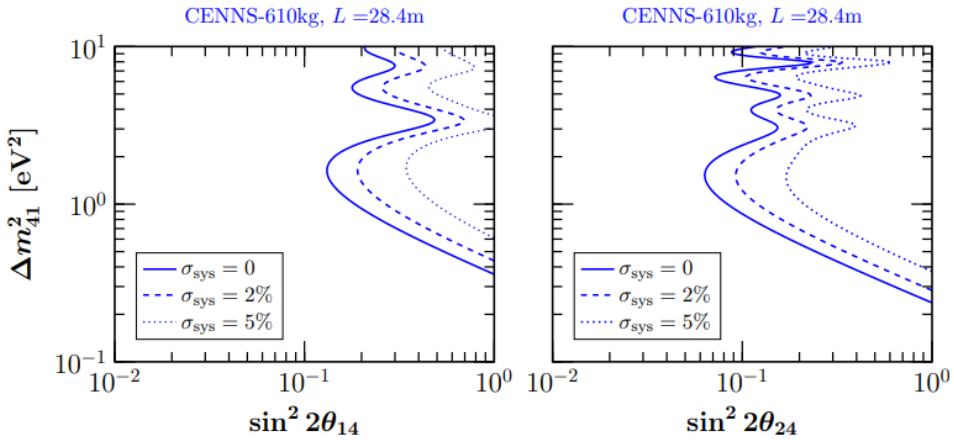

Figure 6.9: Sensitivity for the CENNS-610 to the parameters with a baseline of $L = 28.4$ m [56].

6.3 Non- unitarity

As mentioned in previous sections, the unitarity violation in neutrino oscillations due to the presence of neutral heavy leptons may be detectable in experiments that detect neutrino through a neutral current. CEvNS represent a good approach for this kind of new physics as, shown for sterile neutrinos. In this section, we focus on the next generation of detectors subsystems of COHERENT, namely CENNS, as well as on Coherent Captain-Mills (CCM) experiment at the Los Alamos Neutron Science Center-Lujan facility and on the CEvNS program developed at the European Spallation Source(ESS). We take the same considerations as the previous analysis.

First, we will discuss the CENNS detector of the COHERENT experiment at the SNS. This detector aims to replace the CENNS-10 detector with which the first detection of CEvNS in argon was made. This configuration is planned to contain a 750kg (610kg fiducial) liquid argon scintillation detector, with a 20 KeV threshold and a baseline of 28.4m.

There are two more proposals that we considered for this case since they are planning to measure CEvNS in similar ways, such the as COHERENT collaboration. The first one is the proposed CCM experiment located at Los Alamos National Laboratory, in the Lujan facility. For this experiment, it is planned to install a very large 7 ton liquid argon detector, with an expected threshold of 1 keV. This detector is planned to be placed 20m from the source to reach for sterile neutrinos. The second experiment is the ESS located in Lund, Sweden. This combines the world's most powerful superconducting proton linac with an advanced hydrogen moderator, generating the most intense neutron beam for different purposes.

With this proposal, we will consider two different configurations, the first one considered with a 10kg liquid argon detector with ultra-low 0.1 KeV threshold, and a future next-generation configuration with 1 ton liquid argon detector and a 20 KeV threshold, both of them are located at 20m from the detector.

The major difference between ESS, SNS, and Lujan facilities is the neutrino flux produced in each case. Since ESS is scheduled to reach a power of 5 MW with goal energy of 2GeV by 2023, while SNS (Lujan) will have a power of 1.3 MW, there will be a difference of about one order of magnitude enlargement in the ESS flux with respect to SNS. Finally, it is worth mentioning that in contrast to SNS, the CCM experiment can deploy a very large ton-scale detector. This compensates for the 1-2 orders of magnitude

difference in the proton beam power with respect to SNS and ESS.

As we mentioned, the existence of heavy lepton neutrinos affects the unitarity of the mixing matrix. As a result, we get a zero-distance effect oscillation probability. These probabilities are

$$P_{ee} = \alpha_{11}^4, \tag{6.13}$$
$$P_{\mu\mu} = (|\alpha_{21}^2|^2 + \alpha_{22}^2)^2, \tag{6.14}$$
$$P_{\mu e} = \alpha_{11}^2 |\alpha_{21}|^2, \tag{6.15}$$
$$P_{e\tau} = \alpha_{11}^2 |\alpha_{31}|^2, \tag{6.16}$$
$$P_{\mu\tau} = \alpha_{22}^2 |\alpha_{32}|^2. \tag{6.17}$$

It is important to mention that these parameters must obey some triangle inequalities

$$|\alpha_{21}| \leq \sqrt{(1-\alpha_{11}^2)(1-\alpha_{22}^2)}, \tag{6.18}$$
$$|\alpha_{31}| \leq \sqrt{(1-\alpha_{11}^2)(1-\alpha_{33}^2)}, \tag{6.19}$$
$$|\alpha_{32}| \leq \sqrt{(1-\alpha_{22}^2)(1-\alpha_{33}^2)}. \tag{6.20}$$

This oscillation probability will affect the initial neutrino flux that comes from the spallation source. As a result, the modified fluxes will look like this

$$\frac{d\phi_e^{NU}}{E_\nu} = \frac{d\phi_{\nu_e}^{NU}}{dE_\nu} + \frac{d\phi_{\bar{\nu}_e}^{NU}}{dE_\nu} = P_{ee}\frac{d\phi_{\nu_e}^0}{dE_\nu} + P_{\mu e}\left(\frac{d\phi_{\nu_\mu}^0}{dE_\nu} + \frac{d\phi_{\bar{\nu}_\mu}^0}{dE_\nu}\right), \tag{6.21}$$
$$\frac{d\phi_\mu^{NU}}{dE_\nu} = \frac{d\phi_{\nu_\mu}^{NU}}{dE_\nu} + \frac{d\phi_{\bar{\nu}_\mu}^{NU}}{dE_\nu} = P_{e\mu}\frac{d\phi_{\nu_e}^0}{dE_\nu} + P_{\mu\mu}\left(\frac{d\phi_{\nu_\mu}^0}{dE_\nu} + \frac{d\phi_{\bar{\nu}_\mu}^0}{dE_\nu}\right), \tag{6.22}$$
$$\frac{d\phi_\tau^{NU}}{dE_\nu} = \frac{d\phi_{\nu_\tau}^{NU}}{dE_\nu} + \frac{d\phi_{\bar{\nu}_\tau}^{NU}}{dE_\nu} = P_{e\tau}\frac{d\phi_{\nu_e}^0}{dE_\nu} + P_{\mu\tau}\left(\frac{d\phi_{\nu_\mu}^0}{dE_\nu} + \frac{d\phi_{\bar{\nu}_\mu}^0}{dE_\nu}\right), \tag{6.23}$$

where the terms with super index 0 represent the un-oscillated neutrino energy fluxes given in previous sections.

Note that there will be an additional tau neutrino flux for this case due to the zero-distance effect. Also, this oscillation probability will change the initial energy spectrum of the fluxes. Fig. 6.11 shows the energy spectrum for the initial case and the energy spectrum for the fluxes considering the zero-distances oscillation. As we can see, the effect on the ν_e and ν_μ have a noticeable change with respect to the initial one, on the other hand, the new τ neutrino flux is two orders of magnitude smaller with respect to the other ones, so it is possible to ignore this flux for the present calculations.

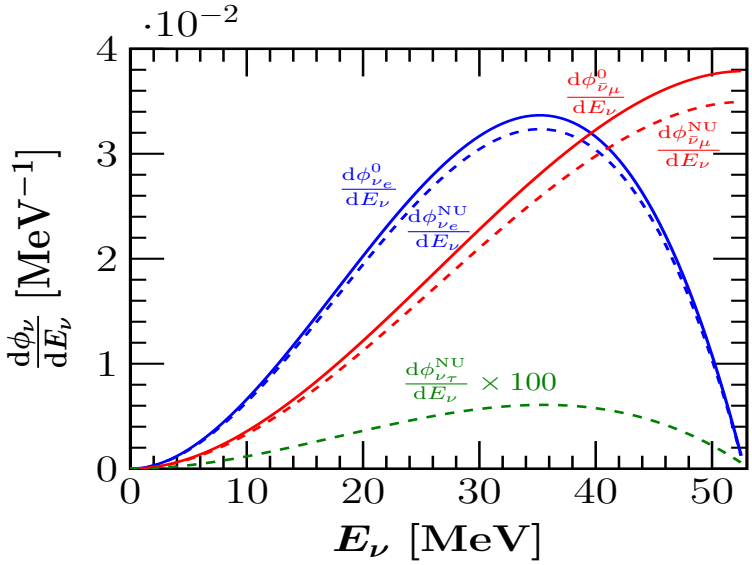

Figure 6.10: Neutrino flux as expected from a π-DAR source (solid line) compared with the excepted flux when considering the zero distance effect (dashed line) [56].

Now we will present an estimate on the prospects for probing the unitarity violating parameters at the future liquid argon detectors. We will do the same analysis using the χ^2 function, but since we do not have information about the different uncertainties of each detector, we consider a reduced χ^2 analysis in the form

$$\chi^2 = \left(\frac{N_{SM} - N_{new}}{\sqrt{N_{SM}}} \right)^2 . \tag{6.24}$$

For definiteness, we will focus on detecting electron and muon neutrinos, so the only relevant parameters become α_{11}, α_{21}, and $|\alpha_{21}|$. First, we only vary one parameter at a time and marginalize the other two. It is necessary to consider the triangular inequalities that exclude some combination of parameters. Fig. 6.11 shows the sensitivity profile for future CEvNS experiments considering the diagonal parameters α_{11} and α_{22}.

We can compare these sensitivities with those derived from global neutrino oscillation data. This is represented in the vertical dashed line. It is possible to see that the CEvNS future experiments, such as CCM and ESS, may become competitive with the current searches. For both cases, the ESS experiment considering 10 kg of mass detector won't be competitive since the intersection at 90% C.L. is more to the left than the vertical line. This is the same for CENNS for both parameters. But, for the case of CCM and the future perspective of ESS with 1 ton detector, it may be possible to improve with respect the current oscillation results.

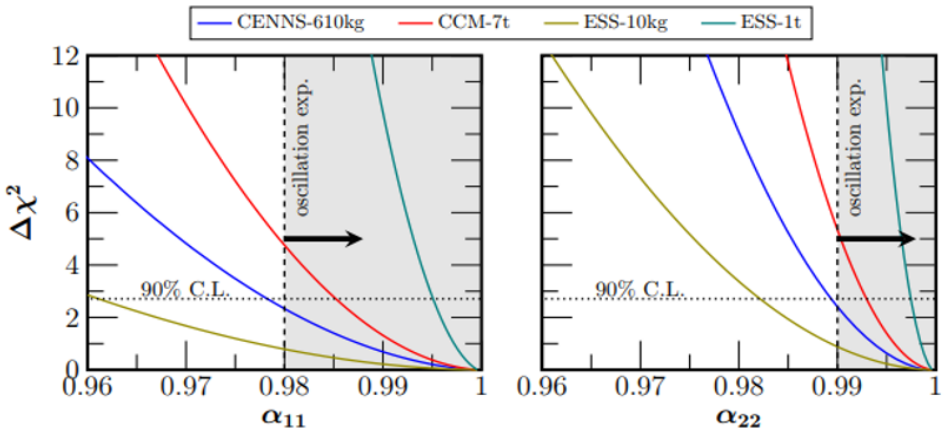

Figure 6.11: Sensitivity to the diagonal parameters α_{11} and α_{22}. For comparison we show the sensitivity obtained from global oscillation data [56].

Fig. 6.12 shows the analysis for the case of the modulus of the non-diagonal parameter α_{21}. Again we compare the results with the upper limits obtained from global oscillation fits and also with the sensitivity of future ICARUS data. For this case, CEvNS experiments can not be competitive with the current bounds, but it is still possible to significantly improve the situation.

We consider possible backgrounds and systematic uncertainties in the calculation for a more realistic approach. Now we explore the projected sensitivities assuming a χ^2 function but considering uncertainties in the following way

$$\chi^2(\alpha_{11}, |\alpha_{21}|, \alpha_{22}) = min_a \left(\frac{(N_{SM} - N_{NU}(\alpha_{11}, |\alpha_{21}|, \alpha_{22})(1+a))^2}{(\sigma_{stat})^2} + (\frac{a}{\sigma_{sys}})^2 \right), \quad (6.25)$$

where the statistical uncertainty is defined as $\sigma_{stat} = \sqrt{N_{SM} + N_{bg}}$, and the number of background events are taken to be $N_{bg} = 10\% N_{SM}$. In this case, a denotes a total

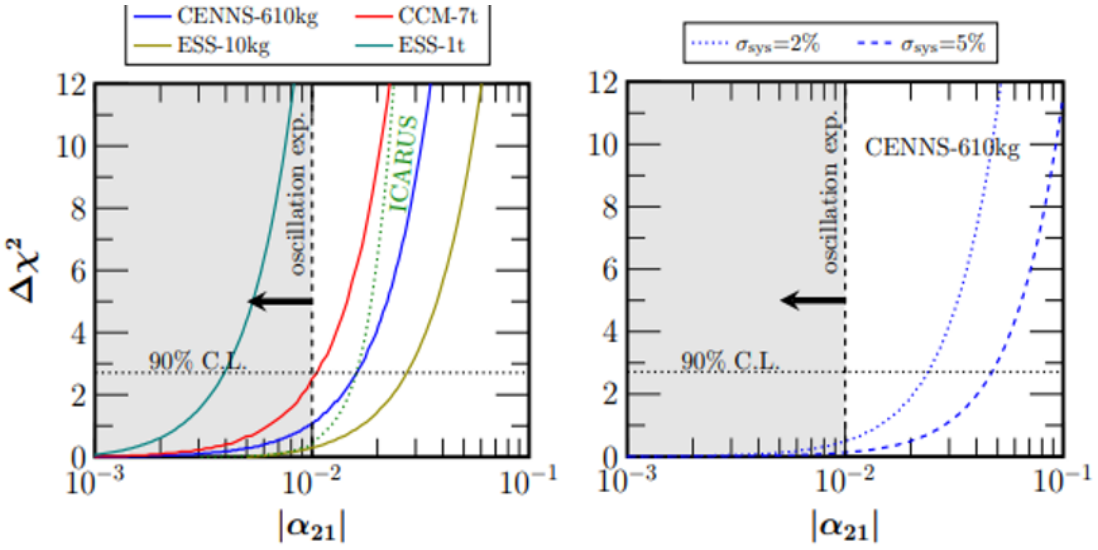

Figure 6.12: Sensitivity to the non-diagonal parameter $|\alpha_{21}|$. The left panel shows the results with no systematic uncertainties and the right panel the systematic uncertainties for the CENNS-610. [56]

normalization nuisance parameter accounting for the systematic uncertainty. For this case, we consider only $\sigma_{syst} = 2\%, 5\%$. The right panel of Fig. 6.12 shows that there may be a reduction in the sensitivity of around 2-4 times with respect to the ideal case, the same maintain for the rest of the experimental setups.

Finally, it is possible to perform a combined χ^2 analysis by simultaneously varying two NU parameters, and marginalizing over the third one. The analysis for the three experiments, CENNS, CCM, and ESS, are presented in the next figure. In this case the triangular inequalities that allow only certain values of the NU parameters are more evident. In both cases, the values below the dashed line represent the physically possible values. The dark-shaded areas in both $\alpha_{11} - |\alpha_{21}|$ and $\alpha_{22} - |\alpha_{21}|$ planes are allowed at 90% C.L. The final possible values for the parameters are determined by the intersection of the gray shaded areas with the allowed region determined by each experiment. From this, it is clear that CENNS and CCM have the potential to probe part of the currently allowed parameter space. But again, the most promising experimental setup is provided by the next phase of ESS.

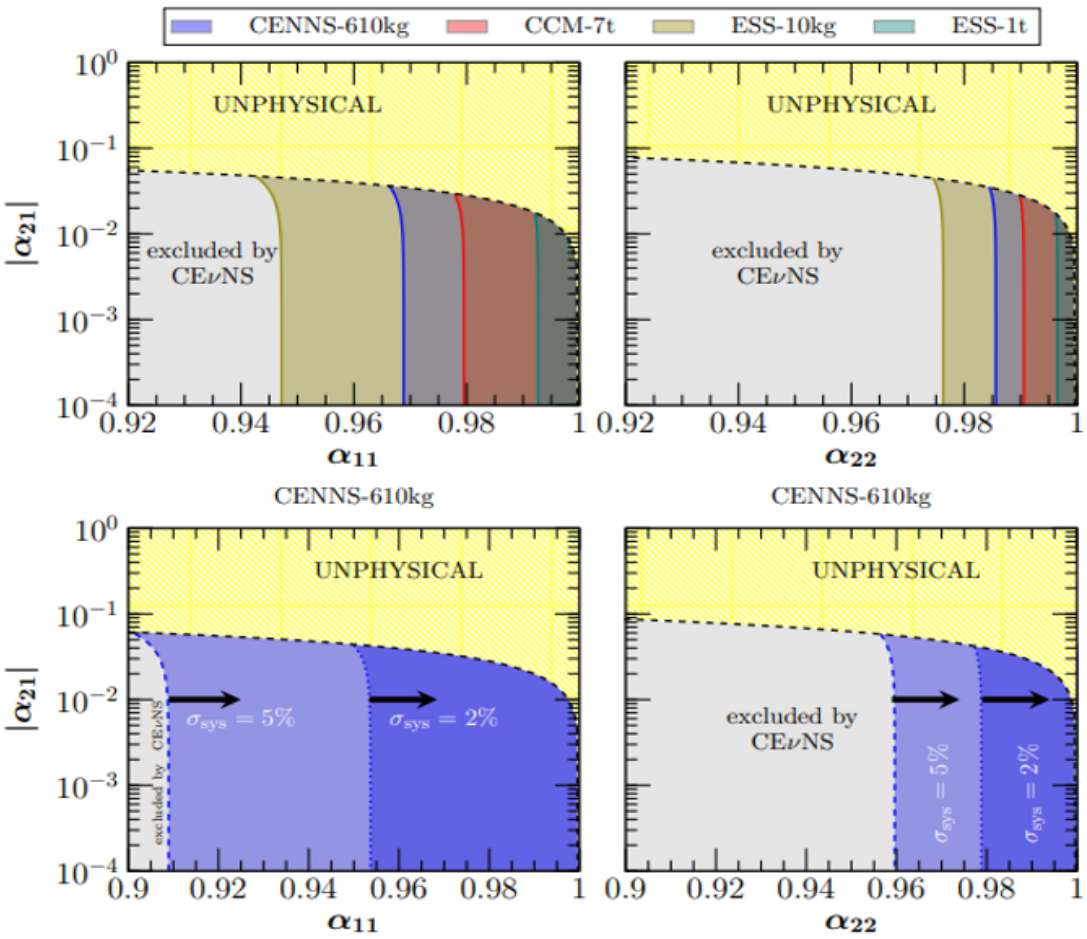

Figure 6.13: Allowed regions at 90 % C.L. in the planes $\alpha_{11} - |\alpha_{21}|$ (left) and $\alpha_{22} - |\alpha_{21}|$ (right). The gray shaded represents the bound given by the triangular inequalities previously mentioned. The upper panel is for the CENNS, CCM, and ESS (10kg) experiments, and the lower panel for the ESS (1ton) [56].

6.4 Neutrino Magnetic Moment

Now we will finish this section with the results obtained from the electromagnetic properties of the neutrinos. In this case, we used both CEvNS and EvES to find the sensitivity to the so-called dipole neutrino portal. First, we assume the neutrino magnetic moment as an effective parameter. Fig. 6.14 shows a summary of our results for all the experiments considered at 90 % C.L. The result for XENON1T for the transition $\nu_\mu \to \nu_s$ and $\nu_e \to \nu_s$ are shown here for comparison.

For the case of COHERENT, we used the CsI and LAr detector measurement data. For the CsI-detector, we considered a mass of 14.57 kg and a light yield $LY = 13.348 PE/KeV_{ee}$

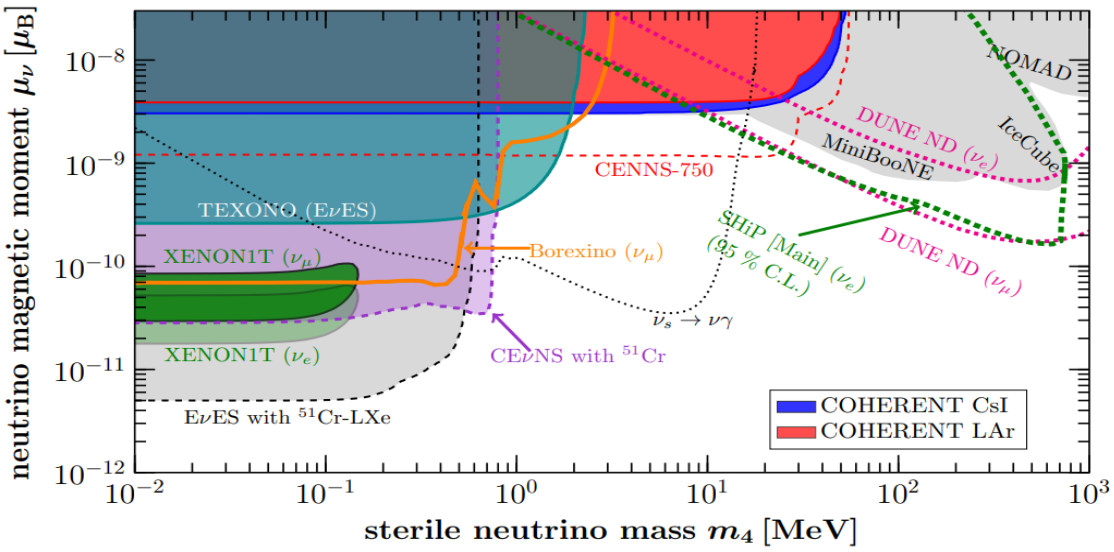

Figure 6.14: Sensitivity of CEvNS and EvES experiments to the effective sterile neutrino transition magnetic moments [57].

to convert the signal into photoelectrons (PE). The statistical analysis was performed using a χ^2 function

$$\chi^2(S) = \sum_{i=4}^{15} \left(\frac{N_i^{exp} - N_i^{CEvNS}(S)[1+a_1] - B_{0n}^i[1+a_2]}{\sqrt{N_i^{exp} + B_i^{0n} + 2B_i^{ss}}} \right)^2 + \left(\frac{a_1}{\sigma_{a_1}}\right)^2 + \left(\frac{a_2}{\sigma_{a_2}}\right)^2 \quad (6.26)$$

where N_i^{exp} and N_i^{CEvNS} are the measured and theoretical number of events in each bin. For this analysis, we only focused on the 12 bins from $i = 4$ to $i = 15$, which corresponds to $6 \leq PE \leq 30$. B_i^{0n} is the beam-on prompt neutron background, and B_i^{ss} is the steady-state background from the AC-ON data. The nuisance parameters a_1 and a_2 quantify the systematic uncertainties of the signal and the background, with $\sigma_{a_1} = 12.8\%$ and $\sigma_{a_2} = 25\%$.

Analogously, for the LAr, we used the 24 kg mass CENNS-10 detector subsystem. First we evaluated the expected signal in keV_{ee} with the reported quenching factor $QF = 0.246 + 7.8 \times 10^{-4} keV_{nr}^{-1}$. Then we convert the signal to reconstructed energy using a normalized Gaussian function with a resolution power $\frac{\sigma}{E} = \frac{0.58}{\sqrt{E(KeV_{ee}}}$. The χ^2 function used for this case reads as follows

$$\chi^2(S) = \sum_{i=1}^{12} \frac{(N_i^{exp} - \eta_{CEvNS} N_i^{CEvNS}(S) - \eta_{PBRN} B_i^{PBRN} - \eta_{LBRN} B_i^{LBRN})^2}{(\sigma_i^{exp})^2 + [\sigma_{BRNES}(B_i^{PBRN} + B_i^{LBRN})]^2} + \left(\frac{\eta_{CEvNS} - 1}{\sigma_{CEvNS}}\right)^2 + \left(\frac{\eta_{PBRN} - 1}{\sigma_{PBRN}}\right)^2 + \left(\frac{\eta_{LBRN} - 1}{\sigma_{LBRN}}\right)^2 \tag{6.27}$$

For this case, we consider the 12 bins in the range of $[0, 120]$ KeV_{ee} of the reconstructed energy, with each bin of 10 KeV_{ee} sizes. N_i^{exp} denotes the measured signal with uncertainty σ_i^{exp}, BRNES is the Beam Related Neutron Energy Shape, while PBRN and LBRN are the Prompt and Late Beam Related Neutron Background data, with $\sigma_{PBRN} = 32\%$ and $\sigma_{LBRN} = 100\%$. The BRNES uncertainty is 1.7%, and the systematic uncertainty of the signal rate is 13.4%.

This data rules out the region with $\mu_{\nu_\mu} \geq 3 \times 10^{-9} \mu_B$ and $m_4 \leq 40 MeV$, and we can see that the CsI detector is a little better in comparison with the LAr detector. Since these experiments are under improvement, we also performed the analysis for the next generation CENNS-750 detector with 610 kg fiducial mass and 3 years of data acquisition. These experiments increased little bit the region compared with the experimental data available.

Now for the case of EvES, the restrictions come from the TEXONO experiment, which reported measurements of EvES using a 187 kg CsI(Ti) detector. The χ^2 function used for the analysis of this is given by

$$\chi^2 = \sum_{i=1}^{10} \left(\frac{N_i^{meas} - N_i^{new}(S)[1+a]}{\sigma_i^{stat}}\right)^2 + \left(\frac{a}{\sigma_{sys}}\right)^2, \tag{6.28}$$

with N_i^{meas} the detected events. We considered the reported 10 bins distributed over the energy range $[3, 8]$ MeV with their associated errors. The systematic uncertainties are $\sigma_{sys} = 20\%$. From here, $\mu_{\bar{\nu}_e} \geq 3 \times 10^{-10} \mu_B$ is excluded. This means that the constraint is improved by an order of magnitude for the neutrino dipole moment coupling with respect to COHERENT results. However, there is a sensitivity loss at $m_4 \approx 10 MeV$ due to the kinematic cut imposed by the low energy reactor neutrinos.

Finally, we also made this analysis for a ^{51}Cr source for neutrinos. This is useful for both CEvNS and EvES measurements. For this case, we use a simplified statistical analysis

because there is no experimental data available

$$\chi^2(S) = \sum_{i=1}^{n} \left(\frac{N_i^{SM} - N_i^{new}(S)[1+a]}{\sigma_i^{stat}} \right)^2 + \left(\frac{a}{\sigma_{sys}} \right), \tag{6.29}$$

with $\sigma_i^{stat} = \sqrt{N_i^{SM} + N_i^{bg}}$. For this case we assumed a fixed background of 20 % from the SM rate, that is $N_i^{bg} = \sigma_{bg} N_i^{SM}$ with $\sigma_{bg} = 20\%$ with systematic uncertainties to be $\sigma_{sys} = 20\%$. For CEvNS, we used $n = 12$ bins on the energy range $[E_r^{thres}, E_r^{max}]$, with E_r^{max} being the maximum recoil energy for each target. For EvES we took $5keV_{ee}$ bins in the range $[1, 601]keV_{ee}$. This leads to a neutrino magnetic moment sensitivity improving in the region $\mu_{\nu_e} \approx 10^{-12}\mu_B$. However, just as in the reactor neutrino case, the low energy of the neutrinos leads to sensitivity loss for masses $m_4 \geq 750KeV$.

Before finishing this section, it is relevant to note the complementarity of the bounds from the analysis of CEvNS and EvES experiments, with those from oscillation experiments. For the $\nu_\mu \to \nu_s$ channel in COHERENT, experiments such as MiniBooNE, NOMAD, IceCube, Borexino, and DUNE near-detector are complementary. While not placing strength constraints on the NMM, the COHERENT experiments cover a larger portion of the previously unexplored parameter space. These regions overlap with other regions probed by the already mentioned large-scale experiments. Similarly, for the TEXONO and ^{51}Cr-based CEvNS and EvES experiments, the relevant experiments to complement are XENON1T, SHiP, and DUNE ND. Also, the Cr-LXe can provide another test of the region indicated by the XENON1T excess.

Finally, we can explore the sensitivities for the TMMs. Adopting this more general TMMs formalism allow us to compare the sensitivities at different experiments in terms of the same parameter λ_{ij}. Also, we can combine the full data set of experiments with multiple neutrino flavors. So, for example, for COHERENT and XENON1T, we don't need to consider one non-zero effective magnetic moment $\mu_{\nu_\alpha}(\alpha = e, \mu, \tau)$ at a time. For the final Fig. 6.15, the relevant parameters μ_{ν_α} are assumed non-vanishing and are expressed in terms of the TMMs λ_{ij}. Fig. 6.15 shows the results taking only one non-vanishing TMM at a time and neglecting the associated CP phases, and it can be seen that the same behavior is observed as for the effective dipole moment.

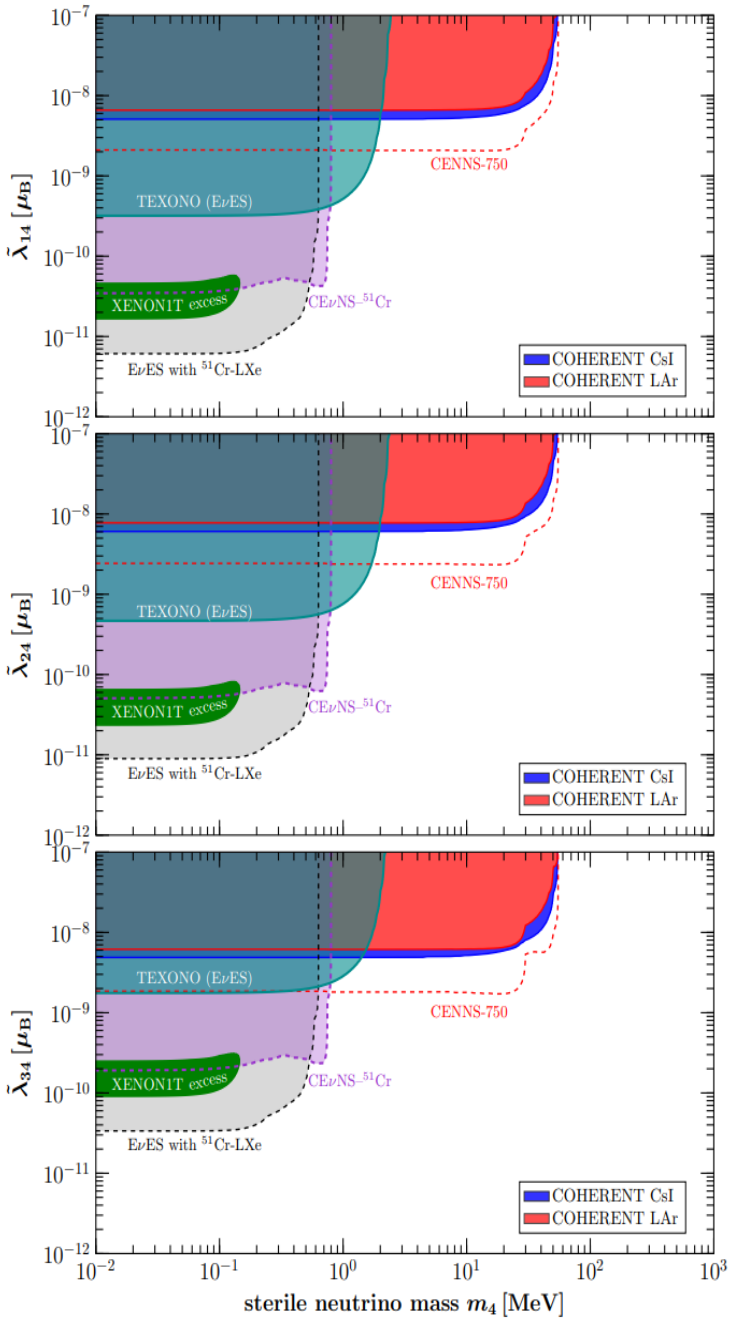

Figure 6.15: Sensitivity to the general TMM formalism. [57]

Chapter 7

Conclusions

Neutrinos are fascinating particles, and it is a fact that we still have a lot to learn about them. The great change in their understanding upon discovering that they actually do have mass has left its mark on their study and continues to date. There are still many questions to answer, and we hope that the future experiments can answer them.

Detecting coherent elastic neutrino neutrino-nucleus scattering has shown us the great progress we have made in technologies for particle detection. It has allowed us to continue studying the Standard Model and its possible extensions, obtaining more and more precise results. In this thesis, we have studied different types of physics beyond the Standard Model and obtained the sensitivity to its different parameters. The results yield four article publications [54–57]. For the case of the experimental results, we have observed that the results obtained can become competitive, as in the case of the mixing angle and the rms radius of the neutron.

For the case of neutrino oscillations into sterile states, we observed that the baselines considered for each experiment are favorable for their study. A distance around 20-30 m is optimal for the values expected for the mass splitting and the mixing angle. The possible existence of sterile neutrinos is still under doubt,but finding more ways to prove or refuse its existence is still important. CEvNS has shown that it is possible to reach the limits actually imposed by other experiments with an increase in mass and data obtained. This is the case of the ESS with the proposed 1-ton mass, which gave the best results of all our analysis.

The non-unitarity neutrino mixing matrix is studied in our analysis by introducing the zero-distance effect. This gives an oscillation probability even though the neutrino was

just produced at the source. From here, we observed that, again, CEVNS experiments with a big mass could be competitive with results obtained from oscillation experiments. Still, if this configuration becomes possible, the results are expected to improve significantly.

Finally, for the neutrino electromagnetic properties, the regions that we reach using CEvNS are unexplored by other experiments, and this is due to the energies considered for this process. This can be complemented using EvES and a Cr^{51} source. Also, the analysis using the fundamental TMM, we were able to study the transitions $\nu_e \to \nu_s$ and $\nu_\mu \to \mu$ separately.

CEvNS is a relatively new process that has opened the doors to many different analyses and has shown their importance. The next step is to combine the different physics scenarios to constrain multiple parameters that are related. Also, the new results and information about the experimental setups will improve our understanding and future perspectives of the results presented in this thesis. We hope that with this thesis, we can set our contribution to a better understanding of our universe.

Appendix A

Cross section calculation

Following Feynman rules, we have that the amplitude is

$$iM = \frac{-ig}{2cos\theta_w}\left(\frac{1}{2}\right)\bar{u}_{r'}(p_1)\gamma^\mu(1-\gamma^5)u_r(k_1)\frac{-i(g_{\mu\nu}-\frac{p_\mu p_\nu}{M_z^2})}{q^2-M_z^2}J^\nu_{nuc}. \tag{A.1}$$

The nuclear current can be represented as

$$J^\nu_{nuc} = \frac{g}{2cos\theta_w}(g^u_L\bar{u}_L\gamma^\mu u_L + g^u_R\bar{u}_R\gamma^\mu u_R + g^d_L\bar{d}_L\gamma^\mu d_L + g^d_R\bar{d}_R\gamma^\mu d_R). \tag{A.2}$$

For nuclei of spin 0, and assuming that parity is not violated, we have

$$\bar{u}_L\gamma^\mu U_L = \bar{U}_R\gamma^\mu U_R = \bar{u}\gamma^\mu u, \tag{A.3}$$

$$\bar{d}_L\gamma^\mu d_L = \bar{d}_R\gamma^\mu d_R = \bar{d}\gamma^\mu d, \tag{A.4}$$

for a nucleus of Z protons and N neutrons

$$u-quarks \to 2Z+N, d-quarks \to 2N+Z. \tag{A.5}$$

For the case of EM current in quarks we get

$$J^\mu_{EM} = \frac{2}{3}\bar{u}\gamma^\mu u - \frac{1}{3}\bar{d}\gamma^\mu d. \tag{A.6}$$

From Feynman rules for this case, we know that the vertex is proportional to $(p_2 + k_2)^\mu$,

$$J^\nu_{nuc} = \gamma(k_2 + p_2)^\nu, \tag{A.7}$$

but also,

$$J^\nu_{nuc} = \frac{g}{2cos\theta_w}(g^u_L(2Z+N) + g^u_R(2Z+N) + g^d_L(2N+Z) + g^d_R(2N+Z))(k_2+p_2)^\nu, \tag{A.8}$$

and from this

$$\alpha = \frac{g}{2cos\theta_w}((2Z+N)g^u_V + (2N+Z)g^d_V), \tag{A.9}$$

$$= \frac{g}{2cos\theta_w}((2Z+N)(\frac{1}{2} - \frac{4}{3}sin^2\theta_w) + (2N+Z)(-\frac{1}{2} + \frac{2}{3}sin^2\theta_2)), \tag{A.10}$$

$$= \frac{g}{2cos\theta_w}(Z - \frac{8}{3}Zsin^2\theta_w + \frac{N}{2} - \frac{4}{3}Nsin^2\theta_w - N + \frac{4}{3}Nsin^2\theta_w - \frac{1}{2}Z + \frac{2}{3}Zsin^2\theta_w), \tag{A.11}$$

$$= \frac{g}{2cos\theta_w}[(1 - 4\sin^2\theta_w)Z - N] = \frac{g}{2cos\theta_w}Q_w. \tag{A.12}$$

Including the form factor for the nucleus

$$J^\nu_{nuc} = \frac{g}{2cos\theta_w}Q_wF(q^2)(k_2+p_2)^\nu, \tag{A.13}$$

and we get to

$$iM = \frac{-ig^2}{8cos^2\theta_w}\left(\frac{1}{2}\right)\bar{u}_{r'}(p_1)\gamma^\mu(1-\gamma^5)u_r(k_1)Q_wF(q^2)\frac{-i(g_{\mu\nu} - \frac{p_\mu p_\nu)}{M_z^2}}{q^2 - M_z^2}(k_2+p_2)_\mu. \tag{A.14}$$

On the limit of $q^2 << M_z^2$ we get that the propagator reduces to $\frac{-g_{\mu\nu}}{M_z^2}$,

$$iM = -i\frac{G_F}{\sqrt{2}}Q_wF(q^2)g^V_L\bar{u}_{r'}(p_1)\gamma^\mu(1-\gamma^5)u_r(k_1)(k_2+p_2)_\mu. \tag{A.15}$$

Now we can find the sum over the spins

$$\begin{aligned}\sum_{rr'}|iM_{rr'}|^2) &= \sum_{rr'}\frac{G_F^2}{2}Q_w^2F^2(q^2)(g_L^v)^2(k_2+p_2)_\mu(k_2+p_2)_\nu\times\\ &\times\bar{u}_{r'}(p_1)\gamma^\mu(1-\gamma^5)u_r(k_1)u_r(k_1)\gamma^\nu(1-\gamma^5)u_{r'}(p_1)\\ &= C\sum_{rr'}[\bar{u}_{r'}(p_1)\gamma^\mu(1-\gamma^5)u_r(k_1)][\bar{u}_{r'}\gamma^\nu(1-\gamma^5)u_r]^\dagger\\ &= CTr[\gamma^\mu(1-\gamma^5)(\not{k}_1\gamma^\nu(1-\gamma^5)\not{P}_1]\\ &= CTr[\gamma^\mu\not{k}_1\gamma^\nu\not{P}_1-\gamma^\mu\not{k}_1\gamma^\nu\gamma^5\not{P}_1-\gamma^\mu\gamma^5\not{k}_1\gamma^\nu\not{P}_1+\gamma^\mu\gamma^5\not{k}_1\gamma^\nu\gamma^5\not{P}_1]\\ &= C(2)Tr[\gamma^\mu\not{k}_1\gamma^\nu\not{P}_1(1-\gamma^5)]\\ &= C(2)[4][k_1^\mu P_1^\nu+P_1^\mu k_1^\nu-g^{\mu\nu}(k_1\cdot P_1)-i\epsilon^{\rho\mu\sigma\nu}k_{1\rho}P_{1\sigma}],\end{aligned}$$

we get

$$\begin{aligned}\sum_{rr'}|M|^2 &= \frac{8G_F^2}{2}Q_w^2F^2(g_L^v)^2(k_2+p_2)_\mu(k_2+p_2)_\nu[k_1^\mu P_1^\nu+P_1^\mu k_1^\nu-\\ &g^{\mu\nu}(k_1\cdot p_1)-i\epsilon^{\rho\mu\sigma\nu}k_{1\rho}P_{1\sigma}]\\ &= 4G_F^2Q_w^2F^2(g_L^v)^2[2k_1\cdot(k_2+p_2)P_1\cdot(k_2+P_2)-(k_2+P_2)^2(k_1\cdot P_1)-\\ &i\epsilon^{\rho\mu\sigma\nu}k_{1\rho}(k_2+P_2)_\mu P_{1\sigma}(k_2+P_2)_\nu]\\ &= 8G_F^2Q_w^2F^2(g_L^v)^2[(k_1\cdot k_2)(p_1\cdot k_2)+(k_1\cdot k_2)(p_1\cdot p_2)+(k_1\cdot p_2)(p_1\cdot k_2)+\\ &(k_1\cdot p_2)(p_1\cdot p_2)-(M^2+k_2\cdot p_2)(k_1\cdot p_1)].\end{aligned}$$

On the Lab. system

$$k_1 = (E,\vec{k}_1), \tag{A.16}$$
$$k_2 = (M,\vec{0}), \tag{A.17}$$
$$P_1 = (E-T,\vec{P}_1), \tag{A.18}$$
$$P_2 = (T+M,\vec{P}_2), \tag{A.19}$$
$$q = k_1-P_1 = k_2-P_2 = (T,\vec{q}), \tag{A.20}$$

with this, we can find the following relations

$$k_1 \cdot k_2 = EM, \tag{A.21}$$

$$P_1 \cdot P_2 = \frac{1}{2}((P_1 + P_2)^2 - P_1^2 - P_2^2) = \frac{1}{2}((k_1 + k_2)^2 - 0 - M^2) \tag{A.22}$$

$$= \frac{1}{2}(k_1^2 + k_2^2 + 2k_1 \cdot k_2 - M^2) \tag{A.23}$$

$$= \frac{1}{2}(M^2 + 2EM - M^2) = EM, \tag{A.24}$$

$$k_2 \cdot P_1 = M(E - T), \tag{A.25}$$

$$k_2 \cdot P_2 = M(T + M), \tag{A.26}$$

$$k_1 \cdot P_1 = (P_1 + P_2 - k_2) \cdot P_1 = P_1^2 + P_1 \cdot P_2 - k_2 \cdot P_1 \tag{A.27}$$

$$= EM - EM + MT = MT, \tag{A.28}$$

$$k_1 \cdot P_2 = k_1 \cdot (k_1 + k_2 - P_1) = k_1^2 + k_1 \cdot k_2 - k_1 \cdot P_1 = EM - MT = M(E - T), \tag{A.29}$$

$$q^2 = (k_1 - P_1)^2 = k_1^2 - 2k_1 \cdot P_1 + P_1^2 = -2MT, \tag{A.30}$$

So we get

$$
\begin{aligned}
|M|^2 &= 8G_F^2 Q_w^2 F^2 (g_L^v)^2 [EM(M(E-T)) + EM(EM) + M^2(E-T)^2 \\
&\quad + M(E-T)EM - (M^2 + M(T+M))MT] \\
&= 8G_F^2 Q_w^2 F^2 (g_L^v)^2 [E^2M^2 - EM^2T + E^2M^2 + EM^2 - 2EM^2T + M^2T^2 + \\
&E^2M^2 - EM^2T - M^3T - M^2T^2 - M^3T].
\end{aligned}
$$

After reducing terms

$$
|M|^2 = 8G_F^2 Q_w^{F\,2} (g_L^v)^2 [4E^2M^2 - 4EM^2T - 2M^3T] \tag{A.31}
$$

$$
= 32G_F^2 Q_w^2 F^2 \left(\frac{1}{2}\right) E^2M^2 [1 - \frac{T}{E} - \frac{MT}{2E^2}]. \tag{A.32}
$$

Using Fermi's golden rule we can find

$$
d\sigma = \frac{|M|^2}{2E_aE_b|v_a - v_b|}(2\pi)^4 \delta(P_a + P_b - \sum_f P_f) \prod_f \frac{d^3P_f}{(2\pi)^3 2E_f}, \tag{A.33}
$$

which for this case results

$$
d\sigma = \frac{|M|^2}{2E_a 2E_b|v_a - v_b|}(2\pi)^4 \delta(P_a + P_b - P_1 - P_2) \frac{d^3\vec{P}_1}{(2\pi)^3 2E_1} \frac{d^3P_2}{(2\pi)^3 2E_2}. \tag{A.34}
$$

On the center of mass frame $\vec{P}_a = -\vec{P}_b$ and $\vec{P}_1 = -\vec{P}_2$

From which we can get

$$
2E_aE_b|v_a - v_b| = 2E_a 2E_b |\frac{P_a^z}{E_a} - \frac{P_b^z}{E_b}| \tag{A.35}
$$

$$
= 2E_a 2E_b |\frac{\vec{P}_a}{E_a} - \frac{\vec{P}_b}{E_b}| \tag{A.36}
$$

$$
= 4E_aE_b |\frac{\vec{P}_a}{E_a} + \frac{\vec{P}_b}{E_b}| = \frac{4E_aE_b}{E_aE_b}|\vec{P}_a|(E_a + E_b), \tag{A.37}
$$

$$d^3\vec{P} = |\vec{P}|^2 d\vec{P} d\Omega = 4|\vec{P}_a|(E_a + E_b), \tag{A.38}$$

so

$$d\sigma = \frac{|M|^2}{16(2)^2(E_a + E_b)|\vec{P}_a|}\delta(E_a + E_b - E_1 - E_2)\delta^3(\vec{P}_a + \vec{P}_b - \vec{P}_1 - \vec{P}_2)\frac{d^3\vec{P}_1 d^3\vec{P}_2}{E_1 E_2}. \tag{A.39}$$

Integrating over $\vec{P}_2$

$$d\sigma = \frac{|M|^2}{16(2\pi)^2(E_a + E_b)|\vec{P}_a|}\delta(E_a + E_b - \sqrt{|\vec{P}_1^2|} - \sqrt{|\vec{P}_1|^2 + M^2})\frac{d^3\vec{P}_1}{|\vec{P}_1|\sqrt{|\vec{P}_1|^2 + M^2}} \tag{A.40}$$

$$= \frac{|M|^2}{16(2\pi)^2(E_a + E_b)|\vec{P}_a|}\delta(E_a + E_b - \sqrt{|\vec{P}_1^2|} - \sqrt{|\vec{P}_1|^2 + M^2})\frac{|\vec{P}_1|^2 d|\vec{P}_1| d\Omega}{|\vec{P}_1|\sqrt{|\vec{P}_1|^2 + M^2}}. \tag{A.41}$$

Using the change of variable

$$u = |\vec{P}_1| + \sqrt{|\vec{P}_1|^2 + M^2}, \tag{A.42}$$

we get that

$$\frac{du}{d|\vec{P}_1|} = 1 + \frac{2|\vec{P}_1|}{2\sqrt{|\vec{P}_1|^2 + M^2}} \tag{A.43}$$

$$= \frac{\sqrt{|\vec{P}_1|^2 + M^2} + |\vec{P}_1|}{\sqrt{|\vec{P}_1|^2 + M^2}} \tag{A.44}$$

$$= \frac{u}{\sqrt{|\vec{P}_1|^2 + M^2}}, \tag{A.45}$$

by doing the substitution

$$d\sigma = \frac{|M|^2}{16(2\pi)^2(E_a+E_b)|\vec{P}_a|}\delta(E_a+E_b-u)\frac{|\vec{P}_1|dud\Omega_{CM}}{u}. \tag{A.46}$$

If we integrate over u

$$d\sigma = \frac{|M|^2}{16(2\pi)^2(E_a+E_b)^2|\vec{P}_a|}|\vec{P}_1|d\Omega_{CM}, d\Omega_{CM} = s\phi d(cos\theta_{CM}), \tag{A.47}$$

and from the kinematics of the interaction on the CM-frame

$$\vec{q} = \vec{P}_a - \vec{P}_1 \rightarrow q^2 = |\vec{P}_a - \vec{P}_1|^2, \tag{A.48}$$

$$q^2 = |\vec{P}_a|^2 + |\vec{P}_1|^2 - 2\vec{P}_a \cdot \vec{P}_1 \tag{A.49}$$

$$= |\vec{P}_a|^2 + |\vec{P}_1|^2 - 2[|\vec{P}_a||\vec{P}_1|cos\theta_{CM}] \tag{A.50}$$

$$\frac{dq^2}{dcos\theta_{CM}} = 0 + 0 - 2|\vec{P}_a||\vec{P}_1|, \tag{A.51}$$

and

$$d\Omega_{CM} = \frac{d\phi dq^2}{-2|\vec{P}_a||\vec{P}_1|}. \tag{A.52}$$

Integrating over ϕ

$$d\sigma = \frac{|M|^2}{16(2\pi)^2(E_a+E_b)^2|\vec{P}_a|}\left(\frac{|\vec{P}_1|2\pi dq^2}{-2|\vec{P}_a||\vec{P}_1|}\right) \tag{A.53}$$

$$\frac{d\sigma}{dq^2} = -\frac{|M|^2}{64\pi(E_a+E_b)^2|\vec{P}_a|^2}. \tag{A.54}$$

Finally

$$S = (P_a + P_b)^2) = (k_1 + k_2)^2, \tag{A.55}$$

we have

$$P_a^2 + P_b^2 + 2P_a \cdot P_b = K_1^2 + K_2^2 + 2K_1 \cdot K_2, \tag{A.56}$$
$$M^2 + 2(E_a E_b - \vec{P}_a \cdot \vec{P}_b) = M^2 + 2EM, \tag{A.57}$$
$$E_a E_b - |\vec{P}_a|^2 = EM, \tag{A.58}$$
$$|\vec{P}_a| E_b - |\vec{P}_a|^2 = EM, \tag{A.59}$$
$$|\vec{P}_a|(E_a + E_b) = EM, \tag{A.60}$$
$$|\vec{P}_a|^2 (E_a + E_b)^2 = E^2 M^2. \tag{A.61}$$

So finally

$$\frac{d\sigma}{dq^2} \frac{-|M|^2}{64\pi E^2 M^2}, \tag{A.62}$$

then, since $q^2 = -2MT \rightarrow \frac{dT}{dq^2} = -\frac{1}{2M}$

$$\frac{d\sigma}{dq^2} = \frac{d\sigma}{dT} \frac{dT}{dq^2}, \tag{A.63}$$

$$\frac{d\sigma}{dT} = -2M \left(\frac{-|M|^2}{64^2 M^2} \right) = \frac{|M|^2}{32\pi E^2 M}, \tag{A.64}$$

and finally we get

$$\frac{d\sigma}{dT} = \left(\frac{1}{32\pi E^2 M} \right) \left(32 G_F^2 Q_w^2 F^2 (\frac{1}{2}) E^2 M^2 [1 - \frac{T}{E} - \frac{MT}{2E^2}] \right), \tag{A.65}$$

$$\frac{d\sigma}{dT} = \frac{G_F^2}{4\pi} Q_w^2 |F(q^2)| M [1 - \frac{T}{E} - \frac{MT}{2E^2}]. \tag{A.66}$$

Bibliography

[1] (2017, December). *Gold Foil Experiment*. Retrieved from https://www.sciencefacts.net/gold-foil-experiment.html,

[2] Griffiths, D. J. (1987). Introduction to elementary particles. New York: Harper Row

[3] J. J. Thomson, Phil. Mag. Ser. 5 **44**, 293-316 (1897) doi:10.1080/14786449708621070

[4] E. Rutherford, Phil. Mag. Ser. 6 **21**, 669-688 (1911) doi:10.1080/14786440508637080

[5] N. Bohr, Phil. Mag. Ser. 6 **26**, 1-24 (1913) doi:10.1080/14786441308634955

[6] T. D. Lee and C. N. Yang, Phys. Rev. **104**, 254-258 (1956) doi:10.1103/PhysRev.104.254

[7] Giunti, C., Kim, C. W. (2007). Fundamentals of neutrino physics and astrophysics. Oxford: Oxford Univ. Press.

[8] P. Janot and S. Jadach, Phys. Lett. B **803**, 135319 (2020) doi:10.1016/j.physletb.2020.135319 [arXiv:1912.02067 [hep-ph]].

[9] M. Tanabashi *et al.* [Particle Data Group], Phys. Rev. D **98**, no.3, 030001 (2018) doi:10.1103/PhysRevD.98.030001

[10] A. Lesov, [arXiv:0911.0058 [physics.hist-ph]].

[11] C. S. Wu, E. Ambler, R. W. Hayward, D. D. Hoppes and R. P. Hudson, Phys. Rev. **105**, 1413-1414 (1957) doi:10.1103/PhysRev.105.1413

[12] B. Pontecorvo, Sov. Phys. JETP **6**, 429 (1957)

[13] B. Pontecorvo, Zh. Eksp. Teor. Fiz. **34**, 247 (1957)

[14] Z. Maki, M. Nakagawa and S. Sakata, Prog. Theor. Phys. **28**, 870-880 (1962) doi:10.1143/PTP.28.870

[15] B. Pontecorvo, Zh. Eksp. Teor. Fiz. **53**, 1717-1725 (1967)

[16] Y. Fukuda *et al.* [Super-Kamiokande], Phys. Rev. Lett. **81**, 1562-1567 (1998) doi:10.1103/PhysRevLett.81.1562 [arXiv:hep-ex/9807003 [hep-ex]].

[17] Q. R. Ahmad *et al.* [SNO], Phys. Rev. Lett. **87**, 071301 (2001) doi:10.1103/PhysRevLett.87.071301 [arXiv:nucl-ex/0106015 [nucl-ex]].

[18] Q. R. Ahmad *et al.* [SNO], Phys. Rev. Lett. **89**, 011301 (2002) doi:10.1103/PhysRevLett.89.011301 [arXiv:nucl-ex/0204008 [nucl-ex]].

[19] K. Eguchi *et al.* [KamLAND], Phys. Rev. Lett. **90**, 021802 (2003) doi:10.1103/PhysRevLett.90.021802 [arXiv:hep-ex/0212021 [hep-ex]].

[20] A. Aguilar-Arevalo *et al.* [LSND Collaboration], Phys. Rev. D **64**, 112007 (2001) doi:10.1103/PhysRevD.64.112007 [hep-ex/0104049].

[21] J. Kopp, P. A. N. Machado, M. Maltoni and T. Schwetz, JHEP **1305**, 050 (2013) doi:10.1007/JHEP05(2013)050 [arXiv:1303.3011 [hep-ph]].

[22] T. Katori and M. Martini, J. Phys. G **45**, no. 1, 013001 (2018) doi:10.1088/1361-6471/aa8bf7 [arXiv:1611.07770 [hep-ph]].

[23] Y. Fukuda *et al.* [Super-Kamiokande Collaboration], Phys. Rev. Lett. **81**, 1562 (1998) doi:10.1103/PhysRevLett.81.1562 [hep-ex/9807003].

[24] K. Abe *et al.* [T2K Collaboration], Phys. Rev. D **88**, no. 3, 032002 (2013) doi:10.1103/PhysRevD.88.032002 [arXiv:1304.0841 [hep-ex]].

[25] A. P. Serebrov, R. M. Samoilov, V. G. Ivochkin, A. K. Fomin, V. G. Zinoviev, P. V. Neustroev, V. L. Golovtsov, S. S. Volkov, A. V. Chernyj and O. M. Zherebtsov, *et al.* Phys. Rev. D **104** (2021) no.3, 032003 doi:10.1103/PhysRevD.104.032003 [arXiv:2005.05301 [hep-ex]].

[26] Y. Abe *et al.* [Double Chooz], Phys. Rev. Lett. **108**, 131801 (2012) doi:10.1103/PhysRevLett.108.131801 [arXiv:1112.6353 [hep-ex]].

[27] F. P. An *et al.* [Daya Bay], Phys. Rev. Lett. **108**, 171803 (2012) doi:10.1103/PhysRevLett.108.171803 [arXiv:1203.1669 [hep-ex]].

[28] J. K. Ahn *et al.* [RENO], Phys. Rev. Lett. **108**, 191802 (2012) doi:10.1103/PhysRevLett.108.191802 [arXiv:1204.0626 [hep-ex]].

[29] S. Böser, C. Buck, C. Giunti, J. Lesgourgues, L. Ludhova, S. Mertens, A. Schukraft and M. Wurm, Prog. Part. Nucl. Phys. **111** (2020), 103736 doi:10.1016/j.ppnp.2019.103736 [arXiv:1906.01739 [hep-ex]].

[30] C. Giunti, X. P. Ji, M. Laveder, Y. F. Li and B. R. Littlejohn, JHEP **10**, 143 (2017) doi:10.1007/JHEP10(2017)143 [arXiv:1708.01133 [hep-ph]].

[31] C. Giunti, Y. F. Li, B. R. Littlejohn and P. T. Surukuchi, Phys. Rev. D **99**, no.7, 073005 (2019) doi:10.1103/PhysRevD.99.073005 [arXiv:1901.01807 [hep-ph]].

[32] W. Hampel *et al.* [GALLEX], Phys. Lett. B **447**, 127-133 (1999) doi:10.1016/S0370-2693(98)01579-2

[33] J. N. Abdurashitov *et al.* [SAGE], Phys. Rev. C **60**, 055801 (1999) doi:10.1103/PhysRevC.60.055801 [arXiv:astro-ph/9907113 [astro-ph]].

[34] A. Aguilar-Arevalo *et al.* [LSND], beam," Phys. Rev. D **64**, 112007 (2001) doi:10.1103/PhysRevD.64.112007 [arXiv:hep-ex/0104049 [hep-ex]].

[35] F. J. Escrihuela, D. V. Forero, O. G. Miranda, M. Tortola and J. W. F. Valle, Phys. Rev. D **92** (2015) no.5, 053009 [erratum: Phys. Rev. D **93** (2016) no.11, 119905] doi:10.1103/PhysRevD.92.053009 [arXiv:1503.08879 [hep-ph]].

[36] J. Schechter and J. W. F. Valle, Phys. Rev. D **24** (1981), 1883-1889 [erratum: Phys. Rev. D **25** (1982), 283] doi:10.1103/PhysRevD.25.283

[37] J. F. Nieves, Phys. Rev. D **26** (1982), 3152 doi:10.1103/PhysRevD.26.3152

[38] B. Kayser, Phys. Rev. D **26** (1982), 1662 doi:10.1103/PhysRevD.26.1662

[39] K. Fujikawa and R. Shrock, Phys. Rev. Lett. **45** (1980), 963 doi:10.1103/PhysRevLett.45.963

[40] C. Broggini, C. Giunti and A. Studenikin, Adv. High Energy Phys. **2012**, 459526 (2012) doi:10.1155/2012/459526 [arXiv:1207.3980 [hep-ph]].

[41] D. Z. Freedman, Phys. Rev. D **9**, 1389-1392 (1974) doi:10.1103/PhysRevD.9.1389

[42] E. A. Paschos and A. V. Kartavtsev, hep-ph/0309148.

[43] J. Barranco, O. G. Miranda and T. I. Rashba, JHEP **0512**, 021 (2005) doi:10.1088/1126-6708/2005/12/021 [hep-ph/0508299].

[44] D. Akimov *et al.* [COHERENT Collaboration], Science **357**, no. 6356, 1123 (2017) doi:10.1126/science.aao0990 [arXiv:1708.01294 [nucl-ex]].

[45] D. Akimov *et al.* [COHERENT], Phys. Rev. Lett. **126**, no.1, 012002 (2021) doi:10.1103/PhysRevLett.126.012002 [arXiv:2003.10630 [nucl-ex]].

[46] M. Cadeddu, C. Giunti, Y. F. Li and Y. Y. Zhang, Phys. Rev. Lett. **120**, no. 7, 072501 (2018) doi:10.1103/PhysRevLett.120.072501 [arXiv:1710.02730 [hep-ph]].

[47] P. S. Barbeau, Y. Efremenko and K. Scholberg, [arXiv:2111.07033 [hep-ex]].

[48] D. Akimov *et al.* [COHERENT], doi:10.5281/zenodo.1228631 [arXiv:1804.09459 [nucl-ex]].

[49] D. Akimov, S. Alawabdeh, P. An, A. Arteaga, C. Awe, P. S. Barbeau, C. Barry, B. Becker, V. Belov and I. Bernardi, *et al.* [arXiv:2204.04575 [hep-ex]].

[50] D. Akimov *et al.* [COHERENT], Science **357**, no.6356, 1123-1126 (2017) doi:10.1126/science.aao0990 [arXiv:1708.01294 [nucl-ex]].

[51] E. Aprile *et al.* [XENON], Phys. Rev. D **102**, no.7, 072004 (2020) doi:10.1103/PhysRevD.102.072004 [arXiv:2006.09721 [hep-ex]].

[52] M. Deniz [TEXONO], Nucl. Phys. B Proc. Suppl. **229-232**, 498-498 (2012) doi:10.1016/j.nuclphysbps.2012.09.135

[53] C. Bellenghi, D. Chiesa, L. Di Noto, M. Pallavicini, E. Previtali and M. Vignati, Eur. Phys. J. C **79**, no.9, 727 (2019) doi:10.1140/epjc/s10052-019-7240-3 [arXiv:1905.10611 [physics.ins-det]].

[54] O. G. Miranda, G. Sanchez Garcia and O. Sanders, Adv. High Energy Phys. **2019** (2019), 3902819 doi:10.1155/2019/3902819 [arXiv:1902.09036 [hep-ph]].

[55] O. G. Miranda, D. K. Papoulias, G. Sanchez Garcia, O. Sanders, M. Tórtola and J. W. F. Valle, JHEP **05** (2020), 130 [erratum: JHEP **01** (2021), 067] doi:10.1007/JHEP05(2020)130 [arXiv:2003.12050 [hep-ph]].

[56] O. G. Miranda, D. K. Papoulias, O. Sanders, M. Tórtola and J. W. F. Valle, Phys. Rev. D **102** (2020), 113014 doi:10.1103/PhysRevD.102.113014 [arXiv:2008.02759 [hep-ph]].

[57] O. G. Miranda, D. K. Papoulias, O. Sanders, M. Tórtola and J. W. F. Valle, JHEP **12** (2021), 191 doi:10.1007/JHEP12(2021)191 [arXiv:2109.09545 [hep-ph]].